

DISSERTATION

Asymptotic theory of marginal turbulent separation

ausgeführt zum Zwecke der Erlangung des akademischen Grades eines Doktors der technischen Wissenschaften unter der Leitung von

O.Univ.-Prof. Dipl.-Ing. Dr. techn. Alfred Kluwick

E322 /

Institut für Strömungslehre und Wärmeübertragung

eingereicht an der Technischen Universität Wien,
Fakultät für Maschinenbau

von

Dipl.-Ing. Bernhard Scheichl

Matrikelnummer: 8725070

Neusiedlerstraße 41/2/3, A-2340 Mödling

Wien, im Juni 2001

VORWORT

Die vorliegende Arbeit entstand in den Jahren 1997–2001 während meiner Tätigkeit als Universitätsassistent am Institut für Strömungslehre und Wärmeübertragung der Technischen Universität Wien.

An dieser Stelle möchte ich meinem Lehrer, Herrn Professor Dr. Alfred Kluwick, für die interessante und herausfordernde Themenstellung danken. Er betreute die Arbeit in fachlich souveräner sowie menschlich großzügiger Weise und erlaubte mir einen ausgesprochen selbständigen Arbeitsstil. In schwierigen Phasen war er jedoch stets bereit, in zahlreichen ergiebigen Diskussionen mit Rat und Tat zur Seite zu stehen und wertvolle Hinweise für den Fortgang der Arbeit zu liefern.

Weiters danke ich Herrn Professor Dr. Helmut Sockel für die Übernahme des Koreferates. Von ihm kenne ich einige interessante Vorschläge in Hinblick auf eine mögliche Validierung der in dieser Arbeit vorgestellten Theorie durch Experimente sowie mittels Direkter Numerischer Simulation.

Allen anderen Kollegen und Institutsmitgliedern sei für das Zustandekommen eines äußerst kollegialen wie motivierenden Arbeitsklimas am Institut gedankt. Insbesondere möchte ich die Herren Dr. Stefan Braun und Professor Dr. Herbert Steinrück erwähnen, die in so manchem fruchtbaren Gespräch Interesse am Fortschritt der Arbeit bekundeten.

Wien, im Juni 2001.

Bernhard Scheichl

Kurzfassung

Die Entwicklung einer asymptotischen Theorie zur turbulenten Ablösung wurde bis heute in erster Linie dadurch verhindert, dass selbst im Grenzfall unendlich hoher Reynolds-Zahlen Re ein Druckanstieg von der $O(1)$ notwendig ist, um Ablösung einer klassischen anliegenden turbulenten Grenzschicht herbeizurufen. Dabei ist die bekannte asymptotische Struktur letzterer im Wesentlichen durch den kleinen Geschwindigkeitsdefekt in Bezug auf die Geschwindigkeit am Grenzschichttrand zufolge der drehungsfreien Außenströmung charakterisiert.

Eine gänzlich andere Situation tritt auf, wenn man eine Grenzschicht betrachtet, welche unter der Wirkung eines aufgeprägten stetigen, positiven (sowie hinreichend starken) Druckgradienten zwar abzulösen vermag, jedoch unmittelbar stromab wieder anlegt. In Übereinstimmung mit den Ergebnissen für laminare marginal abgelöste Strömungen ändert sich der Druckgradient an der Stelle verschwindender Wandschubspannung nur schwach. Ihr Vorzeichenwechsel setzt im turbulenten Fall ebenso wie bei laminarer Strömung einen Geschwindigkeitsdefekt von der $O(1)$ voraus. Diese Beobachtung lässt den Schluss zu, dass der äußere Teil einer sich am Rande der Ablösung befindlichen turbulenten Grenzschicht ein Freistrah-ähnliches Verhalten aufweist, welches durch die reibungsfreien, turbulenten Scherschicht-Gleichungen mit nichtlinearem konvektiven Anteil bestimmt wird. Dabei stellt sich heraus, dass die Dicke der Schicht asymptotisch von der Größenordnung eines kleinen, im Wesentlichen von Re unabhängigen, sogenannten Schlankheits-Parameters ist.

Dieses selbstkonsistente asymptotische Konzept eröffnet die Möglichkeit einer weiteren analytischen Behandlung des turbulenten Ablösemechanismus, sodass unter anderem die Frage geklärt wird, wie das klassische logarithmische Wandgesetz für strikt anliegende Grenzschichten glatt in das bekannte Quadratwurzel-Verhalten des Geschwindigkeitsprofils in Wandnähe für eine gerade ablösende Strömung transformiert wird. Unterstützt von numerischen Rechnungen erhält man als ein wichtiges Ergebnis, dass im Grenzfall $Re^{-1} \rightarrow 0$ die reine Scherschicht-Approximation für den Außenteil der Grenzschicht beim Auftreten von Ablösung reguläre Lösungen für das kleine Rezirkulationsgebiet zulässt, ganz im Gegensatz zu dem aus der Theorie laminarer marginaler Ablösung bekannten singulären Verhalten.

Des weiteren gelingt es zu zeigen, dass im speziellen Fall von Quasi-Gleichgewichtsgrenzschichten mit kleinem Geschwindigkeitsdefekt, die sich in führender Ordnung durch konstanten Rotta–Clauser-Parameter β auszeichnen, der Übergang von der klassischen Defektstruktur zum nichtlinearen Verhalten einer nahezu freien Scherschicht von einer Mehrdeutigkeit der Lösungen im Falle $\beta \rightarrow \infty$ begleitet wird.

Die vorliegenden Untersuchungen stellen sich dabei als im weitesten Sinne unabhängig von der Wahl eines speziellen Schließmodells für die Reynolds-Spannungen heraus.



Abstract

The development of an asymptotic theory of turbulent separation has been hampered severely by the fact that a pressure increase of $O(1)$ appears to be necessary to separate an initially firmly attached turbulent boundary layer, even in the limit of infinite Reynolds number, denoted by Re . According to classical theory, the latter one is characterized by a small velocity defect with respect to the external irrotational flow. A different situation is expected to arise if one considers boundary layers subjected to adverse pressure gradients such that the wall shear stress vanishes eventually but immediately recovers. Similar to the case of laminar marginally separated flows, the pressure changes in the vicinity of the point of vanishing wall shear then are small. But then the difficulty is encountered that separation is not compatible with a small velocity defect but rather requires the existence of a defect of $O(1)$. Thus, separation is seen to be associated with the appearance of a nonlinear wake-like solution describing the outer part of the boundary layer, whose slenderness then is determined by an additional small parameter which is essentially independent of Re . This allows for further analytical progress which suggests a self-consistent description of the separation process and, among others, shows how the classical logarithmic law of the wall is gradually transformed into the well-known square root law that holds at the point of zero skin friction. Supported by numerical calculations, the important result is found, among others, that separation is accompanied by a regular solution of the inviscid wake. It gives rise to a small reverse-flow regime in the limit $Re^{-1} = 0$ within the framework of pure boundary layer theory, strikingly contrasting the singular behaviour known from its laminar counterpart. Moreover, in the special case of quasi-equilibrium flows characterized by an only weakly varying Rotta–Clauser parameter β the transition from the classical defect to the nonlinear wake is found to be associated with non-uniqueness of the solutions in the case $\beta \rightarrow \infty$. The analysis presented is essentially independent of the choice of a specific closure for the Reynolds shear stress.

CONTENTS

1. Introduction	1
2. Problem formulation — governing equations	4
3. Limitations of classical small-defect approach	6
3.1. Small-defect formulation	6
3.1.1. Viscous wall layer	7
3.1.2. Outer defect layer	9
3.1.3. Equilibrium flows	10
3.2. Impossibility of predicting separation	11
3.2.1. Numerical aspects	11
4. Case of quasi-equilibrium flow — bifurcating solutions as $\beta \rightarrow \infty$	15
4.1. Velocity defect flow for large β	15
4.1.1. Transition layer	18
4.2. Analytical homogeneous solution	19
4.3. Connecting flow regime	21
5. General nonlinear theory	27
5.1. Boundary layer approximation: $\alpha \ll 1$, $Re^{-1} = 0$	27
5.1.1. Intermediate layer	28
5.1.2. Combined structure for finite α	32
5.2. Generalized law of the wall and skin friction formula	33
5.2.1. Disturbances in the wake region due to finite Re	36
5.3. Similarity solutions	37
5.3.1. Inviscid limit: $Re^{-1} = 0$	37
5.3.2. Finite values of Re	41
5.4. Small defect — connecting flow	42
6. Separation process	46
6.1. Inviscid limit: $Re^{-1} = 0$	46
6.1.1. Numerical results — marginally separated flow	46
6.1.2. Local analytical solutions for $U_s \rightarrow 0$	50
6.1.3. Reverse-flow regime — multiple solutions	55
6.2. Accounting for finite Re	57
6.2.1. Near-wall structure allowing for separation and reattachment	59
7. Conclusions — further outlooks	62
Appendix A	64
Appendix B	65
Appendix C	65

1. Introduction

A rational asymptotic theory of wall-bounded turbulent shear flows over a smooth surface in the limit of large Re on basis of the full set of the time- or, equivalently, Reynolds-averaged Navier–Stokes equations for the mean motion has been formulated first by Yajnik (1970), Bush & Fendell (1972), Fendell (1972) and Mellor (1972). Their approach accounts for the two-tiered structure of a firmly attached turbulent boundary layer, reflecting different length scales which give rise to an almost inviscid outer region comprising most of the boundary layer and a viscous wall layer which have to be treated separately (cf. also figure 1). The thickness of the latter is established by the kinematic viscosity related to the so-called surface or skin friction velocity, cf. (3.1), and turns out to be transcendently small as compared to the boundary layer thickness. However, the need to distinguish between an outer part dominated by inertia and Reynolds stress terms and a region very close to the surface characterized approximately by the equilibrium between Reynolds shear stress and its viscous counterpart was already pointed out by v. Kármán (1930), Prandtl (1933), by means of dimensional reasoning alone.

The basic assumption that the streamwise mean velocity component in the inviscid outer part of the boundary layer differs from the external free stream velocity imposed at the outer edge of the boundary layer only by the magnitude of the dimensionless skin friction velocity $u_\tau = O(1/\ln Re)$ allows for a self-consistent description of the composite structure by means of matched asymptotic expansions. The requirement of a common domain of validity of the appropriate expansions for the field quantities in both layers this small velocity defect implies among others the famous logarithmic velocity law which spans the gap between the velocity profile scaled by u_τ in the viscous sublayer and the slightly perturbed free stream velocity in the outer defect layer. Thus the convection terms in the equation governing the flow in the latter in leading order turn out to be linearized. However, this property unfortunately prevents the possibility of extending the small-defect theory in a rational manner in order to account for the occurrence of separation ($u_\tau \rightarrow 0$) for high but finite Re . This conclusion is strongly supported by several studies that deal with distortions exerted on that classical type of a turbulent boundary layer, see in particular the work of Sykes (1980) who considered small disturbances in the imposed pressure leading to an asymptotically large gradient. In fact, the results indicate that at least a short-scale pressure rise of $O(1)$ is necessary for provoking separation of the initially strictly attached small-defect flow. However, any theory describing that kind of separation has not been developed at present.

On the other hand, many empirical studies but also analytical investigations in the limit of high Re of the structure of a boundary layer on the verge of separation over the last decades – a representative cross-section is given by Clauser (1954), Schofield (1981), Elsberry *et al.* (2000), the asymptotic approach of Durbin & Belcher (1992) as well as the survey on some features of separating boundary layers given in Townsend (1976), for instance – suggest the need of a nonlinear theory as the velocity defect near separation becomes of $O(1)$. This in turn renders the the two-tiered small-defect formulation invalid but is consistent with the well-known half-power velocity law that holds in the overlap between the outer rather wake-like flow and a viscous wall layer. An asymptotically correct treatment of the latter is outlined in Durbin & Belcher (1992) who recognized that the common description of the flow near the wall ceases to be valid at incipient separation where $u_\tau = O(Re^{-1/3})$ or smaller. The new scaling is based on a reference velocity of that magnitude formed by viscosity and the local pressure gradient and thus holds even for separation as it allows for $u_\tau \rightarrow 0$. It inevitably gives rise to a so-called intermediate layer as the square root profile clearly does not match with the solution at the base of a fully nonlinear outer region. Nevertheless, their approach which is purely based on Re as the single perturbation parameter also implies a dependency on Re in the expressions for any familiar model applicable to the outer part of

the boundary layer which definitely does not exist. Furthermore, it lacks an explanation for the structural change of the classical small-defect flow towards a separating multi-layered wake-like one.

A different approach is adopted in the contributions of Vik. Sychev (1983) and V. Sychev (1987) who addressed the challenging problem of turbulent pressure-induced separation on a blunt body and proposed an overlap regime comprising the viscous sublayer and a nonlinear intermediate region, in order to match the linearly varying shear stress by means of well-known Prandtl's mixing length hypothesis, for the original derivation see Prandtl (1925). Since it is readily verified that this fundamental relation gives rise to a Reynolds shear stress of $O(1)$ for a defect of $O(1)$ it seems difficult to accept their theory as a rational flow description. Moreover, Sychev & Sychev (1987) applied such a three-layered structure also to attached boundary layers for the purpose of providing a framework capable of the transition towards separation. Apart from the outlined inconsistency associated with the questionable need of a nonlinear middle region, it is not clear how the log-law shall be superseded by the square root behaviour. Similar discrepancies arise from the two-layered nonlinear structure proposed by Afzal (1996).

One important clue indicating how these dilemmas one encounters in elaborating an asymptotic theory for high Re , which suffices the correct wall scaling at incipient separation and accounts for the necessity of proposing a large defect, can be avoided is provided by inspection of all commonly used closure for Reynolds shear stress: At least one small dimensionless scaling parameter is noticed which is known from experiments but clearly independent of Re . However, the shear stress gradient must be retained in leading order in a shear layer approximation that exhibits nonlinearly coupled inertia terms for a velocity defect of $O(1)$. Therefore, that small scaling factor then serves as a so-called slenderness parameter measuring both the width of the shear layer as well as the magnitude of the Reynolds stresses. Thus it has to be interpreted as a second perturbation parameter besides Re . This idea was put forward first by Melnik (1989) who attacked the problem of separation caused by an imposed smooth adverse pressure gradient. His approach gives rise to a slip velocity at the base of the nonlinear region that matches with the logarithmic velocity profile in the case of attached flow but tends to zero as separation is approached. However, the log-region does never dissolve for high but finite Re . This serious handicap arises from the proposed skin friction law which states that the slenderness parameter is of $O(1/\ln^2 Re)$ and thus prevents a true two-parameter asymptotics.

Melnik's concept giving rise to a shear layer with a finite width even in the limit $Re^{-1} = 0$ in connection with the special case of equilibrium flow exhibiting overall vanishing skin friction has been pursued in Gersten & Herwig (1992) and Schlichting & Gersten (2000). Despite the correct treatment of the wall layer the analysis must be considered as incomplete as the question how the log-law transforms into the square root law if a firmly attached boundary layer is driven towards separation has not been answered satisfactory from an asymptotic point of view. Nevertheless, first hints are given on the non-uniqueness of self-similar flow which is inevitably due to the existence of a nonlinear structure even for attached flow. This topic will be examined rigorously in the present study.

Adopting the assumption of a Re -independent slenderness parameter will be shown to give rise to genuine two-parameter expansions which among others allow for a self-consistent description of the process how an initially attached flow is gradually transformed into a separated one. Furthermore, the new theory also properly accounts for the mixing length distribution in an asymptotic sense, resulting in a two-layered wake structure in the limit $Re^{-1} = 0$. As a consequence, the well-understood small-defect structure may be re-interpreted as a three-layered one. Restricting the turbulence closure in the overlap with the viscous wall layer to simple Prandtl's mixing length hypothesis, which holds in leading order and is solely based on dimensional arguments, the range of application of the analysis will even cover the possibility of a mild

separation bubble totally lying within the wall layer. In order to avoid the subtle difficulties associated with wall layer modelling the theory will be completed by some empirical data which account for the universal structure of the near-wall flow. Although experimental results regarding such flow configurations are rarely available (a more recent study has been performed by Alfing & Fernholz, 1996) the present analysis may provide some background to an asymptotically correct Reynolds stress modelling, even for future effort in the case of larger reverse-flow regimes.

2. Problem formulation — governing equations

We consider an incompressible fully turbulent boundary layer exhibiting steady two-dimensional mean motion of a fluid with uniform density $\tilde{\rho}$ and constant kinematic viscosity $\tilde{\nu}$, respectively, along a smooth impermeable solid surface.

It has been well established that a turbulent shear layer is characterized by a rather distinct edge which separates the region close to the wall where Reynolds shear stresses arising from usual Reynolds-averaging are important from the non-turbulent outer free stream flow. Apart from the weak effect of viscous forces the latter one may be regarded as strictly irrotational; see e.g. Rotta (1972), Gersten & Herwig (1992), or Schneider (1991) for a more detailed discussion. For the sake of completeness we note that the fully turbulent boundary layer mean flow regime and the outer irrotational bulk flow region are connected by means of a so-called viscous superlayer. Its lateral extent is exponentially thin compared to the thickness of the boundary layer and can be expressed in terms of well-known Kolmogoroff's length $\tilde{\ell}_K$, i.e. the scale measuring the size of the smallest eddies where dissipation takes place. The latter one appears to be essential for the understanding of the mechanism which carries the entrainment of the irrotational outer flow into the boundary layer. This topic is treated rigorously, for example, in Rotta (1972). Some more critical remarks regarding that model of the outer edge are found in Schneider (1991); cf. also the last paragraph in §6.2.1. However, from the point of view of Reynolds-averaging, this natural concept of a finite thickness, denoted by $\tilde{\delta}$ in the following, will be pursued consequently in our analysis (though a laminar-like asymptotic decay of the turbulent stresses in the transition to the outer flow field would not alter the essential results presented substantially).

Since wall curvature effects on the behaviour of the boundary layer will be neglected, the surface may be regarded to be plane. Thus, let x, y denote Cartesian coordinates in streamwise direction and perpendicular to the surface, respectively, which are non-dimensional with a global reference scale of length, \tilde{L} , characterizing the free stream flow outside the boundary layer. The streamwise velocity \tilde{U}_0 at some designated location x_0 resulting in the inviscid limit, i.e. $\tilde{\nu} = 0$, of the outer flow is chosen as the global reference velocity. The Reynolds-averaged stream function ψ and pressure p are made non-dimensional with $\tilde{L}\tilde{U}_0$ and $\tilde{\rho}\tilde{U}_0^2$, respectively, and the dimensionless velocity components are $u = \psi_y$, $v = -\psi_x$. Furthermore, we introduce the shear component τ and both normal components $\sigma_{(x)}$ and $\sigma_{(y)}$ acting in the x - and y -direction, respectively, of the Reynolds stress tensor, that is also non-dimensionalized with respect to $\tilde{\rho}\tilde{U}_0^2$. Reynolds-averaging of the Navier–Stokes equations then yields the the well-known Reynolds equations in dimensionless form

$$\psi_y\psi_{yx} - \psi_x\psi_{yy} = -p_x + \tau_y + \sigma_{(x)x} + Re^{-1}\nabla^2\psi_y; \quad (2.1a)$$

$$-\psi_y\psi_{xx} + \psi_x\psi_{xy} = -p_y + \tau_x + \sigma_{(y)y} - Re^{-1}\nabla^2\psi_x, \quad (2.1b)$$

where

$$Re = \tilde{U}_0\tilde{L}/\tilde{\nu} \gg 1 \quad (2.2)$$

defines an appropriate global Reynolds number, which is assumed to be sufficiently large.

This set of equations has to be supplemented with the usual no-slip conditions at the wall. Furthermore, since the outer flow is assumed to be strictly non-turbulent, that means fluctuating irrotationally, cf. Rotta (1972), the Reynolds shear stresses have to vanish for $y \geq \delta(x)$. Therefore,

$$\left. \begin{aligned} y = 0 : \quad \psi_x = \psi_y = \tau = \sigma_{(x)} = \sigma_{(y)} = 0; \\ y = \delta(x) : \quad \tau = 0, \quad \psi, p, \tau, \sigma_{(x)}, \sigma_{(y)} \dots \text{smooth.} \end{aligned} \right\} \quad (2.3)$$

The condition of zero wall velocity holding for the total unsteady motion causes vanishing fluctuations,

and, as a consequence, implies identically vanishing Reynolds stresses. This requirement is in accordance with the earlier considerations regarding the definition of a sharp boundary layer edge as the viscous superlayer will be neglected in the following.

As an important principal assumption which is supported by experimental observations, the scaling of the (a priori unknown) distribution along the x -axis of the boundary layer thickness,

$$\delta(x) = \tilde{\delta}(x)/\tilde{L} \ll 1, \quad (2.4)$$

permits a thin shear layer approximation. For what follows, the equations of mean motion (2.1) together with the conditions (2.3) serve as a starting point allowing for developing a theory of boundary layer separation on a rational basis. As far as possible we shall use an asymptotic approach to elucidate properties of the flow holding in the limit of high Re , independent of any specific closure model. In contrast to the asymptotic theory of laminar boundary layers which inherently implies a slenderness of $O(Re^{-1/2})$, arising from a singular perturbation problem, the assumption (2.4) will be seen to be compatible with two different asymptotic formulations of a turbulent boundary layer: First, the ‘classical’ theory, which, in the form available at present, is capable of describing attached flow. It is derived by means of the method of matched asymptotic expansions applied to the full set of Reynolds equations where Re appears as the single perturbation parameter. This procedure is supplemented with only a few assumptions concerning the nearly inviscid nature of turbulent flow, see e.g. Gersten & Herwig (1992). It gives rise to the well-known self-consistent two-tiered structure comprising an exponentially thin viscous wall layer and the outer fully turbulent main layer. The latter exhibits a small relative velocity defect $(U_e - u)/U_e$ where $u = U_e(x)$ denotes the non-dimensional imposed streamwise velocity at the outer edge, $y = \delta(x)$, in the limit $Re^{-1} \rightarrow 0$, i.e. the free stream velocity at the wall due to the outer potential flow. Thus in the outer part convective terms are linearized about U_e .

Second, an extension of that classical attached-flow concept which allows to account also for separation will inevitably lead to the introduction of the small slenderness parameter mentioned in §1 which is essentially independent of Re . As the behaviour on the verge of separation is strongly associated with the appearance of nonlinear inertia terms and a velocity defect of $O(1)$ that second perturbation parameter besides Re will restrain the unbounded increase of δ in order to justify a shear layer approximation. That new approach leading to a nonlinear theory will be elaborated in §5.

3. Limitations of classical small-defect approach

Before outlining the substantial shortcomings of the classical small-defect formulation with regard to separation it is necessary to briefly summarize its essential features. To this end we follow the extensive pioneering papers of Yajnik (1970), Bush & Fendell (1972), Fendell (1972) and Mellor (1972), but adopt the notation of the more recent contributions by Gersten & Herwig (1992), Walker (1998) and Gersten in Schlichting & Gersten (2000).

3.1. Small-defect formulation

Apart from the assumption of a small-velocity defect holding in the outer main part of the boundary layer classical theory is essentially based on the so-called related skin friction velocity which provides the principal perturbation parameter. It is defined by

$$\gamma(x) = \frac{u_\tau(x)}{U_e(x)} = O(1/\ln Re), \quad \text{with} \quad u_\tau(x) = \text{sgn}(\tau_w) |\tau_w(x)|^{1/2}, \quad (3.1)$$

where τ_w denotes the (at first strictly positive) wall shear stress. The logarithmic dependency on Re will arise from the subsequent analysis.

In order to account for the small-velocity deficit of $O(\gamma)$ in the outer fully turbulent main part of the boundary layer the appropriate defect transformation

$$\left. \begin{aligned} \eta &= y/\delta(x), & \delta(x) &= \gamma \Delta(x); & \psi(x, y) &= \delta U_e (\eta - \gamma F(x, \eta)), \\ \tau(x, y) &= \gamma^2 U_e^2 T(x, \eta), & \sigma_{(x), (y)}(x, y) &= \gamma^2 U_e^2 S_{(x), (y)}(x, \eta), \\ p(x, y) &= p_0(x) + \gamma U_e^2 P(x, \eta), & \text{with} & \quad p_{0x} = -U_e U_{ex}, \end{aligned} \right\} \quad (3.2)$$

is applied. It introduces a rescaled stream function F , Reynolds stresses T and $S_{(x), (y)}$ and a boundary layer coordinate η , respectively, where the latter is of $O(1)$ in the main region of the boundary layer. Therefore, the magnitude of the boundary layer thickness $\delta(x)$, which is part of the solution, is assumed to be of $O(\gamma)$. For the sake of clarity the dependency of the dependent field quantities on Re given by (2.2) and thus on γ , in particular, has not been indicated in (3.2). The function $\gamma(x; Re)$ is unknown, and its prediction is one main goal of the theory.

According to the assumption of a small-velocity defect the pressure gradient p_x deviates only slightly from $-U_e U_{ex}$ due to Bernoulli's law, evaluated along the wall streamline of the outer potential flow field. In general, it is assumed to be positive and of $O(1)$ throughout this work; for an exception see § 3.2 where the effect of an imposed strong pressure rise acting along a short streamwise scale will be studied.

Reynolds normal stresses are assumed to be of same magnitude as the Reynolds shear component which is strongly supported by the well-known Kolmogoroff's hypothesis of locally isotropic turbulence. The latter is widely accepted in statistical theories of turbulence, even in the case of globally highly non-isotropic flow situations, e.g. shear layers (for further details see e.g. Rotta 1972). We will return to this point later at levels of the asymptotic analysis when higher-order effects due to normal stresses will have to be estimated.

Inserting (3.2) into the momentum balance in streamwise direction, (2.1a), yields for the fully turbulent main part of the boundary layer

$$\begin{aligned} & \frac{(\delta U_e)_x}{\gamma U_e} \eta F'' - \delta \frac{(\gamma U_e^2)_x}{\gamma^2 U_e^2} F' + \delta \frac{(\gamma U_e)_x}{\gamma U_e} F'^2 - \frac{(\delta \gamma U_e)_x}{\gamma U_e} F F'' - T' \\ & - \left(\frac{\delta}{\gamma} - \delta F' \right) F'_x - \delta F_x F'' = \frac{1}{\gamma^2 U_e^2} (\delta \partial_x - \delta_x \eta \partial_\eta) [\gamma^2 U_e^2 (-P + S_{(x)})], \end{aligned} \quad (3.3)$$

where primes denote derivatives with respect to η . Since turbulent momentum transport dominates over

its counterpart due to molecular viscosity over most of the boundary layer with the exception of a very thin near-wall region, the divergence of the viscous stress tensor giving rise to an asymptotically small term of $O(1/(Re \delta u_\tau))$ in (3.3) has been discarded. Therefore, a viscous sublayer has to be introduced where Reynolds stresses become of equal magnitude as their viscous counterparts, $Re^{-1}u_y$.

3.1.1. Viscous wall layer

In that region the sum of both the molecular and Reynolds shear stresses, i.e. the total stress, equals the (positive) wall shear stress u_τ^2 in leading order as $Re^{-1} \rightarrow 0$ since convective terms are asymptotically small throughout the wall layer. Supported by dimensional considerations, see e.g. Gersten & Herwig (1992), u_τ defined in (3.1) is assumed to provide the only velocity scale near the wall. Balancing Reynolds and viscous shear stresses shows that the thickness of that wall layer is of $O(1/(Re u_\tau))$ and gives rise to the familiar scalings

$$y = \delta^+ y^+, \quad \delta^+ = 1/(Re |u_\tau|); \quad u = u_\tau u^+, \quad \tau = u_\tau^2 \tau^+. \quad (3.4)$$

Furthermore, in the case of boundary layers subjected to a pronounced pressure gradient it is convenient to introduce the so-called pressure parameter or frequently termed Bradshaw parameter K (cf. Gersten & Herwig 1992) defined by

$$K = \frac{-U_e U_{ex}}{Re u_\tau^3} = O\left(\frac{\ln^3 Re}{Re}\right). \quad (3.5)$$

Its magnitude results from (3.1). Note that in the interesting case of an adverse pressure gradient K is negative for separated flows we will deal with later. In the high- Re limit the x -momentum balance integrated with respect to the wall layer coordinate y^+ is then written as

$$\tau^+ + u_{y^+}^+ = 1 + K y^+ + \frac{1}{Re u_\tau} \frac{U_{ex}}{U_e} \int_0^{y^+} u_0^{+2}(z) dz + \dots, \quad (3.6a)$$

immediately suggesting the appropriate expansion for the streamwise velocity u^+ ,

$$u^+ = u_0^+ + K u_1^+ + \frac{1}{Re u_\tau} \frac{U_{ex}}{U_e} u_2^+ + \dots. \quad (3.6b)$$

Therefore, K measures the magnitude of the linearly varying contribution to the shear stress due to the imposed local pressure gradient, $-U_e U_{ex}$, relative to the skin friction. As already indicated in the expression for the convective part in (3.6a), we stress that u^+ and thus τ^+ are assumed to depend only weakly on x , such that higher-order terms not considered in the expansion for τ^+ include, among others, also the gradient of the Reynolds normal stress, $S_{(x)}$. The apparent neglect of terms proportional to γ_x in (3.6a) will be justified by the relation (3.16) below.

Assuming fully developed profiles of velocity u^+ and shear stress τ^+ , common dimensional reasoning suggests (cf. Gersten & Herwig, 1992; Vieth, 1996), at least as the leading orders are concerned where Re and x do not explicitly influence the expansions (3.6a) and (3.6b), that K is the only dimensionless group determining the properties of the flow near the wall apart from y^+ . But as K is asymptotically small the leading order terms depend solely on y^+ . Thus the profiles $u_0^+(y^+)$ and $\tau_0^+(y^+)$ are commonly termed universal ones as specific conditions imposed by the flow in the fully turbulent outer part have no significant influence. Therefore, the (as $Re^{-1} \rightarrow 0$, asymptotically weak) dependency of u^+ and τ^+ on x , respectively, enters the flow description at most parametrically via K , whereas the scaling velocity u_τ is affected by the outer-flow conditions expressed through these quantities.

The dependency of γ on Re as stated in (3.1) as well as on the imposed outer-flow velocity distribution

U_e and thus the magnitude of K given in (3.5) arises from matching that universal wall layer solution to the fully turbulent flow regime as $y^+ \rightarrow \infty$, i.e. $\eta \rightarrow 0$. In view of the general nonlinear theory to be developed in §5 it proves advantageously to perform the matching procedure formally on basis of well-known Prandtl's mixing length concept (Prandtl, 1925)

$$\tau = \ell^2 u_y |u_y|, \quad \text{or} \quad T = -l^2 F'' |F''| \quad \text{with} \quad l = \ell/\delta, \quad (3.7)$$

where $\ell = O(\delta)$ denotes a macro-length scale made non-dimensional with the global length scale \tilde{L} . Then the related counterpart l is a quantity of $O(1)$ in the outer fully turbulent region. As the overlap region between both layers is characterized by vanishing viscous effects, exploitation of dimensional arguments there yields

$$\ell \sim \kappa_0 y = \kappa_0 \delta \eta \quad \text{as} \quad y, \eta \rightarrow 0 \quad \text{and} \quad Re^{-1} \rightarrow 0, \quad (3.8)$$

where κ_0 denotes the well-known v. Kármán's constant; see e.g. Gersten & Herwig (1992) for a more detailed discussion. This universal relation (3.8) has originally been deduced by Prandtl (1925) on basis of the few assumptions concerning the flow in the viscous wall layer outlined so far and thus is commonly termed Prandtl's mixing length distribution. Integration in turn yields the famous logarithmic law of the wall,

$$u_0^+ \sim \frac{1}{\kappa_0} \ln y^+ + C^+, \quad y^+ \rightarrow \infty, \quad \text{with} \quad \kappa_0 \approx 0.41, \quad C^+ \approx 4.9. \quad (3.9)$$

The numerical values are obtained empirically and refer to the case of a perfectly smooth wall. Combination of the matching conditions (3.8), (3.9) with (3.6a) now allows to determine the asymptotic behaviour of the wall quantities u^+ and τ^+ for $Re^{-1} \rightarrow 0$ and $y^+ \rightarrow \infty$:

$$u^+ \sim \frac{1}{\kappa_0} \ln y^+ + C^+ + \frac{K y^+}{2 \kappa_0} + \dots, \quad \tau^+ \sim 1 - \frac{1}{\kappa_0 y^+} + K y^+ + \frac{U_{ex}/U_e}{Re u_\tau} \left(\frac{y^+}{\kappa_0^2} \ln^2 y^+ + \dots \right).$$

Higher-order terms denoted by dots may be affected by the choice of a specific wall closure. According to the scalings adopted in (3.2), the Reynolds shear in the outer main layer is required to match to the finite wall shear in leading order.

We note that the derivation of (3.9) on basis of the near-wall hypothesis (3.8) for the mixing length ℓ presented here, closely following Gersten & Herwig (1992) and the original one by Prandtl (1925), is in accordance with Millikan's argument (Millikan, 1938) adopted by other authors, cf. Narashima (1996), for instance, referring it to as the method of 'matching of gradients'. That approach was also employed in the pioneering work using asymptotic methods by Mellor (1972) where the log-region immediately follows from matching the wall layer to the outer defect hypothesis given by (3.1) and (3.2) due to the so-called 'generation gap' $U_e - u_\tau u^+ = O(1)$. In contrast, Walker (1998) regards the log-law in the universal overlap region as an experimentally justified starting point for further asymptotic analysis.

For the sake of completeness, we close the discussion of the viscous wall layer by focussing on the model-independent properties of the flow in the immediate vicinity of the wall: From the continuity equation that is satisfied by the velocity fluctuations themselves and the no-slip condition together with (3.6a) the relationships

$$\tau^+ \sim A^+(K) y^{+3}, \quad u^+ \sim y^+ + K/2 y^{+2} - A^+(K)/4 y^{+4}, \quad \text{as} \quad y^+ \rightarrow 0, \quad K \rightarrow 0, \quad (3.10)$$

can be derived where A^+ is to be expressed by a correlation of second and first, respectively, spatial derivatives of the velocity fluctuations. As K is small, cf. (3.5), A^+ is commonly approximated by a constant $A_0^+ = A^+(0)$, whose value of about 6.1×10^{-4} is known from measurements; see e.g. Gersten & Herwig (1992), p. 376. We will return to that topic in §6.2.1 where the effect of finite K , which even tends to infinity as separation is approached, on the flow within the viscous sublayer is studied.

With regard to the results for separated flows discussed later, cf. §5.3, we stress that the asymptotic structure of the wall layer pointed out above for positive u_τ is apparently independent of the sign of u_τ .

3.1.2. Outer defect layer

In the outer main part of the boundary layer, the nonlinearly coupled inertia terms of the Reynolds equations (2.1) suggest expansions of the form

$$Q = Q_0 + \gamma Q_1 + \gamma^2 Q_2 + \dots, \quad \text{with } Q = \Delta, F, T, S_{(x),(y)}, P. \quad (3.11)$$

Inserting (3.11) into the set of Reynolds equations (2.1) yields the leading-order problem for the unknowns F_0, T_0, Δ_0 ,

$$\frac{(\Delta_0 U_e)_x}{U_e} \eta F_0'' - 2 \Delta_0 \frac{U_{ex}}{U_e} F_0' - \Delta_0 F_0' = T_0', \quad (3.12a)$$

subjected to the boundary conditions

$$\eta \rightarrow 0: F_0 \rightarrow 0, T_0 \rightarrow 1; \quad \eta = 1: F_0' = T_0 = 0. \quad (3.12b)$$

As the flow exhibits a velocity defect of $O(\gamma)$ the convection terms in (3.12a) are linearized about $u = U_e(x)$. Kolmogoroff's hypothesis mentioned before implies that the leading-order terms of $S_{(x),(y)}$ vanish smoothly in addition to T_0 for $\eta = 1$ and also outside the boundary layer, so that Bernoulli's law is satisfied automatically up to $O(\gamma^2)$ at the outer edge of the boundary layer. Thus in the expression (3.11) for the pressure P defined in (3.2) we set $P_0 \equiv 0$ and the expansions for the free stream velocity and the pressure gradient at the distinct outer edge $y = \delta(x)$ read

$$u = U_e \left(1 - \gamma^2 U_e^{(1)}(x) + \dots \right), \quad p_x = p_{0x} + \frac{d}{dx} \left(\gamma^2 U_e^2 U_e^{(1)} \right) + \dots = \\ -U_e U_{ex} + (\partial_x - \Delta_{0x}/\Delta_0 \partial_\eta)|_{\eta=1} \left(\gamma^2 U_e^2 P_1(x, \eta) + \dots \right). \quad (3.13)$$

Therefore, the induced disturbances denoted by superscript (1) in the outer potential flow are of $O(\gamma^2)$ and still irrotational in leading order. The quantity $U_e^{(1)}$ is the velocity at $y = 0$, resulting from a solution of a linearized Euler problem in the free stream flow region. It represents a higher-order effect as it is induced by the displacement effect resulting from the normal velocity component due to $F_0(x, 1)$ and may be computed e.g. by means of thin-airfoil theory. The value of the corresponding induced pressure at $\eta = 1$, see (3.13), provides the boundary condition for the pressure response inside the boundary layer characterized by a gradient perpendicular to the wall which follows from an expansion of (2.1b) according to (3.11). We will return to these considerations in §4.1.

The representation (3.7) for τ provides the natural physical concept which an asymptotically correct shear stress closure shall be based on, mainly due to the simple transition to Prandtl's universal near-wall law (3.8). Furthermore, it has τ , thus u_y and even τ_y , respectively, vanishing smoothly at $y = \delta(x)$ where ℓ is in general assumed to be finite and smooth. The validity of the latter properties are strongly supported by the considerations regarding the distinct outer edge as elucidated in §2, also cf. (2.3) together with an inspection of (2.1a) at the boundary layer edge. Making use of the defect notation, we conclude that F' and T vanish quadratically up to all orders as $\eta \rightarrow 1$.

Evaluation of (3.8) for $\eta \rightarrow 0$ by taking into account (3.9) yields

$$T_0 = 1 + \frac{2}{\kappa_0} \frac{\Delta_0 U_{ex}}{U_e} \eta \ln \eta + O(\eta), \quad F_0' = -\frac{1}{\kappa_0} \ln \eta - C_0(x) - \frac{\Delta_0 U_{ex}}{\kappa_0^2 U_e} \eta \ln \eta + O(\eta) \quad (3.14)$$

where the $O(1)$ -quantity $C_0(x)$ is obtained from the leading-order problem for the outer defect. Higher orders are expected to behave regularly, i.e. $F_1' \sim -C_1(x)$ etc. also cf. Walker (1998); the functions $C_i(x)$, $i = 0, 1, 2, \dots$, strongly depend on the outer-layer closure chosen for modelling T_i .

In addition, one finds that $T_i \rightarrow 0$ as $\eta \rightarrow 0$ for $i = 1, 2, \dots$ as contributions to the defect layer expansions (3.11) due to deviations in τ^+ from $\tau_0^+ \equiv 1$ are only exponentially small in terms of Re , cf. (3.5 and (3.6a), (3.6b).

Finally, and as has been mentioned earlier, due to the logarithmic profile in the overlap region matching of the velocity with the viscous wall layer reveals self-consistency of the a priori proposed small-defect structure, according to the assumptions expressed by (3.1)–(3.2) and yields the well-known skin friction law which determines the distribution of the related wall shear velocity γ , defined by (3.1), in the limit of high Re :

$$\gamma^{-1} = \kappa_0^{-1} \ln(Re \delta u_\tau) + C^+ - C_0 - \gamma C_1 + O(\gamma^2). \quad (3.15)$$

Differentiation with respect to x gives

$$\frac{d\gamma}{dx} = \frac{\gamma^2}{\kappa_0} \left[-\frac{d \ln(\Delta_0 U_e)}{dx} + \kappa_0 \frac{dC_0}{dx} \right] + O(\gamma^3), \quad (3.16)$$

which implies $\gamma_x = O(\gamma^2)$, justifying a posteriori the neglect of terms proportional to γ_x in the derivation of the leading-order equation (3.12a).

By integration of (3.12a) across the boundary layer, i.e. from $\eta = 0$ to $\eta = 1$, one obtains an important local relationship between the leading-order terms of the stream function at the outer edge and the rescaled thickness Δ ,

$$(\Delta_0 F_{e0} U_e^3)_x = U_e^3 \quad (3.17a)$$

where F_e denotes $F(x, 1)$ and F_{e0} represents the leading-order contribution of its expansion according to (3.11). Subsequent integration with respect to x starting at an arbitrary location x_0 gives

$$(\Delta_0 F_{e0} U_e^3)(x) = (\Delta_0 F_{e0} U_e^3)(x_0) + \int_{x_0}^x U_e^3(s) ds. \quad (3.17b)$$

3.1.3. Equilibrium flows

We close this general survey of the classical small-defect theory of turbulent boundary layers by outlining the special case of self-similar or self-preserving flow, sometimes also termed equilibrium flow in the sense of Mellor & Gibson (1966) and Townsend (1976), respectively. Following Schlichting & Gersten (2000), the well-known Rotta–Clauser parameter (cf. Clauser, 1956)

$$\beta = -\frac{\delta^* U_e U_{ex}}{\tau_w} = -\frac{\Delta F_e U_{ex}}{U_e}, \quad \text{with} \quad \delta^* = \delta\gamma \int_0^1 F' d\eta, \quad (3.18)$$

is introduced which is assumed to be of $O(1)$ in general. Here δ^* denotes the turbulent displacement thickness. Expanding β as suggested by (3.11) then shows that similarity solutions, i.e. solutions having $F_{0x} \equiv 0$ or equivalently $F_0 = F_0(\eta)$ and thus $T_0 = T_0(\eta)$, are characterized by a constant value of β_0 . All commonly used shear stress models allow for such profiles.

By means of (3.17a), the momentum balance (3.12a) reduces to an ordinary differential equation which requires the boundary layer thickness to vary linearly with x in leading order:

$$(1 + 2\beta_0) \eta F_0'' + 2\beta_0 F_0' = F_{e0} T_0', \quad \Delta_0 F_{e0} = (1 + 3\beta_0)(x - x_o). \quad (3.19)$$

Here x_o denotes the (arbitrary) so-called virtual origin. The second relation in (3.19) replaces (3.17b) in the case of equilibrium flow. As we restrict ourselves to non-accelerating flows, a further necessary condition for the existence of self-similarity is provided by a power law for the imposed outer-edge velocity

$U_e(x)$,

$$U_e \propto (x - x_o)^m, \quad m = -\beta_0 / (1 + 3\beta_0); \quad 0 \geq m > -1/3 \quad \text{or} \quad 0 \leq \beta_0 < \infty. \quad (3.20)$$

As pointed out by Mellor & Gibson (1966), Schlichting & Gersten (2000), $F_0 = O(\beta^{1/2})$, $T_0 = O(\beta)$ and $\Delta_0 = O(\beta^{1/2})$, respectively, in the limit $\beta_0 \rightarrow \infty$ which in turn implies a breakdown of the small-defect approach. We will return to this important point in § 4.3.

3.2. Impossibility of predicting separation

One extension of the classical theory which is of relevance here has been performed by Sykes (1980): He investigated an initially firmly attached boundary layer exposed to a short and gentle surface hump such that the asymptotically small increase of the pressure is accompanied by a large gradient of $O(\gamma^{-1/2})$, giving rise to a so-called blending layer, located between the outer defect and the wall layer. Here *gamma* pertains to the oncoming undisturbed boundary layer under zero pressure gradient. With respect to (3.16), the wall shear stress is then perturbed according to $\tau^+ \sim 1 + O(\gamma^{1/2})$. Therefore, the results seem to indicate that a step-like pressure rise of at least $O(1)$ is necessary for evoking separation, even in the limit $Re^{-1} \rightarrow 0$. The analysis of the associated change in the asymptotic structure of an oncoming incompressible ‘classical’ defect boundary layer due such a more severe form of rapid distortion has not been addressed rigorously. Moreover, numerical solutions of (3.12) obtained so far by means of a simple algebraic model do not indicate any structural change of the flow but render the conclusion that a large pressure step will cause separation at least questionable; some details will be presented in the next section.

A further hint on the impossibility of provoking separation within the framework of the small-defect structure is provided by numerical calculations carried out by Neish & Smith (1992) who considered turbulent separation on a bluff body: Their analysis gives strong evidence that the defect-based formulation of the attached oncoming flow shifts the regime where separation takes place towards the rear stagnation point as Re tends to infinity.

Both findings cited are in agreement with an early argument put forward by Prandtl (Prandtl, 1904) in an attempt to explain the mechanism which causes the separation of any boundary layer (laminar or turbulent) due to a rapid distortion: In the case of a turbulent one the passive wall layer, which is exponentially thin as compared to δ , vanishes in the limit $Re^{-1} \rightarrow 0$ and the flow in the outer part is inertia-driven and thus approximately governed by Bernoulli’s law; therefore, reverse flow which always associates separation is only to be evoked by a pressure rise of $O(1)$. This strikingly contrasts the laminar case where the velocity defect is always of $O(1)$ and separation may take place in a viscous sublayer, even in the limit $Re^{-1} \rightarrow 0$. That difference concerning the profiles is depicted in figure 1.

3.2.1. Numerical aspects

The considerations outlined so far are strongly supported by numerical studies carried out in the present investigation: The calculations start with the flat-plate solution ($U_e = U_{e0}$, $m = 0$), then U_e decreases over some distance downstream, i.e. $U_{e,x} \leq 0$, giving rise to a peak in the adverse pressure gradient, to take finally again a similarity form with a negative $m = m_\infty > -1/3$, in agreement with (3.20). Due to the deceleration of the boundary layer flow the solutions of F_0' , T_0 and Δ_0 , respectively, are not in equilibrium, even if the imposed outer-edge velocity U_e obeys the power law already, but are found to exhibit a pronounced relaxing behaviour before attaining their final similarity form.

The case $m_\infty = 0$ in which the distance over which the imposed non-equilibrium pressure rise acts becomes very small is of special interest: Then the distribution of U_e includes a distinct step with a height of $O(1)$. Calculations for that extreme case of a short-scale pressure rise have been carried out by the author, using a Keller–Box scheme. Following the study in Schlichting & Gersten (2000), dealing

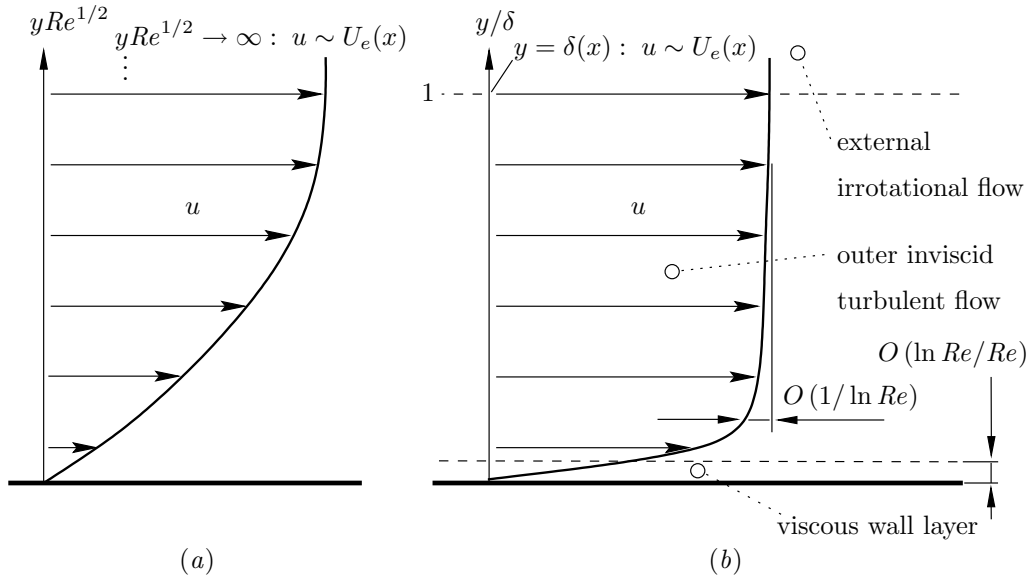


FIGURE 1. (a) Laminar vs. the (b) turbulent boundary layer structure for attached flow.

with general non-equilibrium solutions of (3.12), the well-known algebraic Michel's mixing length closure (Michel, Quémard & Durant 1969), which satisfies the asymptotic near-wall condition given by (3.8), was used but in a slightly modified form so that it includes the well-known Klebanoff's intermittency factor $I(\eta)$, in order to achieve an improved treatment of the flow near the outer edge:

$$\ell = c_\ell I(\eta)^{1/2} \delta(x) \tanh \frac{\kappa_0 y}{c_\ell \delta(x)}; \quad I(\eta) = (1 + 5.5 \eta^6)^{-1}, \quad c_\ell = 0.085. \quad (3.21)$$

Specifically, the velocity distribution at the boundary layer edge is assumed to be of the form

$$U_e(x; \epsilon) = \begin{cases} 1.0 & \dots x < 1.0, \\ 1.0 - 0.5 \tanh((x - 1.0)^2/\epsilon), & \epsilon \ll 1 \dots x \geq 1.0. \end{cases} \quad (3.22)$$

which tends to a step function in the limit $\epsilon \rightarrow 0$.

Even if the imposed velocity drop is fairly close to a sharp step the solutions seem to remain bounded and tend to a limit solution. However, downstream of the pressure increase relaxation towards the flat-plate solution becomes more and more pronounced, see figure 2.

Calculations were performed within the range $10^{-1} \geq \epsilon \geq 10^{-3}$. With ϵ decreasing the differences in the solutions decrease also and the result for the minimum value 10^{-3} is expected to be extremely close to the limiting solution $\epsilon = 0$. That limiting behaviour observed numerically is strongly supported by analytical considerations based on the integral balance (3.17b) together with (3.12a), which implies that the scaled defect represented by F_e as well as the scaled thickness Δ maintain their $O(1)$ -magnitude downstream of the location of the onset of the pressure rise $x_0 = 1.0$, even for $\epsilon \rightarrow 0$, at least as long as $x - x_0$ may be regarded to be of $O(1)$.

Thus separation will not be provoked at all as the small-defect flow solutions will remain bounded, even if a discontinuous pressure rise is imposed on the boundary layer ($\epsilon = 0$), giving rise to discontinuous responses of the global flow parameters depicted in figure 2. Therefore, the small-defect approach remains valid, and, as a consequence of the skin friction law (3.15) holding in the high- Re limit, the distribution of the skin friction velocity u_τ strictly follows the imposed outer-flow velocity $U_e(x)$.

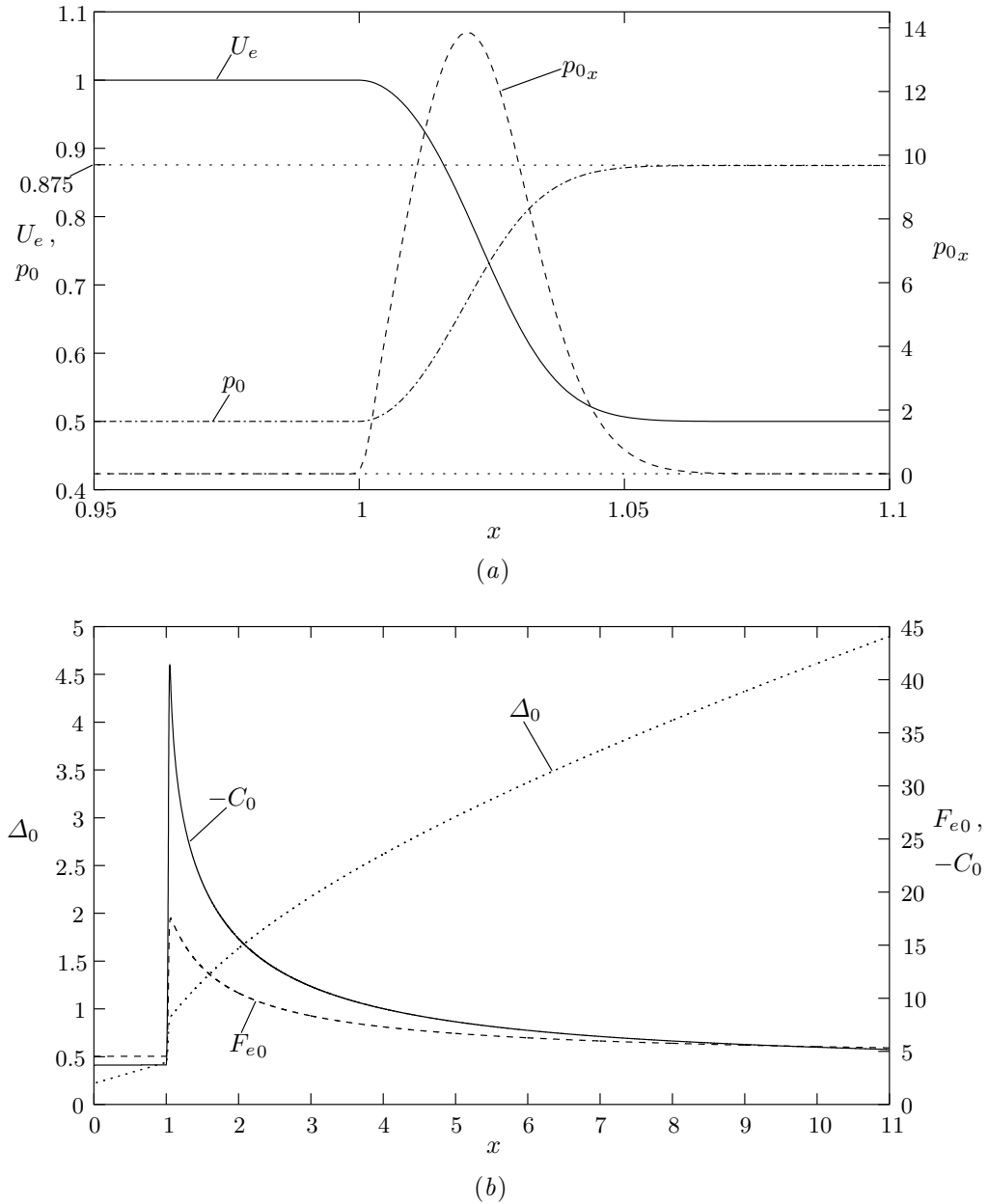


FIGURE 2. Distributions of the key quantities of the solution to the linearized defect problem (3.12) with U_e given by (3.22) in the case $\epsilon = 10^{-3}$: (a) $U_e(x)$ changes rapidly from $U_e \equiv 1$ to $U_e \equiv 0.5$ starting at $x = 1.0$ (abscissa zoomed), $p_0(x) = 1 - U_e^2(x)/2$, $p_{0x} = -U_e U_{ex}$; (b) step function response: bounded jumps in $\Delta_0(x)$, $F_{e0}(x)$, $-C_0x$.

However, our final aim here is to examine *marginal* separation, i.e. to investigate flows where the boundary layer is driven towards the verge of separation by an adverse pressure gradient $p_x = O(1)$ which acts along a streamwise distance $x - x_0$, also of $O(1)$: To this end, the distribution of the imposed outer-edge velocity, $U_e(x)$, has to be strictly smooth. Therefore, the distortions are not triggered by instantaneous changes as it is the case in the previous investigations but by rather smooth variations.

As a consequence, one concludes that boundary layer separation is less likely to occur than before in the high- Re if the initial upstream flow is described by means of the defect structure governed by (3.12).

4. Case of quasi-equilibrium flow — bifurcating solutions as $\beta \rightarrow \infty$

As has been pointed out in § 3.2 the small-defect theory predicts a velocity defect of $O(1/\ln Re)$ in the limit $Re^{-1} \rightarrow 0$, consistent with the basic assumptions. We now consider the case of a relatively large defect, i.e. with a magnitude much larger than of $O(1/\ln Re)$.

4.1. Velocity defect flow for large β

Inspection of (3.19) leads to the conclusion that flows with a relatively large defect may occur for high values of the Rotta–Clauser parameter β defined in (3.18), at least if we are dealing with self-preserving boundary layers, cf. the comments in § 3.1.3 supplementing (3.20). According to (3.18), the following considerations will concentrate on flows with an adverse pressure gradient of $O(1)$. However, expanding the relationship for m in (3.20) for $\beta_0 \gg 1$ gives

$$m = -1/3 + 1/(9\beta_0) + O(\beta_0^{-2}), \quad (4.1)$$

representing the integral momentum balance (3.17) for self-similar flow in the case of high β_0 . Thus the – strictly positive – deviation from the limiting value $-1/3$ reflects the influence of the still positive wall shear. Expansions for high β in the case of self-preserving flows have already been carried out by e.g. Mellor & Gibson (1966) in order to investigate solutions of (3.19) from a numerical point of view. A more detailed discussion of this topic will be presented in § 4.3 but at first we will focus on the general properties of large-defect flows with arbitrary distributions of U_e , giving rise to an adverse pressure gradient.

We now ask what happens if the relative defect, $\gamma F'$, of the initial velocity profile at some $x = x_0$, e.g. a similarity profile, is asymptotically larger than γ but small enough to allow for the linearization of the convective terms. It then immediately follows from (3.12a) that $\beta_0(x) \gg 1$ for the Re -independent leading-order term in the expansion (3.11) of $\beta(x; \gamma)$. For the sake of convenience the value $\beta_0(x_0)$ characteristic for the initial profile will be abbreviated by β_0 in the following. Then equations (3.3) and (3.7) together with (3.8) suggest a possible extension of the classical small-defect flow theory to boundary layers with a ‘moderately’ large defect, distinguished by β large and a rescaled skin friction parameter denoted by $\bar{\gamma}$ which satisfies the following inequality:

$$\bar{\gamma} \equiv \gamma \beta_0^{1/2} \sim p_{0x} \delta^*/\gamma \ll 1, \quad \text{as } \beta_0 \gg 1. \quad (4.2)$$

Taking into account (3.18) with β large and the previous results, cf. § 3.1.2 and § 3.1.3, the appropriate generalization of the expansions (3.11) is found to be

$$Q = \beta_0^{1/2} [Q_0 + \gamma Q_{01} + \dots + \bar{\gamma} (Q_1 + \gamma Q_{11} + \dots) + \bar{\gamma}^2 (Q_2 + \dots) + \dots], \quad (4.3a)$$

with $Q = \Delta, F, P$.

In order to account for their change in magnitude the corresponding expressions of the Reynolds stresses have to be modified too,

$$R = \beta_0 [R_0 + \gamma R_{01} + \dots + \bar{\gamma} (R_1 + \gamma R_{11} + \dots) + \bar{\gamma}^2 (R_2 + \dots) + \dots], \quad (4.3b)$$

with $R = T, S_{(x)}, S_{(y)}$.

Evaluation of β according to (3.18) together with the scaling of the leading-order terms in (4.3a) yields at the location

$$x = x_0 : \Delta_0 F_{e0} = -U_e/U_{ex}. \quad (4.4)$$

Also $\beta \gg 1$ itself has to be expanded according to

$$\beta = \beta_0 [B_0(x) + \dots + \bar{\gamma} (B_1(x) + \dots) + \dots], \quad \text{with } B_0(x_0) = 1, \quad (4.5)$$

where the definition of β_0 has been taken into account.

It will become clear later that (3.15) remains formally valid for large β_0 if C_0 is replaced by $\beta_0^{1/2}C_0$ such that

$$\gamma_x/\gamma^2 = \beta_0^{1/2}dC_0/dx + O(\gamma); \quad (4.6)$$

cf. the last paragraph of the subsequent section. The expansions marked by double subscripts and dots, respectively, in (4.3) and (4.5) arise from the terms abbreviated by $O(\gamma)$ in the modified skin friction law (4.6); up to leading order these are still given by the first expression on the right-hand side of (3.16).

The yet unknown scaling of Δ follows from the requirement that shear stress gradient and linearized convection terms are balanced. Consequently, the leading-order quantities are still governed by (3.12a) and $P_0 \equiv 0$. However, that equation is subjected to the boundary conditions (3.12b) which have to be modified by accounting for the fact that the wall shear stress now represents a term of higher order, causing in turn the moderately large defect to behave as a linearized wake. Integrating (3.12a) from 0 to η under consideration of (3.12b) then yields

$$\frac{(\Delta_0 U_e)_x}{U_e} \eta F_0' - \frac{(\Delta_0 F_0 U_e^3)_x}{U_e^3} = T_0, \quad (4.7a)$$

subjected to the remaining purely homogeneous boundary conditions

$$\eta \rightarrow 0: T_0 \rightarrow 0; \quad \eta = 1: F_0' = T_0 = 0. \quad (4.7b)$$

By evaluation of (4.7a) at $\eta = 1$ one recovers (3.17b) in the case of vanishing wall shear where this relation reduces to

$$\Delta_0 F_{e0} U_e^3 = C > 0, \quad -C = (U_e^4/U_{ex})(x_0), \quad \text{or} \quad B_0(x) = -C (U_{ex}/U_e^4)(x), \quad (4.8)$$

taking into account the initial condition (4.4). Therefore, if U_e satisfies a power law as in (3.20) one obtains $B_0 = (x/x_0)^{-3m-1}$. Strict similarity of the leading-order solution, characterized by $B(x) \equiv 1$, is only expected in the limit $m + 1/3 \rightarrow 0_+$, as already suggested by means of (3.20).

By adopting any defect layer closure for T_0 and prescribing $U_e(x)$ as well as an initial profile F_0 at a (in principle arbitrary) selected position x_0 , downstream integration of (4.7) is expected to give rise to a non-trivial solution F_0, T_0, Δ_0 of the zeroth-order problem. This is supported by the considerations of § 4.2 where an analytical solution based on the specific choice $l = l(\eta)$ of (3.7) will be presented.

In particular, we expect the resulting velocity defect profile to exhibit a non-zero wall slip denoted by $C_0(x) = -F_0'(x, 0)$, cf. the behaviour (3.14) in the case of the classical small defect. From (4.7) one then infers that T_0 tends to zero linearly in η as $\eta \rightarrow 0$. Furthermore, application of Prandtl's mixing length hypothesis, cf. (3.8), to the overlap region of the velocity profile then shows that the departure of the velocity from its value C_0 at the wall is given by a square root law in leading order:

$$\left. \begin{aligned} F_0' &= -C_0 - 2\kappa_0^{-1}(\lambda\eta)^{1/2} + O(\eta), \quad \lambda(x) = \frac{\Delta_0 (C_0 U_e^2)_x}{U_e^2} > 0; \\ T_0 &= \lambda\eta + \frac{4}{3\kappa_0} \left[\frac{\Delta_0 \lambda_x}{2\lambda} - \frac{(\Delta_0 U_e^3)_x}{2U_e^3} \lambda^{1/2} \right] \eta^{3/2} + O(\eta^2). \end{aligned} \right\} \quad (4.9)$$

Apart from the function C_0 , this result is independent of any closure. The behaviour of F_0' at the base of the outer fully turbulent region expressed in (4.9) replaces the universal log-law of the wall (3.9), characteristic for the classical small-defect theory. This is well-known already from structures dealing with the properties of velocity profiles on the verge of separation; see e.g. Mellor & Gibson (1966), Mellor

(1966), Townsend (1976), Schofield (1981) and Gersten & Herwig (1992). We will return to that issue in §5.1.1.

From (4.7a) and (4.9) it is readily seen that $T_0 \geq 0$. Furthermore, taking into account (3.7) one concludes that $F'' \leq 0$ according to the definition of the defect, see (3.2). Thus $F' \geq 0$ and, consequently, $C_0 \leq 0$, in accordance with (4.7b).

As the skin friction does not enter the solution we now focus on the equation which governs the first-order quantities denoted by subscript 1 and exhibits inhomogeneities, in particular due to nonlinear coupling of the convection terms, cf. (3.3). To this end it is useful to rewrite (3.12a) in the form $L(F_0, \Delta_0) = T_0'$, where L indicates the bilinear differential operator due to the linearized inertia terms. Paying regard to (4.6), the equation determining F_1 , T_1 and Δ_1 , which follows from insertion of (4.3) into (3.3), then reads

$$\begin{aligned} & L(F_0, \Delta_1) + L(F_1, \Delta_0) - T_1' = \\ & \frac{dC_0}{dx} \Delta_0 (F_0' - \eta F_0'') + \frac{(\Delta_0 U_e)_x}{U_e} F_0 F_0'' - \Delta_0 \frac{U_{ex}}{U_e} F_0'^2 \\ & + \Delta_0 (F_{0x} F_0'' - F_0' F_{0x}') + \frac{1}{U_e^2} (\Delta_0 \partial_x - \Delta_{0x} \eta \partial_\eta) [U_e^2 (-P_1 + S_{(x)0})]. \end{aligned} \quad (4.10a)$$

Equation (4.10a) is subjected to the boundary conditions

$$\eta \rightarrow 0: F_1 \rightarrow 0, T_1 \rightarrow 1/\Gamma; \quad \eta = 1: F_1' = U_e^{(1)}(x), T_1 = 0, \quad (4.10b)$$

where Γ defines the coupling parameter

$$\Gamma = \gamma \beta_0^{3/2}. \quad (4.10c)$$

Inspection of the definition of (4.10c) indicates that the classical small-defect theory for $\beta = O(1)$ will be recovered from the present results by taking $\Gamma = O(\gamma)$, which tends to zero for $Re^{-1} \rightarrow 0$. In that case the inhomogeneities appearing in (4.10a) do not affect the asymptotic analysis essentially as all the interesting properties of the small-defect flow are governed by the leading-order problem (3.12). According to the expansion (4.3), which implies (3.11) if $\beta = O(1)$, the match to the overall wall shear stress in leading order then is expressed by $\beta_0 T_0 \rightarrow 1$ for $\eta \rightarrow 0$. Therefore, if $\Gamma \rightarrow 0$ the second wall condition in (4.10b) will be modified into $T_1 \rightarrow 0$ in order to recover the first-order problem following (3.12) in the case of the classical small defect.

Furthermore, inspection of (4.3) and (3.7), (3.8) and taking into account (4.10b) yields the small- η behaviour of the first-order perturbations of the shear stress and the velocity, respectively,

$$T_1 \sim 2(\kappa_0 \eta)^2 F_0'' F_1'', \quad F_1' = (\kappa_0 \Gamma)^{-1} (\lambda \eta)^{-1/2} + F_1'(x, 0) + O(\eta^{1/2}). \quad (4.11)$$

According to (3.13), the velocity defect F_1' has to be patched to the leading-order perturbation $U_1^{(1)}$ of the outer velocity field, $U_1^{(1)}$, accounting for the displacement effect caused by F_{e0} at $\eta = 1$. Expanding (2.1b) and integrating the leading-order balance between convection of the imposed free stream potential flow with respect to the distance from the wall, the pressure gradient normal to the wall as well as $S_{(y)}$ in y -direction is seen to be given by

$$P_1(x, \eta) - S_{(y)0}(x, \eta) = P_{e1}(x) + \frac{\Delta_0^2}{2} \frac{d}{dx} \left(\frac{U_{ex}}{U_e} \right) (\eta^2 - 1). \quad (4.12)$$

The value P_{e1} of P_1 at the outer edge of the boundary layer is determined by (4.10a) if evaluated for $\eta = 1$. In agreement with the classical case discussed in §3.1.2 we note that, apart from the condition

$S_{(x)_0}(x, 1) = S_{(y)_0}(x, 1) = 0$ holding for the Reynolds normal stresses, the gradients with respect to η of $T_1 = 2lF_0''F_1''$ as well as $S_{(x)_0}$ have to vanish at $\eta = 1$, too. Making use of (3.12b) and (4.10b) one then obtains the relationship

$$\begin{aligned} \frac{d}{dx} \left(U_e^2 U_e^{(1)} \right) &= \left(\partial_x - \frac{\Delta_{0x}}{\Delta_0} \partial_\eta \right) \Big|_{\eta=1} (U_e^2 P_1) \equiv \\ &= \frac{d}{dx} (U_e^2 P_{e1}) - \Delta_0 \Delta_{0x} (U_e U_{e,xx} - U_{e,x}^2), \end{aligned} \quad (4.13)$$

which is equivalent to the differential form of Bernoulli's law, linearized about $u = U_e$, that holds at $y = \delta(x)$, cf. (3.13).

With Re and β_0 given, Γ follows from the skin friction law (3.15), which is modified by rescaling C_0 according to (4.6) as pointed out above. Similar to equation (4.7) for F_0 , T_0 and Δ_0 , equation (4.10) is expected to represent a well-posed problem for determining F_1 , T_1 and Δ_1 , respectively, if a specific shear stress closure is adopted. Integrating (4.10a) from $\eta = 0$ to $\eta = 1$ establishes a relationship between Δ_1 and the perturbed stream function F_{e1} at the outer edge of the boundary layer. Therefore, this asymptotically correct higher-order contribution to the large- β form (4.8) of the leading-order integral momentum balance, (3.17a), exhibits inhomogeneities arising not only from the finite wall shear (as expressed through Γ and C_0) but also from the displacement effect exerted on the outer-edge flow, the pressure gradient perpendicular to the wall as well as nonlinearly coupled inertia terms and the sum of the Reynolds normal stresses $\sigma_{(x)} + \sigma_{(y)}$, respectively:

$$\begin{aligned} \frac{d}{dx} \left[(\Delta_1 F_{e0} + \Delta_0 F_{e1}) U_e^3 \right] &= \frac{U_e^3}{\Gamma} - 2 \Delta_0 F_{e0} U_e^3 \frac{dC_0}{dx} \\ &+ \frac{d}{dx} \left(\Delta_0 U_e^{(1)} U_e^3 \right) - \frac{\Delta_0^3 U_e}{3} \frac{d}{dx} (U_e U_{e,xx} - U_{e,x}^2) \\ + U_e \frac{d}{dx} \left[\Delta_0 U_e^2 \int_0^1 (F_0'^2 - S_0) d\eta \right], \quad &\text{with } S_0 = S_{(x)_0} + S_{(y)_0}. \end{aligned} \quad (4.14)$$

In order to eliminate P_{e1} we made use of (4.12) and (4.13), having integrated the term ηP_1 in (4.10a) by parts. As will be shown in §4.3 the integral relation (4.14) contains the whole information that allows for a theoretical explanation of the phenomenon of non-uniqueness in large-defect equilibrium flow.

4.1.1. Transition layer

The approximately linear shear stress distribution at the base of the outer defect region, see (4.9), does not match with the finite wall shear stress inside the viscous wall layer, where $T \sim 1$. In order to eliminate this mismatch and to account for the change in the logarithmically varying velocity profile in the overlap region, cf. (3.9), to the square root behaviour more away from the wall a so-called transition layer has to be introduced: In that region the total shear equals the Reynolds shear stress as viscous effects are still exponentially small. Furthermore, the linearly varying part, $T \sim \bar{\gamma}^2 \lambda \eta$, becomes of the same order as the wall shear stress γ^2 which in turn determines the thickness of the layer to be of $O(\delta/\beta_0)$.

Introducing the stretched inner coordinate

$$\bar{\eta} = \beta_0 \eta$$

and combining (3.3), (4.3) with (4.9) and (3.8) yields the appropriate inner expansions

$$F' = \beta_0^{1/2} (-C_0 + \gamma U_{01} + \dots) + \bar{U}_1 + \dots + O(\beta_0^{-1/2}), \quad T = \bar{T}_0 + \gamma T_{01} + \dots + \beta_0^{-1/2} (\bar{T}_1 + \dots) + O(\beta_0^{-1}).$$

Dots in parentheses are to be interpreted by analogy to (4.3). Note that the scalings of this layer expressed in terms of large β_0 are independent of the assumed magnitude of the coupling parameter Γ and solely

arise from the shear stress distribution. Integration of the leading-order problem given by

$$\bar{T}_0 = 1 + \lambda\bar{\eta} = -(\kappa_0 \bar{\eta})^2 |\partial_{\bar{\eta}} \bar{U}_1| \partial_{\bar{\eta}} \bar{U}_1, \quad (4.15)$$

reflecting the mixing length hypothesis (3.8), leads in turn to a generalized velocity law in the near-wall regime:

$$\bar{U}_1 = \kappa_0^{-1} \left\{ -\ln(\lambda\bar{\eta}) + 2 \ln \left[(1 + \lambda\bar{\eta})^{1/2} + 1 \right] - 2(1 + \lambda\bar{\eta})^{1/2} \right\}. \quad (4.16)$$

Note that the sign of \bar{U}_1 is chosen in view of the requirement $\partial_{\bar{\eta}} \bar{U}_1 \leq 0$, cf. the comment above. The logarithmic portion of the velocity profile near $\eta = 0$ is gradually replaced by a square root behaviour at larger distances from the wall:

$$\bar{U}_1 = \kappa_0^{-1} \begin{cases} -2(\lambda\bar{\eta})^{1/2} + (\lambda\bar{\eta})^{-1/2} - (\lambda\bar{\eta})^{-3/2} / 12 + O(\bar{\eta}^{-5/2}) & \dots \bar{\eta} \rightarrow \infty, \\ -\ln \bar{\eta} - \ln(\lambda/4) - 2 - \lambda\bar{\eta}/2 + (\Lambda\zeta)^2 / 16 + O(\bar{\eta}^3) & \dots \bar{\eta} \rightarrow 0. \end{cases} \quad (4.17)$$

It is readily verified that the large- $\bar{\eta}$ variation corresponds to the outer layer behaviour for $\eta \rightarrow 0$ given in (4.9) and (4.11), respectively. Matching of the solution (4.16) to the terms of the outer expansion (4.3) requires an arbitrary contribution of $O(1)$ caused by integration to vanish. Finally, inspection of (4.17) reveals that a match of the profile \bar{U}_1 to (3.6b) holding in the universal wall layer justifies to maintain the skin friction relation (3.15) in the large- β form, according to the above considerations leading to (4.6).

In the classical case where $\beta = O(1)$ the transition layer merges with the outer defect layer and the linear variation of Reynolds shear stress is altered into the $\eta \log \eta$ -behaviour in (3.14) as the square root portion in the velocity profile disappears.

The interesting feature of multi-valued moderate-defect solutions which is addressed in the next sections is essentially caused by the inhomogeneities arising in (4.10a) due to the nonlinear convective terms. However, as these terms do not affect the universal velocity distribution (4.16), we will solely consider the properties of the flow in the outer defect wake layer in the following.

4.2. Analytical homogeneous solution

Downstream integration of (4.7) supplemented with a closure for T_0 will in general have to be carried out numerically. However, since the problem has purely homogeneous boundary conditions, cf. (4.7b), an analytical solution for F_0 can be obtained by means of separation of variables in the case of an algebraic closure and an appropriate choice of the initial profile at $x = x_0$. All commonly used shear stress models, also eddy viscosity-based ones, allow for the ansatz

$$F_0(x, \eta) = g(x) H(\eta), \quad T_0(x, \eta) = g^2(x) R(\eta). \quad (4.18)$$

If specifically a mixing length concept is employed, then $R = (lH'')^2$.

We shall apply this strategy using a simple model with $l = l(\eta)$ and $l \sim \kappa_0 \eta$ as $\eta \rightarrow 0$; see (3.21) for instance: Insertion of (4.18) into (4.7a), taking into account (4.7b) yields after integration

$$\frac{g(x)}{g(x_0)} = \frac{(\Delta_0 U_e^3)(x_0)}{(\Delta_0 U_e^3)(x)}, \quad \frac{(\Delta_0 U_e)(x)}{(\Delta_0 U_e)(x_0)} = \left[1 + \frac{4}{H(1)} \frac{(g U_e)(x_0)}{\Delta_0(x_0)} \int_{x_0}^x \frac{ds}{U_e(s)} \right]^{1/2}. \quad (4.19)$$

The first relation in (4.19) follows immediately from the fact that F_0' is strictly positive (and monotonically decreasing) such that overshooting boundary layers are excluded. Thus $H(1)$ is positive clearly and this relation agrees with (4.8) as $F_{e0} = g(x)H(1)$. Therefore, according to our choice of defining β_0 at the beginning of § 4.1 together with the assumption that U_e and its derivative at $x = x_0$ are known, the product of the (positive) initial values $g(x_0)$, $\Delta_0(x_0)$ and $H(1)$ have to satisfy the condition (4.4). As $g(x_0)$ may be chosen arbitrarily the remaining problem determining $H(\eta)$ is normalized without any

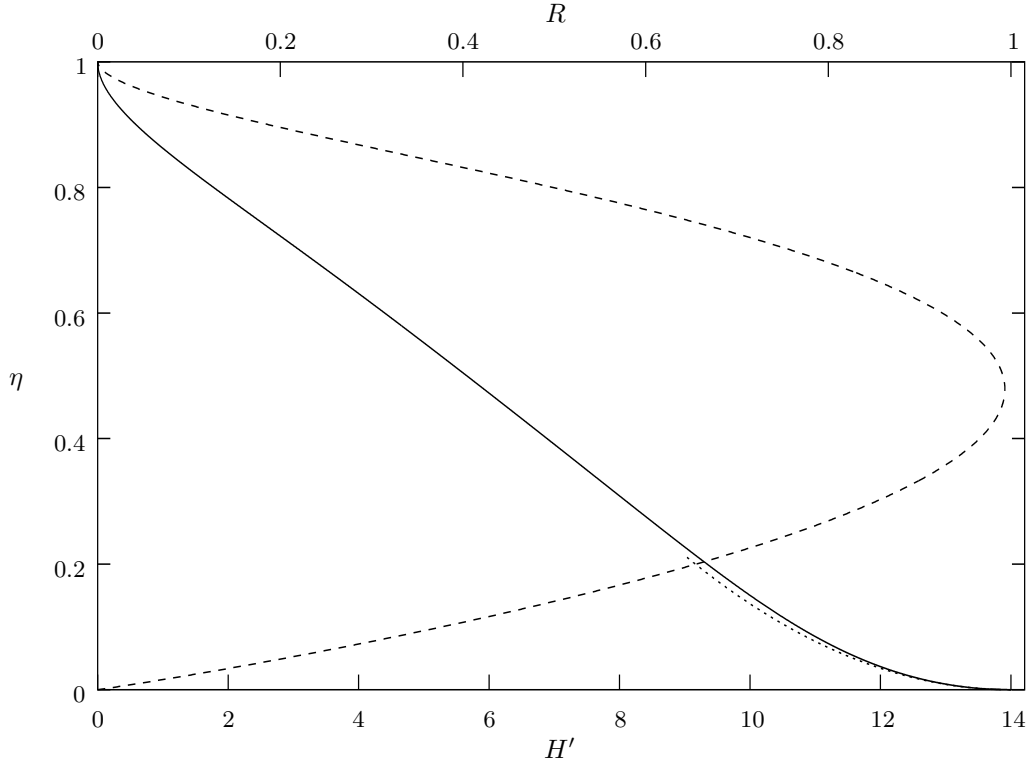


FIGURE 3. Normalized distributions of F_0' and T_0 as $\beta \rightarrow \infty$, given by H' (solid) and R (dashed), respectively. Notice the asymptote (dotted) and the linear rise in R for small η according to (4.21); due to the mixing length closure (3.7) both H' and R vanish quadratically for $\eta \rightarrow 1$.

restriction of generality in fixing the in principle also arbitrary coefficient $4/H(1)$ in the second relation in (4.19). Then H is seen to be a non-trivial solution of the thereby reduced problem (4.7),

$$2\eta H' = H(1) R; \quad H(0) = R(0) = 0, \quad H'(1) = 0 \iff R(1) = 0. \quad (4.20)$$

The construction of such a solution is outlined in Appendix A. Results based on the closure (3.21) are plotted in figure 3.

The square root behaviour of H' near the wall is clearly visible. Furthermore, a pronounced maximum in the distribution of R is observed. According to (4.9) and (4.18), the small- η behaviour of that limiting profile is given by

$$H'(\eta) = H'(0) - \frac{2}{\kappa_0} \left(\frac{H'(0)}{H(1)} 2\eta \right)^{1/2} + O(\eta) \quad \text{as } \eta \rightarrow 0; \quad \lambda = 2g(x)^2 \frac{H'(0)}{H(1)}. \quad (4.21)$$

It will turn out subsequently that these mixing length-based normalized profiles H , R as well as Δ_0 collapse to the solution of (4.7) in the case of *quasi*-equilibrium flow. Following Gersten & Herwig (1992) and Schlichting & Gersten (2000), this term is used to characterize boundary layers where U_e deviates only slightly from the self-preserving distribution $U_e \propto x^m$, cf. (3.20). The close context between the general type of large- β flow and the self-similar case may, for example, made evident by expressing the nonlinear inertia term in (4.14) according to the definition of a shape parameter that accounts for the

influence of nonlinearity:

$$G(x) \equiv \frac{\bar{\gamma}}{F_0'^2} \int_0^1 F_0'^2 d\eta = \bar{\gamma} g(x) G_0, \quad \text{with} \quad G_0 \equiv \frac{1}{H(1)} \int_0^1 H'^2 d\eta \quad (4.22)$$

denoting the equilibrium shape parameter in the sense of Schlichting & Gersten (2000). By inspection of problem (4.10) for the first-order quantities, and in particular the inhomogeneous matching condition for T_1 given in (4.10b), it is readily deduced that a separation ansatz (4.18) will generally fail. We will see that this is true even in the case of strict equilibrium of the leading order approximation, unless a certain solvability condition which predicts a minimum value $m_{min} > -1/3$, tending to the critical value $-1/3$ for $Re^{-1} \rightarrow 0$, of the exponent m in the power law obeyed by U_e , see (3.20), is met. This will give rise to double-valued class of solutions that exhibit complete similarity up to the first order.

4.3. Connecting flow regime

Inspection of (4.7a) shows that the leading-order problem (4.7) apparently implies a special case if and only if the second term on the left-hand side vanishes for any η . This in fact is satisfied identically by (4.18) and, if more general solutions are considered, if $F_{0,x} \equiv 0$, i.e. for self-preserving flows. With respect to the analytical solution (4.19), that means $g \equiv g(x_0)$. Indeed, taking into account (4.4), it follows from (4.8) and (4.18) that self-similar solutions are restricted to $F_0 \equiv H(\eta)$ or, equivalently, $g \equiv 1$ and $B_0 \equiv 1$. Then $\Delta_0 U_e^3 = const$ according to (4.8), where the imposed outer flow velocity and the leading order of the boundary layer thickness must satisfy

$$\frac{U_e(x)}{U_e(x_0)} = [*]^{-1/3}, \quad \frac{\Delta_0(x)}{\Delta_0(x_0)} = [*]; \quad [*] = 1 + \frac{3x_0}{H(1)\Delta_0(x_0)} \left(\frac{x}{x_0} - 1 \right). \quad (4.23)$$

Thus (4.7a) reduces to the normalized form (4.20), independently of any specific closure hypothesis. Also note that this equation is seen to equal the large- β limit of (3.19), integrated from $\eta = 0$. Clearly, as F_0 enters this simplified problem determining F_0' solely via $F_{e1} = H(1)$ its order has been reduced such that each of the boundary conditions at $\eta = 1$ in (4.7b) now includes the other. Furthermore, without loss of generality, in (3.19), (3.20) the virtual origin x_o may be set to zero. Taking into account (4.4), strict similarity in the sense of classical firmly attached boundary layers then is given if

$$\Delta_0(x_0)/x_0 = \Delta_{0x}(x_0) = 3/H(1) \implies [*] = x/x_0.$$

Here the symbol $[*]$ defined in (4.23) was used.

From (3.18) and the expression for the exponent m in (3.20) the case of quasi-equilibrium solutions for $\beta \rightarrow \infty$ may be obtained by adding a small positive term $\mu(x)$ to the exponent $m = -1/3$ in (4.23), implying in turn an appropriate expansion of U_e of the form:

$$U_e = U_0 \left(1 + \mu(x) \ln[*] + O(\mu^2) \right), \quad U_0 = [*]^{-1/3}; \quad \mu(x) = m + 1/3 = O(\beta_0^{-1}). \quad (4.24)$$

For reasons becoming evident below it is convenient to regard μ asymptotically as a quantity of the same magnitude as $\bar{\gamma} = O(\beta_0^{-1})$. As a consequence, cf. the definition (4.10c), the coupling parameter Γ is seen to be of $O(1)$ indeed. Moreover, considering (4.3) and (4.5), we assume a double expansion for μ ,

$$\mu = \bar{\gamma}(\mu_1(x) + \dots) + \gamma^2(\mu_2(x) + \dots) + \dots, \quad (4.25)$$

with (in principle arbitrary) functions μ_1, μ_2, \dots of $O(1)$. Then the leading-order solution is governed by (4.20), (4.23) and, with respect to (4.5), $B_0 \equiv 1$. Taking into account (4.25) with some non-zero $\mu_1(x)$ and inserting the corresponding expansions for U_e given in (4.24) into the bilinear convective part of the leading-order equation, (4.7a), a perturbation of $O(\bar{\gamma})$ of the zeroth-order solution governed by (4.20)

gives rise to an additional term in the first-order problem, (4.10). Integrating (4.10a), from $\eta = 0$ by paying regard to (4.10b), (4.8), the skin-friction law according to (4.6) and the expansions (4.24), (4.25), yields in the case of quasi-equilibrium flow

$$\begin{aligned} & \frac{(\Delta_1 U_0)_x}{U_0} \eta H' - \frac{(\Delta_1 U_0^3)_x}{U_0^3} H + \frac{2}{H(1)} \eta F_1' - \Delta_0 F_{1x} \\ & - (\eta H' + 3H) \frac{d}{dx} \Delta_0 (\mu_1 \ln[*]) - T_1 + \frac{1}{\Gamma} = \int_0^\eta (\dots) d\bar{\eta}. \end{aligned} \quad (4.26)$$

Here Δ_0 is given by (4.23). The dots denote the inhomogeneity on the right-hand side of (4.10a) where U_e has to be replaced by U_0 and η by the variable of integration $\bar{\eta}$, respectively. As the integrand is determined by the self-similar leading-order solution of (4.20), characterized by a $\Delta_0(x)$ which is linearly growing, $F_0 = H(\eta)$, $C_0 = -H'(0)$ and – as an apparent consequence arising from (3.2) – $S_0 = S_0(\eta)$ where S_0 is defined in (4.14), it now does not depend on x . Furthermore, application of thin-airfoil theory to the displacement exerted by $F_{e0} = H(1)$ due to $U_e(x) = U_0(x)$ gives rise to a constant $U_e^{(1)}$. Therefore, as self-similarity with respect to the first-order quantities means vanishing x -dependency of F_1 , T_1 , the first-order solution is characterized by an also linearly varying distribution of Δ_1 , or $\Delta_1/\Delta_0 = \text{const}$.

It is evident that for an arbitrarily prescribed $\mu_1(x)$ the problem (4.26) has to be solved numerically in general, in order to obtain a first-order correction to the leading-order problem in the case of quasi-equilibrium flow. However, evaluation of that equation at $\eta = 1$ using (4.8) reveals a simplified form of the first-order integral momentum balance (4.10a). By means of (4.8) it provides the following relationship between Δ_1 , F_{e1} and μ_1 for quasi-equilibrium flows:

$$H(1) \frac{d}{dx} \left(\frac{F_{e1}}{H(1)} + \frac{\Delta_1}{\Delta_0} + 3\mu_1 \ln[*] \right) = \left[\frac{1}{\Gamma} + \frac{8}{H(1)^3} + \frac{1}{H(1)} \int_0^1 (F_0'^2 - S_0) d\eta \right] \frac{1}{\Delta_0}.$$

Since Reynolds normal stresses are strictly negative (away from the wall), the constant inhomogeneity within the parentheses is undoubtedly positive. In addition to the effect of finite wall shear represented by Γ it includes contributions originating from the effect of displacement as well as the normal pressure gradient P_1 .

Abbreviating the bracketed term by dots and using the leading-order results (4.23), integration yields

$$3 \left(F_1/H(1) + \Delta_1/\Delta_0 \right) \Big|_{x_0}^x = \left\{ [\dots] - 9\mu_1(x) \right\} \ln[*]. \quad (4.27)$$

Taking into account (3.18), (4.5) and (4.25), a similar relation is seen to hold for $B_1(x)$. For any prescribed $\mu_1(x)$ the first-order problem will admit self-similar solutions only if the term in brackets on the left-hand side in (4.27) is a constant. Then the left-hand side vanishes, requiring in turn the coefficient of the logarithmically varying term to the right to be zero. Therefore, if the self-similar zeroth-order solution characterized by $\mu = 0$ is disturbed due to some even constant $\mu > 0$, the first order perturbation will exhibit a strict self-preserving structure only if the condition

$$9\mu_1 = \frac{1}{\Gamma} + G_0 + \Pi_0^2, \quad \text{with} \quad \Pi_0^2 = \frac{8}{F_{e0}^3} - \frac{1}{F_{e0}} \int_0^1 S_0 d\eta, \quad (4.28)$$

is met. Here we have used (4.22) and $H(1) = F_{e0}$. In fact, μ is seen to be strictly positive. A numerical estimate is obtained in Appendix A on basis of the model (3.21) as well as an appropriate asymptotically correct simple normal stress closure.

To make the analysis as simple as possible we have initiated the derivation of (4.28) at the beginning of § 4.1 by prescribing a sufficiently high value of Re , and some large β_0 which is independent of Re and measures the magnitude of the defect. Then γ and, considering (4.2), also $\bar{\gamma}$ are already determined by

means of (3.15) and (4.6), respectively. Finally the coupling parameter Γ is fixed by (4.10c). Therefore, according to (4.28) a single distinct value for μ_1 is allowed only for obtaining strict equilibrium as all other quantities are already known. However, with respect to engineering applications, e.g. diffuser flows, it appears much more preferable to prescribe μ , in order to seek the wake-like solutions describing the moderately large defect flow which will withstand a given adverse equilibrium pressure gradient that is only slightly weaker than its maximum reached in the limit $Re^{-1} = 0$, given by $m = -1/3$. As the magnitude of the defect can also be measured by the shape parameter $G = O(\bar{\gamma})$ defined in (4.22) in the case $g \equiv 1$, we eliminate Γ from (4.28) by means of the asymptotic coupling condition (4.10c). It is convenient to introduce the rescaled $O(1)$ -quantities

$$\bar{\mu} = \frac{\mu}{(\gamma/G_0)^{2/3} (1 + \Pi_0^2/G_0)^{2/3}}, \quad \bar{G} = \frac{G (1 + \Pi_0^2/G_0)^{1/3}}{(\gamma/G_0)^{2/3}}, \quad (4.29)$$

based on the normalized shape parameter G_0 , which in turn allows for eliminating β_0 according to the definition of $\bar{\gamma}$ in (4.2). It follows from (4.22), (4.29) and the coupling condition (4.10c) that $\bar{G} = \gamma^{1/3} \beta^{1/2} G_0 = O(1)$ as $Re^{-1} \rightarrow 0$ and is thus asymptotically proportional to $\beta_0^{1/2}$ for a given γ .

The condition (4.28) then assumes in leading order the canonical form

$$9\bar{G}^2\bar{\mu} - 1 - \bar{G}^3 = 0. \quad (4.30)$$

The graph of this universal relation determining the reduced shape parameter \bar{G} for a given $\bar{\mu}$ is plotted in figure 4.

According to (4.30) no equilibrium solutions are possible if $\bar{\mu} < \bar{\mu}_{min}$. However, for $\bar{\mu} > \bar{\mu}_{min}$ there exist two values of \bar{G} and thus two solutions differing in the magnitude of the velocity defect by an factor which is of $O(1)$ in general. As a result, for any prescribed values of Re (or, equivalently by taking into account (3.15), any given γ) and $m + 1/3 \rightarrow 0_+$ there exist two different values for G , leading in turn to different values for the Rotta–Clauser parameter $\beta \sim \beta_0$, with respect to (4.22) and (4.10c). In original variables the critical quantities limiting the existence of equilibrium solutions are related by

$$G_{crit} \sim \frac{6}{1 + \Pi_0^2/G_0} \mu_{min}. \quad (4.31)$$

Due to the contributions in the denominator arising from the effects of boundary layer displacement as well as Reynolds normal stresses the coefficient on the right-hand side is smaller than 6. For a numerical estimate of that coefficient by means of a simple but asymptotically correct turbulence closure scheme the reader is referred to Appendix A. It seems worth mentioning that in Schlichting & Gersten (2000) an equivalent relation

$$G_{crit} \approx 5\mu_{min} \quad (4.32)$$

is cited. The latter presumably results from empirical data but agrees surprisingly well with the asymptotically exact one, which has been derived here purely on basis of the Reynolds equations without adopting any specific closure.

In order to obtain some insight into the dynamics of flows if the condition (4.30) for strict equilibrium is perturbed due to a rather rapid distortion, we start with a similarity solution given by (4.20) at $x = x_0$ for given values of γ and μ , fixing $\bar{\mu}$ by means of (4.29) and thus a point denoted by A on the lower branch in figure 4. We now increase the imposed pressure gradient $-U_e U_{e,x}$ as compared to the equilibrium distribution such that the outer-flow velocity $U_e(x)$ exhibits a distinct step-like form beginning at some $x = x_s$ over a distance $x - x_s$ which at first is regarded to be of $O(1)$. Far downstream, however,

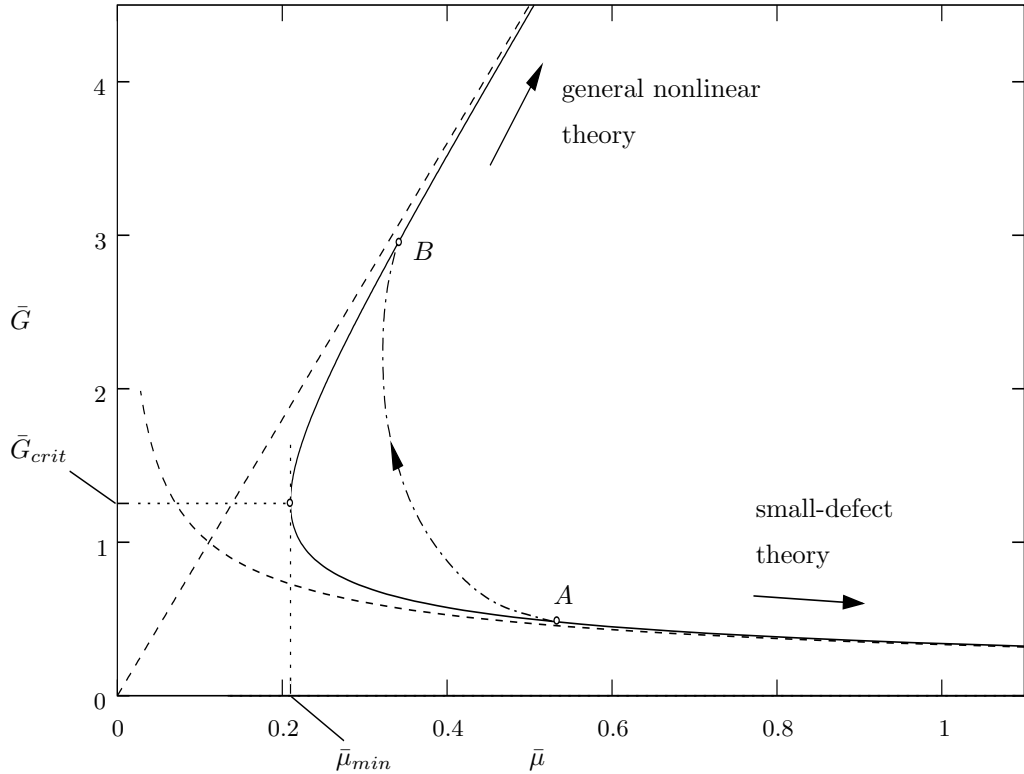


FIGURE 4. Bifurcation diagram for quasi-equilibrium flows. Asymptotes according to (4.33) are dashed; critical values determining the turning point: $\bar{\mu}_{min} = 2^{1/3}/6 \doteq 0.2100$, $\bar{G}_{crit} = 2^{1/3} \doteq 1.260$.

the boundary layer is assumed to asymptote to a new state of equilibrium which is characterized by a (different) value of $\bar{\mu}$ as indicated by the point B on the upper branch.

We examine this situation by choosing a pressure rise comparable to the one implied by (3.22). Thus we assume the distance $x - x_s$ where the condition for similarity in the distribution of $U_e(x)$ is violated to approach zero. In contrast to the case of firmly attached small-defect flow investigated numerically in §3.2.1, the relaxing behaviour of the solution of the zeroth-order problem (4.7) towards a state of self-similarity reached in the limit $x/x_0 \rightarrow \infty$ may be described analytically – at least in the case of an algebraic shear stress closure – by means of the solution (4.19). For the sake of simplicity we consider the extreme example of a sharp step decreasing U_0 by an amount U_a at $x = x_s$:

$$\frac{U_0(x)}{U_0(x_0)} = \begin{cases} (x/x_0)^{-1/3} & \dots x \leq x_s, \\ (1 - \Phi^2)(x/x_0)^{-1/3} & \dots x > x_s; \end{cases} \quad \text{with} \quad \Phi^2 = \frac{x_s}{x_0} \frac{U_a}{U_0(x_0)} < 1.$$

Therefore, $U_e(x)$ changes between two distributions each of which alone allows for strict similarity according to (4.23). As is seen from (4.8) yielding the distribution for $B_0(x)$ and the change in leading order of β expressed by (4.5), due to this abrupt drop $B_0(x)$ jumps from $B_0 \equiv 1$ for $x \leq x_s$ to the value $B_0 \equiv (1 - \Phi^2)^{-3}$ for $x > x_s$. According to (3.18), (4.19) and the definitions (4.2), (4.22) of $\bar{\gamma}$ and G , respectively, the related increase of β_0 given by (4.5) causes \bar{G} to increase and attaining a final equilibrium value far downstream, qualitatively following the sketched curve in figure 4. The latter is determined by the properly chosen distribution of $\mu_1(x)$ which has to allow for the rise of $\bar{G}(x)$ towards a new equilibrium

solution in leading order. It is obtained from the explicit solution (4.19) of the zeroth-order problem:

$$\Delta_0(x); g(x) = \begin{cases} \frac{3x}{H(1)}; 1 & \dots x \leq x_s, \\ \frac{3x}{H(1)} \frac{[1 - \Phi^2(x_s/x)^{4/3}]^{1/2}}{(1 - \Phi^2)^{3/2}}; (1 - \Phi^2)^{-3/2} [1 - \Phi^2(x_s/x)^{4/3}]^{-1/2} & \dots x > x_s. \end{cases}$$

Here $\Delta_0(x_0)$ has been eliminated with the aid of (4.4). For $x/x_s \rightarrow \infty$ it follows $g \rightarrow (1 - \Phi^2)^{-3/2}$. With the aid of the considerations outlined above and applying the scaling (4.29) to (4.22), the related increase of \bar{G} between the points of equilibrium A and B for a prescribed γ then turns out to be given by $(1 - \Phi^2)^{-3}$ for $Re \rightarrow \infty$.

The asymptotic description of double-valued turbulent boundary layers presented here appears to agree well with effects observed in many experiments, the first ones carried out by Clauser (1954). His attempt of maintaining equilibrium by holding β – defined by (3.18) if δ^* is replaced by the momentum thickness – constant failed, most probably due to instabilities, where the resulting pressure gradient became so large that $m \approx -0.29$. We will see in §5.3 that the nonlinear theory predicts a separating equilibrium profile besides the classical one with a small defect near that value for the outer-flow velocity exponent. However, the profiles rapidly assumed a second state, exhibiting a much more pronounced defect, but sometimes approached even separation. Clauser's observation of non-uniqueness has been supported by some early theoretical considerations put forward by Townsend (1961) but lacking a rational asymptotic basis. It is mentioned also by Durbin & Belcher (1992) who studied self-preserving boundary layers under the action of a strong adverse pressure gradient within the framework of a nonlinear approach. From a semi-empirical point of view the existence of a maximum pressure gradient, characterized by μ_{min} , self-similar flows are capable to withstand has already been attributed to the peculiarity of non-uniqueness by Winter & East (1982) in their study of diffuser flows. For this application of equilibrium flows it is important to recognize that μ_{min} is distinctly smaller than the value where separation occurs.

The limiting behaviour of $\bar{\mu}(\bar{G})$ in figure 4 for $\bar{G} \rightarrow 0$ and $\bar{G} \rightarrow \infty$, associated with the upper and lower branch, respectively, bifurcating at $\bar{G} = \bar{G}_{crit}$ is given by

$$\bar{\mu} \sim 1/(9\bar{G}^2), \quad \bar{\mu} \sim \bar{G}/9. \quad (4.33)$$

As one might expect from the influence of wall shear on the relation for the exponent $m(\beta_0)$ in (3.20) regarding firmly attached equilibrium boundary layers governed by (3.19), the first asymptote corresponds to vanishing significance of nonlinearity and allows for a match of condition (4.30) to the expansion of m with respect to $\beta_0 \rightarrow \infty$, see (4.1). It shows that the value of μ is limited due to finite wall shear, giving rise to the difference between the linearized leading-order momentum balances (3.17) and (4.8) for moderate and high β_0 , respectively.

Contrarily, nonlinear convection terms dominate in the other limit, such that the theory characterized by a linearized inertia due to a small velocity defect ceases to be valid as the defect measured by G becomes large, i.e. if $\bar{\gamma} = O(1)$ or, with reference to (4.10c), $\Gamma = O(\beta)$. In order to examine such flows, the next section focuses on the derivation of a nonlinear theory for a velocity defect of $O(1)$. As will be demonstrated later, cf. §5.3, this new theory contains the results presented so far if the defect becomes asymptotically small again. In fact, in the particular case of quasi-similarity solutions that limiting behaviour will allow for a match with. This possibility of a continuation of the upper branch describing the possible states of equilibrium in figure 4 even if $G = O(1)$ and the reduction to the

classical small-defect theory gives rise to the notation *connecting* flow for the multivalued solution in the case $\Gamma = O(1)$.

5. General nonlinear theory

As has already been mentioned, see § 1, any commonly used boundary layer closure model is essentially based on the existence of a dimensionless small parameter, in the following termed α , that is independent of Re . Its value determined from experiments serves as a scaling factor in the expressions concerning the Reynolds shear stress closure, which is usually based on the assumption of a thin shear layer, i.e.

$$\partial_x = O(1), \quad \partial_y = O(1/\alpha).$$

This observation strongly suggests how a generalized nonlinear boundary layer theory can be developed in a fully rational manner: Firstly, as α turns out to be $\ll 1$ for any accepted boundary layer closure it may be regarded as a measure of the magnitude of Reynolds stress, i.e. $\tau \sim \alpha$, as the velocity defect is assumed to be of $O(1)$. Secondly, in order to retain the Reynolds shear stress gradient normal to the wall in a shear layer approximation of (2.1a) that leaves the nonlinear convection terms unchanged, the boundary layer has to be slender. Therefore, $\delta \sim \alpha$ and α may also be interpreted as a slenderness parameter.

It is crucial for what follows that a theory based on these assumptions allows for a distinguished shear layer limit if α , possibly a function of Re , remains finite even in the limit $Re^{-1} = 0$. Therefore, in the following α will be considered as strictly independent of Re . Viscous effects then vanish and the resulting limiting form of the nonlinear boundary layer equations, see (5.2a), give rise to a solution that has to be obtained numerically. In § 5.2 and § 5.2.1 that limiting solution will be perturbed due to the effect of high but finite Re .

As in the previous sections, the mixing length concept, see (3.7), will be adopted for reasons pointed out in § 3.1.2. One of the simplest examples for an adequate closure based on this concept is Michel's model, see (3.21), which implies $\alpha = c_\ell^2$. Models appropriate for free shear layers commonly use numerically higher values up to $\alpha \approx 0.1$, cf. Schneider (1991), Schlichting & Gersten (2000). If in contrast a model based on the eddy viscosity ansatz (as e.g. in the case of the most widely used two-equation closure, the k - ϵ model) is employed, there exists also a slenderness parameter α ; for example, in the well-known Baldwin–Lomax model the eddy-viscosity is scaled accordingly such that $\alpha \approx 0.018$.

It has been emphasized already in § 1 that the first approach of constructing a Re -independent theory must be attributed to Melnik (1989) and is based on the Cebeci–Smith model which exhibits a constant $\alpha \approx 0.0168$.

At the end of this section we will show how this new theory can formally be reduced to the classical defect formulation for strictly attached flow discussed so far. In contrast, Melnik's theory appears to disagree with the classical small-defect approach due to an imposed coupling between α and u_τ which does not allow for linearization of the convective terms about $u = U_e(x)$.

Most important, the new theory presented here will turn out to be capable of describing separation in a self-consistent manner, see § 6. However, Melnik's approach is seen to fail as the imposed coupling of α to Re prevents a gradual transformation of the log-law of the wall into the well-known square root behaviour holding at separation, cf. (4.9). Both laws are an immediate consequence of Prandtl's mixing length formula, (3.8), allowing for finite or zero shear stress, respectively, at the base of the fully turbulent inviscid main layer.

5.1. Boundary layer approximation: $\alpha \ll 1$, $Re^{-1} = 0$

We start with the structure of the inviscid limit, i.e. $\alpha \ll 1$ fixed but $Re^{-1} = 0$. Following the preliminary considerations concerning the appropriate shear layer approximation we introduce a stretched boundary

layer variable

$$\bar{y} = y/\alpha$$

and expand each field quantity into powers of α :

$$p = p_0 + \alpha p_1 + O(\alpha^2); \quad q = \alpha q_0(x, \bar{y}) + O(\alpha^2), \quad \text{with } q = \delta, \psi, \tau, \sigma(x), \sigma(y). \quad (5.1)$$

Inserting (5.1) into the full set of Reynolds equations, (2.1), then yields the boundary layer approximation

$$\psi_{0\bar{y}}\psi_{0\bar{y}x} - \psi_{0x}\psi_{0\bar{y}\bar{y}} = -p_{0x} + \tau_{0\bar{y}}, \quad p_{0x} = -U_e U_{ex}; \quad p_{0\bar{y}} \equiv 0. \quad (5.2a)$$

As in the previous sections, $p_0 = p_0(x)$ denotes the leading-order pressure imposed by the outer irrotational flow. Equations (5.2a) are supplemented with the boundary conditions

$$\bar{y} = 0: \quad \psi_0 = \tau_0 = 0; \quad \bar{y} = \delta_0(x): \quad \psi_{0\bar{y}} = U_e(x), \quad \tau_0 = 0. \quad (5.2b)$$

The first condition at the base of the shear layer, i.e. at $\bar{y} = 0$, accounts for vanishing normal velocity component. The second condition is a direct consequence of the fact that viscous stresses do not enter the flow description in the limit $Re^{-1} = 0$ which in turn implies a zero wall shear as the Reynolds shear stress has to vanish due to zero turbulent fluctuations of the v -component at the wall. On the other hand, vanishing viscosity effects allow for the existence of non-zero streamwise velocity at the surface; Reynolds-averaging therefore gives rise to a so-called wall slip denoted by $u_s(x)$, which in general will be a quantity of $O(1)$, and in turn a leading-order contribution denoted by $\Lambda_0(x)$ to the convection terms in (5.2a) as $\bar{y} \rightarrow 0$, forcing this wake-like flow:

$$u_s = \psi_{0\bar{y}}(x, \bar{y} = 0) \leq U_e(x) \quad \Lambda_0 = u_s u_{sx} - U_e U_{ex} = O(1).$$

Inspection of (5.2a) then shows that τ_0 varies linearly with \bar{y} , $\tau_0 \sim \Lambda_0 \bar{y}$ near the wall. Due to the absence of the usual no-slip condition in the limit $Re^{-1} = 0$ this balance between inertia and shear gradient strikingly contrasts the y^3 -behaviour proposed by (3.10), which accounts for the viscous shear stress at the wall.

Of course, the ‘trivial’ solution $u \equiv U_e(x)$ describes strictly irrotational flow right down to the wall and thus, having $\tau \equiv 0$, represents a possible solution to problem (5.2). Apart from this, the asymptotic analysis, however, strongly suggests the existence of additional self-consistent non-trivial solutions; this will be supported later by means of numerical results in § 5.3 and § 6.1.1.

The conditions in (5.2b) holding at the outer edge of the boundary layer have already been discussed in the context of the classical small-defect flow, see § 3.1. Note that a finite mixing length at the boundary edge yields $\psi_{0\bar{y}} = 0$ and, considering Bernoulli’s law in (5.2a), in turn $\tau_{0\bar{y}}$ at $\bar{y} = \delta_0(x)$, providing a smooth transition to the outer flow. In the outer irrotational flow regime perturbations of $O(\alpha)$ are caused by the displacement effect due to $\delta_0(x)$, which must be considered as a part of the solution of the nonlinear leading-order problem (5.2). Together with effects due to variations in the pressure but also Reynolds stress normal components, they give rise to the higher-order approximations indicated in (5.1) and, as a consequence, further contributions to the slip velocity u_s .

5.1.1. Intermediate layer

The scalings adopted in (5.1) together with the general mixing length formulation (3.7), immediately imply $\ell = O(\alpha^{1/2}\delta)$ or, equivalently, $\ell = O(\alpha^{3/2})$ due to a velocity defect of $O(1)$ but $\tau = O(\delta)$ for nonlinear flow. Thus the Reynolds shear stress is expressed by

$$\tau_0 = \bar{\ell}^2 \psi_{0\bar{y}\bar{y}} |\psi_{0\bar{y}\bar{y}}|, \quad \text{with } \ell = \alpha^{3/2} \bar{\ell}. \quad (5.3)$$

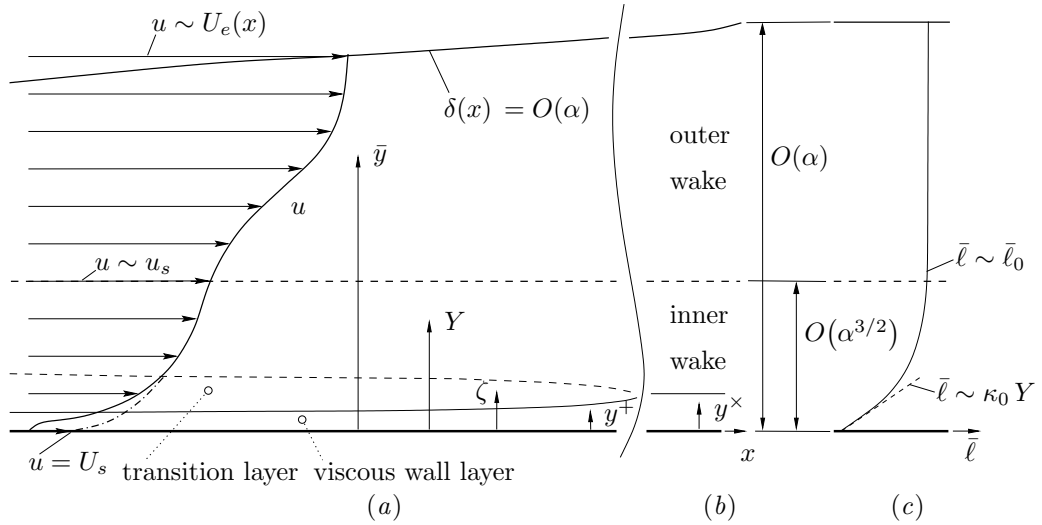


FIGURE 5. Asymptotic structure for both α and Re finite: (a) General nonlinear case – dash-dotted: square root law at the wall in the case $Re^{-1} = 0$; (b) at incipient separation where $\delta^+/\delta^x = O(1)$; (c) mixing length distribution (qualitatively), according to a simple model like (3.21).

Obviously this relation is inconsistent with the universal near-wall behaviour of ℓ given by (3.8), which must be satisfied by any asymptotically correct model – both aspects may be readily verified e.g. by Michel’s model, (3.21). This explains why any attempt of matching the viscous wall layer to a nonlinear region where the defect is assumed to be of $O(1)$ by means of (3.8) – as proposed for example by Sychev (1983) in his work on turbulent massive separation on a blunt body or used in Afzal’s two-tiered boundary layer concept, for a summary see Afzal (1996) – leads to serious and unsurmountable difficulties. As already indicated by Melnik (1989), due to that lack of consistency it becomes delicate to accept such an approach.

The impossibility to match the proposed square root law holding on the verge of separation and already well-known on basis of dimensional reasoning, see e.g. Townsend (1976), in the region between the viscous wall layer and an outer nonlinear regime led Durbin & Belcher (1992) to the formulation of an intermediate or transition layer. In accordance with the authors cited so far, their analysis is based on Re as a single perturbation parameter. This implies an algebraic Re -dependency not only of the thickness δ but in particular of the eddy viscosity which, unfortunately, is inconsistent with any commonly accepted closure.

In order to avoid these difficulties a sublayer or so-called inner wake layer is introduced here, see figure 5(a). It also serves as an intermediate region between the outer wake discussed above and the near-wall regime for Re large but finite, which will be demonstrated in § 5.2.

According to the near-wall condition (3.8), we define an inner coordinate Y and a scaled mixing length denoted by $\bar{\ell} = O(1)$, respectively:

$$y = \alpha^{3/2} Y; \quad \ell = \alpha^{3/2} \bar{\ell}, \quad \text{with} \quad \bar{\ell} \sim \kappa_0 Y \quad \text{as} \quad Y \rightarrow 0. \quad (5.4)$$

As a direct consequence from the mixing length concept (3.7), the inner layer exhibits a thickness of $O(\alpha^{3/2})$, having the same magnitude as the dimensionless mixing length. Therefore, in both layers $\ell = O(\alpha^{3/2})$, which immediately suggests the existence of a finite overlap limit denoted by $\bar{\ell}_0$. It is a

quantity of $O(1)$ and does neither dependent on \bar{y} nor on Y , such that

$$\bar{\ell} \rightarrow \bar{\ell}_0 \quad \text{as} \quad \bar{y} \rightarrow 0 \quad \text{and} \quad Y \rightarrow \infty. \quad (5.5)$$

For the sake of simplicity both the distributions of the mixing length in the outer and inner layer are denoted by $\bar{\ell}$. Due to the inherent small parameter α an asymptotic analysis of all commonly used models based on the mixing length formulation reveals the existence of a near-wall region where ℓ varies more rapidly. Thus the scaling of the two wake layers reflects the asymptotic properties of the mixing length ℓ and gives rise to the proposed behaviour (5.5) in the transition to the outer part, cf. the sketched distribution of $\bar{\ell}$ in figure 5(c). For example, the simple algebraic mixing length closure (3.21) allows for a first approximation $\bar{\ell} \propto \delta_0$ in the outer main layer. However, the strong variation due to the *tanh*-function towards Prandtl's formula (3.8) holding at the wall primarily takes place in an inner regime where $y/\delta = O(\alpha^{1/2})$.

The need for a double-layered structure which is essentially independent of Re has been recognized first by Melnik (1989), who applied an eddy viscosity closure throughout his study. In contrast, the present investigation is motivated primarily by physical considerations and thus appears to be more general: The only assumption concerning the existence of a second Re -independent perturbation parameter, α , inevitably leads to the asymptotic representation of the mixing length distribution discussed so far. The intermediate layer then accounts for its universal near-wall behaviour, Prandtl's law (3.8), that may be derived purely by means of dimensional arguments in the limit $Re^{-1} \rightarrow 0$, see e.g. Gersten & Herwig (1992), Vieth (1996) or Narashima (1996). It turns out as a matching condition between the viscous wall regime and the outer inviscid but fully turbulent flow. As it stems from the assumption of vanishing influence of viscosity on the shear gradient in the overlap region it remains valid even in the case $Re^{-1} = 0$, where the viscous wall layer disappears.

To the author's knowledge the first attempt to apply a true two-parameter expansion based on a finite slenderness parameter α in addition to Re for establishing a nonlinear boundary layer structure is found in Schlichting & Gersten (2000) where the very special case of Stratford flow, i.e. a boundary layer with identically vanishing wall shear, is investigated. But although the square root law in the overlap between the wake and the viscous wall layer is proposed, the necessity of an inner wake layer is not mentioned. We will return to that kind of flow in §5.3.

In addition, it must be noted that the concept of treating α as a perturbation parameter has been adopted before in the asymptotic theory of free turbulent shear layers which have been proposed by Schneider (1991): In his approach the introduction of an intermediate layer with a thickness of $O(\alpha^{3/2})$ is founded on the asymptotic analysis of the well-known transport equation governing the budget of the specific turbulent mean kinetic energy $k = O(\tau)$, made non-dimensional with \tilde{U}_0^2 , which allows for a shear layer approximation

$$uk_x + vk_y \sim \tau u_y - \varepsilon + D_y. \quad (5.6)$$

From this the well-established conclusion is drawn that turbulent production τu_y balances turbulent dissipation ε (non-dimensionalized with respect to \tilde{U}_0^3/\tilde{L}) in the outer main wake whereas in the inner layer also the gradient of the diffusion term D must be retained in the leading order. Moreover, the analysis shows that a further breakdown of the simple main layer approximation entails the introduction of an outermost layer where $y - \delta = O(\alpha^{3/2})$. Without going into detail, we only note that apart from turbulent diffusion also turbulent convection accounting for the transport of k enters the energy budget for this region in leading order, such that (5.6) is fully retained. Following Prandtl (1945), on grounds of common dimensional reasoning it is argued then that expressing the Reynolds shear stress τ

on either the eddy viscosity hypothesis or the mixing length model will equally lead to (3.7), at least as the leading order in the main layer is concerned. However, the mixing length formulation is preferred then, particularly in order to account for the finite width of the shear layer.

We emphasize that all these results remain valid also in the case of wall-bounded flows in the limit $Re^{-1} = 0$ considered here.

Inspection of (5.1) together with the boundary layer approximation (5.2) in the small- \bar{y} limit finally implies the appropriate form of the expansions in the intermediate region,

$$\psi = \alpha^{3/2} u_s(x) Y + \alpha^{9/4} \Psi, \quad \Psi = \int_0^Y \Psi_{\bar{Y}}(x, \bar{Y}; \alpha) d\bar{Y} = \Psi_1 + O(\alpha^{1/4}); \quad (5.7a)$$

$$\tau = \alpha^{3/2} T, \quad T = A_0 Y + \alpha^{3/4} \int_0^Y [(u_s \Psi_{1\bar{Y}})_x - u_{sx} \bar{Y} \Psi_{1\bar{Y}\bar{Y}}] d\bar{Y} + O(\alpha); \quad (5.7b)$$

$$p = p_0(x) + \alpha p_1(x, \bar{y} = 0) + O(\alpha^{3/2}). \quad (5.7c)$$

These asymptotic relationships have to satisfy the conditions of vanishing normal velocity component and Reynolds stress, respectively, at the wall. Neglected terms in (5.7) account for influences due to the normal pressure gradient, cf. the expansion (5.1), as well as Reynolds normal stresses. As in the outer layer the latter ones are considered to be of the magnitude of the shear component τ , cf. also §3.1. However, these effects are beyond the scope of a pure boundary layer approximation to which the following analysis will be restricted. Within this approximation the momentum balance in streamwise direction then reduces to the relationship (5.7b). Owing to the fact that this equation results from the pure linearization of the outer shear layer problem given by (5.2) about $u = u_s$ the intermediate layer may be considered as passive to leading order.

Adopting the mixing length concept the leading-order velocity perturbation may be written as

$$\Psi_{1Y} = U_1(x) + \int_0^Y (A_0 \bar{Y})^{1/2} \bar{\ell}^{-1} d\bar{Y}, \quad U_1(x) = \int_0^\infty (A_0 \bar{Y})^{1/2} (\bar{\ell}_0^{-1} - \bar{\ell}^{-1}) d\bar{Y}, \quad (5.8)$$

where U_1 denotes the leading order perturbation of the slip velocity $u_s(x)$ contributed by the inner layer solution. The integral defining U_1 exists only if $\bar{\ell}_0 - \bar{\ell} = o(Y^{-3/2})$ for $Y \rightarrow \infty$. Therefore, for any arbitrary distribution of $\bar{\ell}$ across the intermediate layer, U_1 is determined by the requirement that in the large Y -behaviour of Ψ_{1Y} any term of $O(1)$ shall vanish. With respect to (5.7b), matching the velocity to the results holding in the main layer then does not alter the expansion (5.1) up to $O(\alpha^2)$.

Due to the passive behaviour of the flow in the inner layer the expansions of all the quantities, and in particular of ψ and τ , are expected to match term by term with their counterparts in the outer wake expansions, (5.1), independent of the specific turbulence model chosen. The overlap behaviour (5.5) within the framework of pure boundary layer theory results from the investigation of problem (5.2) in the outer limit $\bar{y} \rightarrow 0$, or by means of examining the inner quantities for $Y \rightarrow \infty$:

$$\psi_0 \sim u_s \bar{y} + \frac{4}{15} \frac{A_0^{1/2}}{\bar{\ell}_0} \bar{y}^{5/2} + \frac{N}{90 \bar{\ell}_0 A_0^{1/2}} \bar{y}^4, \quad \tau_0 \sim A_0 \bar{y} + \frac{4C}{15} \bar{y}^{5/2}; \quad \Psi_1 \sim \frac{4}{15} \frac{A_0^{1/2}}{\bar{\ell}_0} Y^{5/2},$$

$$\text{where } N = u_s \frac{d}{dx} \left(\frac{A_0^{1/2}}{\bar{\ell}_0} \right) - \frac{u_{sx}}{2} \frac{A_0^{1/2}}{\bar{\ell}_0}. \quad (5.9)$$

It is interesting to note that the first three terms of the velocity profile are independent of any specific closure hypothesis. The \bar{y}^4 -behaviour of the third term may also be found directly by examining the leading-order behaviour of the integral in (5.7b) for $Y \rightarrow \infty$. Its response from the outer wake layer gives rise to a disturbance denoted by $\alpha^{3/4} \Psi^*(x, Y)$ in the expansion for Ψ , (5.7a). According to (3.7) we may

then rewrite these expansions in the form

$$\Psi = \Psi_1 + \dots + \alpha^{3/4} \Psi^* + \dots, \quad T = \Lambda Y + \dots + \alpha^{3/2} 2 \bar{\ell}^2 \Psi_{1YY} \Psi^*_{YY} + \dots; \quad (5.10)$$

Inserting (5.10) into the streamwise momentum balance (2.1a) gives rise to the term Ψ^* within the shear layer approximation. However, the latter term in the expansion of T of $O(\alpha^{3/2})$ already accounts for a contribution of $O(\alpha^{3/2})$ to the shear gradient τ_y which is already of the same magnitude as the Reynolds normal stress gradient σ_x in the intermediate layer.

As stated before, turbulent diffusion becomes important in the energy balance of the intermediate layer. Therefore, at least as far as the intermediate region is concerned, one may regard any model of the turbulent macro-length scale, i.e. $\bar{\ell}$, that solely depends on local properties of the flow field like the distribution in (3.21), as an undue simplification. Of course, more complex half-, one- and two-point closures account also for transport effects such as upstream history etc. However, due to the aforementioned universal quality of the mixing length concept in the main layer approximation the asymptotic analysis for $\bar{y} \rightarrow 0$, $\bar{\ell} \rightarrow \bar{\ell}_0$ will render the overlap behaviour (5.9) universal, even if ℓ exhibits a very complex dependency on the actual flow configuration. On the other hand, for the outer main region the mixing length formulation appears to be universal in an asymptotic sense as it includes a wide range of models.

By analogy to (4.9) holding for a linearized wake, we finally apply Prandtl's near-wall mixing length to the approximately linearly varying shear stress, cf. (5.7b), leading in turn to the universal square root behaviour dominating the near-wall velocity distribution of the inviscid wake:

$$\Psi_{1Y} \sim U_1 + 2 \kappa_0^{-1} (\Lambda_0 Y)^{1/2}, \quad \Lambda_0 Y \sim (\kappa_0 Y)^2 (\Psi_{1YY})^2 \quad \text{as } Y \rightarrow 0. \quad (5.11)$$

Assuming that Prandtl's hypothesis, see (5.4), remains valid within the framework of a pure shear layer approximation governed by (5.2a), a behaviour similar to that in (5.11) is found to hold also for the $O(\alpha^{3/4})$ -term in (5.7b) and the resulting velocity perturbation, Ψ^* . Therefore, Prandtl's law as quoted in (5.4) is seen to be applicable even to the corresponding term of $O(\alpha^{3/2})$ in the extended expansion of T given in (5.10).

5.1.2. Combined structure for finite α

According to (5.7), the overall slip velocity U_s as well as the corresponding convective term denoted by Λ that results from evaluating (2.1a) at $y = 0$ in the limit $Re^{-1} = 0$ are given by

$$U_s(x; \alpha) \equiv u_s(x) + \alpha^{3/4} \Psi_Y(x, Y = 0) = u_s + \alpha^{3/4} U_1 + O(\alpha^{3/2}), \quad (5.12a)$$

$$\Lambda(x; \alpha) \equiv U_s U_{sx} + p_x(x, y = 0) = \Lambda_0(x) + \alpha^{3/4} (u_s U_1)_x + O(\alpha). \quad (5.12b)$$

Note that from (5.8) together with the asymptotic behaviour of $\bar{\ell}$ given in (5.4) and (5.5) follows $U_1 < 0$ and, as one expects, in turn $U_s < u_s$. The effect of the intermediate layer on the overall profile of the streamwise velocity u is depicted in a disproportionate but qualitatively correct manner in figure 5.

Expansions (5.12) account for higher-order contributions to u_s and Λ_0 , respectively, due to the full wake solution comprising both layers as governed by the inviscid limit of the Reynolds equations, (2.1), where the no-slip condition in (2.3) is abandoned in favour of requiring vanishing wall shear stress, cf. (5.2b). In the next section we shall see that the whole information needed to determine the skin friction in the physically meaningful case of high but finite Re is provided if both U_s and Λ are known. In fact, a drastic simplification of the genuine two-parameter asymptotics due to both α and Re finite will be obtained in the following where the two-tiered inviscid wake limit will be treated as one single layer. This procedure allows for subsuming higher-order effects due of finite α in the terms U_s and Λ .

In particular, this approach will prove advantageously for the investigation of separation. It will turn

out that the emergence of a reverse-flow region is always associated with vanishing U_s in the inviscid limit $Re \rightarrow 0$ that is examined in § 6.1. However, if the magnitude of the leading-order velocity in the intermediate layer, u_s , becomes comparable to $\alpha^{3/4}U_1$ a breakdown of the asymptotic structure presented so far will be encountered. Therefore, an asymptotic analysis of the wake flow covering that case has to account for the influence of the inner layer due to finite α on the solution in the outer part as $u_s \rightarrow 0$. This topic is beyond the scope of the present thesis and will be dealt with separately. Nevertheless, the present suggestion seized in § 6 of combining both the outer and the intermediate layer even for $U_s \rightarrow 0$ will appear to be sufficient for outlining the essential asymptotic features of the viscosity-effected near-wall flow structure which undergoes a dramatic change as separation is approached. The latter item will be pointed out in detail in § 6.2.

With respect to the full set of Reynolds equations, (2.1), and the outer expansion (5.1) the (non-trivial, i.e. $U_e - u_s = O(1)$) solutions ψ_0, τ_0 of the leading-order problem (5.2), which governs the inviscid wake in the limit $\alpha \rightarrow 0$, are perturbed primarily due to terms quoted explicitly in (5.7a) and (5.7b). Therefore, in order to capture the effect of finite α in the case $U_s = O(\alpha^{3/4})$, the underlying boundary layer approximation (5.2) may be formally left unchanged but supplemented with an asymptotically correct closure with α adopting a default value, see e.g. (3.21). Numerical results presented in § 5.3 and § 6.1.1 accounting for that two-tiered wake structure due to the change of $\bar{\ell} \sim \bar{\ell}_0$ as $Y \rightarrow \infty$ to the generalized form of Prandtl's mixing length (3.8),

$$\bar{\ell} \sim \kappa(K)Y \quad \text{as } Y \rightarrow 0, \quad (5.13)$$

demonstrate that U_s may even change sign. Anticipating the considerations in § 6.2, we replaced $\kappa_0 = \kappa(0)$ holding for strictly attached flow in (5.13) by $\kappa(K)$, where K is given by (3.5). This characterizes a distinguished limit $K = O(1)$ arising from the inevitable coupling between U_s and Re for high but finite Re on the verge of separation.

Clearly, higher-order perturbations of u_s arising from Reynolds normal stresses and the variations of induced pressure, cf. (5.1) and (5.7), will affect this somewhat *ad hoc*-boundary layer approximation only quantitatively.

5.2. Generalized law of the wall and skin friction formula

If we now consider the physically meaningful case of high but finite Re , matching the outer inviscid wake solution to the universal wall layer arising from the significance of viscous shear stress, see § 3.1.1, must fail as τ varies linearly at the bottom of the outer part, cf. (5.7b), but equals $\tau_w = u_\tau^2$ up to leading order in the near-wall regime, giving rise to a log-region at its outer edge. Since in the inner high- Re limit the solutions for u^+, τ^+ are assumed to be universal throughout, at least in leading order, the results holding in the viscous sublayer where $y = O(\delta^+)$ known from the classical defect approach are left unchanged. As far as the procedure of logarithmic matching the solution to the fully turbulent flow region is concerned, cf. § 3.1.2, only $U_e(x)$ has to be replaced by the slip velocity $U_s(x; \alpha)$, which is assumed to be of $O(1)$ in general. Therefore, recalling the arguments at the beginning of § 4.1.1 in the linearized case of a moderately large defect, that is

$$U_s \sim U_e(1 - \bar{\gamma}C_0), \quad A \sim \bar{\gamma}(C_0U_e^2)_x \quad (5.14)$$

with respect to (4.3a), (4.9) and (5.12), a transition layer has to be introduced which emerges in the distinguished limit $\tau \sim \tau_w + Ay$ in leading order. To this end, we define a coordinate ζ by

$$y = u_\tau^2 \zeta$$

and relate the skin friction velocity to the slip velocity, which yields a Re -dependent perturbation parameter

$$\gamma_s = u_\tau/U_s \equiv \gamma U_e/U_s = O(1/\ln Re) \quad \text{as} \quad Re^{-1} \rightarrow 0.$$

As in the classical case, the parameter γ is defined by (3.1) and the logarithmic dependency on Re will turn out subsequently from matching with the viscous wall layer, see (5.20) below.

The convective part of the boundary layer equations, see (5.2a), (5.7b), suggests a velocity defect differing from $u = U_s$ by $O(u_\tau)$ and in turn expansions of the form

$$u = U_s (1 + \gamma_s U_1 + \gamma_s^2 U_2 + \dots) + \dots, \quad \tau = u_\tau^2 (T_1 + \gamma_s T_2 + \dots) + \dots \quad (5.15)$$

Here dots denote higher-order terms arising from switch-back effects induced by the corresponding expansions holding in adjacent layers and those which account for the influence of viscous stresses, respectively. The following analysis will reveal the importance of the first two higher-order corrections quoted in (5.15) for the understanding of the induced perturbations in the inviscid wake flow, especially if separation is approached, which will be shown in § 6.2.

The derivation of Prandtl's mixing length distribution has originally been based on the existence of an overlap region that is characterized by vanishing influence of viscosity and lies between the wall layer and the outer mainly inviscid flow. This overlap regime characteristic for the two-tiered defect theory has to be replaced by the particular transition layer where Prandtl's universal law provides an asymptotically exact Reynolds shear stress model, which is applicable at least to the leading-order relation. Therefore, by analogy to (4.15),

$$T_1 = 1 + A\zeta = (\kappa_0 \zeta)^2 (\partial_\zeta U_1)^2. \quad (5.16)$$

The defect flow $u - U_s$ is in local equilibrium then in the sense of Townsend (1961). Quadrature of (5.16) yields the generalized law of the wall,

$$U_1 = \kappa_0^{-1} \left\{ \ln(A\zeta) - 2 \ln \left[(1 + A\zeta)^{1/2} + 1 \right] + 2(1 + A\zeta)^{1/2} \right\}. \quad (5.17)$$

Therefore, if U_s is replaced by U_e the behaviour (4.16) of the transition layer in the case of a moderately large defect case is revealed, cf. § 4.1.1. Accordingly, the solution for U_1 exhibits a finite slip as $\zeta \rightarrow 0$ which results from integration and is chosen to avoid a term of $O(1)$ in the large- ζ behaviour of U_1 , which would induce a contribution to U_s of $O(\gamma_s)$ in the intermediate layer expansion (5.7a); on basis of the same argument the higher order disturbances, U_2, \dots , of the velocity profile have to be fixed. The precise behaviour of U_1 near and far away from the wall may follow immediately from (4.17) and then is given by

$$U_1 = \kappa_0^{-1} \begin{cases} 2(A\zeta)^{1/2} - (A\zeta)^{-1/2} + (A\zeta)^{-3/2}/12 + O(\zeta^{-5/2}) & \dots \zeta \rightarrow \infty, \\ \ln \zeta + \ln(A/4) + 2 + A\zeta/2 - (A\zeta)^2/16 + O(\zeta^3) & \dots \zeta \rightarrow 0. \end{cases} \quad (5.18)$$

Thus the square root law, followed by purely algebraically decaying terms for $\zeta \rightarrow \infty$, substitutes the log-law which holds to account for finite shear stress in the viscous wall region and is followed by a regular expansion as $\zeta \rightarrow 0$.

The form of relationship (5.17) has been suggested by a number of authors, see e.g. Mellor (1966), Townsend (1976), Melnik (1989) and Afzal (1996). They recognized the need of a transition region at incipient separation caused mainly by the change in the behaviour of the Reynolds shear stress at the outer edge of the viscous sublayer where τ takes on τ_w in the attached case but approaches a linear distribution balancing the pressure gradient as τ_w tends to zero. The specific algebraic eddy-viscosity models Melnik employed are asymptotically correct as they exhibit Prandtl's law for small distances from the wall. As a consequence arising from the aforementioned improper coupling between α and Re ,

the velocity distribution (5.17) holds at the base of the inner wake layer. On the other hand, Gersten & Herwig (1992) following Afzal (1996) restricted (5.17) to the overlap region to the viscous wall layer as a generalized matching condition accounting also for the case of separation. Both of these different approaches, however, appear to be questionable as they ignore the existence of a distinguished limit leading to the transition layer with a thickness of $O(\tau_w)$.

None of the authors cited so far put these considerations on an asymptotically self-consistent firm basis. This seems less surprising as it has been pointed out before that any attempt to formulate a theory which accounts for the transformation of the outer inviscid flow from an attached small defect to a nonlinear wake-like one must fail, cf. § 3.2.

For completeness and reasons given above, we also quote the large- ζ behaviour of the terms entering at second order, that will be useful for matching with the inner wake region we face in the next section:

$$\frac{T_2}{U_s} = a_{\frac{3}{2}} \zeta^{3/2} + a_{\frac{1}{2}} \zeta^{1/2} + a_0 + O(\zeta^{-1/2}), \quad \frac{U_2}{U_s} = c_1 \zeta + c_{\log} \ln \zeta + c_{-\frac{1}{2}} \zeta^{-1/2} + O(\zeta^{-1}), \quad (5.19a)$$

where the x -dependent coefficients are given by

$$\left. \begin{aligned} a_{\frac{3}{2}} &= \frac{2(U_s \Lambda)_x}{3 \kappa_0 \Lambda^{1/2}}, & a_{\frac{1}{2}} &= \frac{U_s \Lambda_x - 7 \Lambda U_{sx}}{\kappa_0 \Lambda^{3/2}}, & a_0 &= \frac{-2 U_s \Lambda_x + 10 \Lambda U_{sx}}{3 \kappa_0 \Lambda^2}, \\ c_1 &= \frac{(U_s \Lambda)_x}{3 \kappa_0^2 \Lambda}, & c_{\log} &= \frac{U_s \Lambda_x - 11 \Lambda U_{sx}}{3 \kappa_0^2 \Lambda^2}, & c_{-\frac{1}{2}} &= \frac{2 U_s \Lambda_x - 10 \Lambda U_{sx}}{3 \kappa_0^2 \Lambda^{5/2}}. \end{aligned} \right\} \quad (5.19b)$$

Expansion (5.19a) results from applying Prandtl's mixing length closure stated in (5.16) up to second order terms since normal stresses etc. do not enter the solution at this stage as we confine our analysis to pure boundary layer approximation. An arbitrary term of $O(1)$ caused by integration in the expansion for U_2 is required to vanish due to the same argument supplementing the large- ζ form (5.18) of U_1 . For ζ small one obtains

$$\begin{aligned} \frac{T_2}{U_s} &= \frac{U_s \Lambda_x + \Lambda U_{sx} (2 \ln(\Lambda \zeta / 4) - 1)}{\kappa_0 \Lambda} \zeta + \frac{U_s \Lambda_x - \Lambda U_{sx}}{4 \kappa_0} \zeta^2 + O(\zeta^3), \\ \frac{U_2}{U_s} &= \frac{U_s \Lambda_x \ln(4/\Lambda) + \Lambda U_{sx} (12 + 11 \ln(\Lambda/4))}{3 \kappa_0^2 \Lambda} + \frac{U_s \Lambda_x + \Lambda U_{sx} (2 \ln(\Lambda \zeta / 4) - 3)}{2 \kappa_0^2 \Lambda} \zeta + O(\zeta^2 \ln \zeta, \zeta^2). \end{aligned}$$

The contribution in the representation of T_2 not given explicitly possesses a purely regular expansion. Terms varying with ζ match term by term with the corresponding terms in the expansions (3.6a), (3.6b) for $y^+ \rightarrow \infty$ if (3.8) is adopted.

Matching the logarithmic velocity profile given by (5.18) to the viscous sublayer yields the generalized skin friction law,

$$\gamma_s^{-1} = \kappa_0^{-1} \ln(Re |u_\tau|^3) + C^+ - \kappa_0^{-1} (\ln(\Lambda/4) + 2) - \gamma_s C_2(x) + O(U_s^2 \gamma_s). \quad (5.20)$$

It is seen to be similar to the one in classical linearized theory where U_e and γ replace U_s and γ_s , respectively, cf. (3.15). Again, the pure log-behaviour is confined to the first order in (5.15). Thus higher-order terms denote the finite limits $U_i \rightarrow C_i(x)$, $i = 2, 3, \dots$, as $\zeta \rightarrow 0$, perturbing the inviscid slip velocity U_s . Moreover, matching the higher orders of T and U , therefore, appears to be a self-consistent process. Inversion of (5.20) leads to

$$\begin{aligned} \gamma_s &= \frac{\kappa_0}{\ln Re} \left[1 + 3 \frac{\ln(\ln Re)}{\ln Re} + \frac{D(x)}{\ln Re} + 9 \frac{\ln^2 \ln Re}{\ln^2 Re} + (6 D(x) - 9) \frac{\ln(\ln Re)}{\ln^2 Re} \right] + O\left(\frac{1}{\ln^3 Re}\right), \\ D(x) &= 2 - \kappa_0 C^+ - \ln(4 \kappa_0^3 U_s^3 / \Lambda); \end{aligned}$$

higher-order terms depend on $C_i(x)$. As a result, $\gamma_s \sim \kappa_0 / \ln Re$ or $\gamma = O(U_s / \ln Re)$. Differentiation

yields

$$\frac{d\gamma_s}{dx} = \frac{\gamma_s^2}{\kappa_0} \frac{d \ln(\Lambda/U_s^3)}{dx} + O(\gamma_s^3),$$

which justifies expansion (5.15) if inserted into the boundary layer approximation, cf. (5.2a) and (5.7b).

As long as U_s may be regarded to be of $O(1)$, the Bradshaw parameter K defined by (3.5) has the same magnitude as for the linearized defect. In section §6.2.1 we will discuss how it may change to $O(1)$ if U_s becomes small, i.e. as separation is approached. As this is the case the flow in the viscous wall layer can still be regarded as universal but depends also on K , which becomes of $O(1)$ then such that the wall shear stress will turn out to be determined by the local properties of the flow in the near-wall part of the wake region.

5.2.1. Disturbances in the wake region due to finite Re

Matching terms in (5.15) with subscripts 1 and 2 to the inviscid wake flow regime gives rise to additional terms in the intermediate layer expansions, (5.7), causing a two-parameter (namely α and u_τ) asymptotics in the wake region:

$$\begin{aligned} \psi = & \dots + u_\tau^2 \alpha^{3/4} \left[\bar{\Psi}_1 + \alpha^{3/4} \left(b_{\log}(x) Y \ln \frac{\alpha^{3/2}}{u_\tau^2} + \bar{\Psi}_2 \right) + O\left(\alpha^{3/2} \ln \frac{\alpha^{3/2}}{u_\tau^2}\right) \right] + u_\tau^3 \left[d_0(x) \right. \\ & \left. + \alpha^{3/4} \hat{\Psi}_1 + \alpha^{3/2} \left(-\frac{(d_0 u_s^3)_x}{\kappa_0^2 u_s^3} Y \ln \frac{\alpha^{3/2}}{u_\tau^2} + \hat{\Psi}_2 \right) + \dots \right] + O\left(\frac{u_\tau^4}{\alpha^{3/4}}\right), \quad d_0 = \frac{2}{3 \kappa_0 \Lambda_0}; \quad (5.21a) \end{aligned}$$

$$\tau = \dots + u_\tau^2 \left[1 + \alpha^{3/4} \bar{T}_1 + O\left(\alpha^{3/2} \ln \frac{\alpha^{3/2}}{u_\tau^2}\right) \right] + u_\tau^3 \left[b_0(x) + \alpha^{3/4} \hat{T}_1 + \dots \right] + O(u_\tau^4), \quad (5.21b)$$

due to finite skin friction $\tau_w = u_\tau^2$ and in accordance with (5.18) and (5.19a). Here and in the following coefficients denoted by b denote the corresponding terms a and c , respectively, with the same subscript in (5.19b) but if the quantities Λ and U_s are replaced by their leading-order counterparts Λ_0 and u_s . Each of the functions $\bar{\Psi}_i$, $\hat{\Psi}_i$ and \bar{T}_i , \hat{T}_i etc. respectively, with $i = 1, 2, \dots$ in the scheme generated is supposed to vanish for $Y \rightarrow 0$ whereas the shift $d_0(x)$ in the expansion for ψ at $O(u_\tau^3)$ is determined by the behaviour of $\int_0^\zeta U_1(\Lambda\bar{\zeta}) d\bar{\zeta}$ for $\zeta \rightarrow \infty$. The dots on the right of the equality signs in (5.21) denote the unperturbed expansions for $Re^{-1} = 0$, cf. (5.7).

Making use of Prandtl's law (3.8) and integration of the expanded streamwise momentum balance, cf. (5.7b), yields the leading-order disturbances

$$\bar{\Psi}_{1Y} = -\kappa_0^{-1} (\Lambda_0 Y)^{-1/2} + \frac{1}{2} \int_0^Y (\Lambda_0 \bar{Y})^{-1/2} \left[\bar{\ell}^{-1} - (\kappa_0 \bar{Y})^{-1} \right] d\bar{Y}, \quad (5.22a)$$

$$\bar{T}_1 = u_{sx} (4\bar{\Psi}_1 - Y \bar{\Psi}_{1Y}) + u_s \bar{\Psi}_{1x}. \quad (5.22b)$$

One obtains in turn the small- Y relations

$$\begin{aligned} \bar{\Psi}_{1Y} = & -\kappa_0^{-1} (\Lambda_0 Y)^{-1/2} + o(1), \quad \bar{\Psi}_{2Y} = \frac{b_{\frac{1}{2}}}{2 \kappa_0 \Lambda_0^{1/2}} \ln Y + o(1), \quad \bar{T}_1 \sim b_{\frac{1}{2}} Y^{1/2} + o(1); \\ \hat{\Psi}_{1Y} = & b_{-\frac{1}{2}} Y^{-1/2} + o(1), \quad \hat{\Psi}_{2Y} = -\frac{(d_0 u_s^3)_x}{\kappa_0^2 u_s^3} \ln Y + o(1), \quad \hat{T}_1 \sim -\frac{2(d_0 u_s^3)_x}{\kappa_0 u_s^3} (\Lambda_0 Y)^{1/2} + o(1). \end{aligned}$$

Here (arbitrary) contributions of $O(1)$ resulting from integration to the streamwise velocity for $Y \rightarrow 0$ have been set to zero in order to leave expansion (5.15) undisturbed, at least up to orders indicated there. Conversely, the logarithmically varying perturbations of the velocity profile are caused by the transition layer solution. In turn, they induce terms of logarithmic magnitudes in the intermediate layer expansions (5.21), that are retained in the outer wake perturbations. As they inevitably prescribe a disturbance

of the wall slip distribution, in turn corresponding disturbances of the same order are triggered in the external flow.

The outer layer exhibits disturbances, primarily stimulated by the behaviour of (5.22) for $Y \rightarrow \infty$, are expressed by

$$q = \dots + u_\tau^2 (\bar{q}_1 + \dots) + u_\tau^3 (\bar{q}_2 + \dots), \quad \text{with } q = p - p_0, \psi, \delta, \tau, \sigma_{(x)}, \sigma_{(y)}. \quad (5.23)$$

Here the dots on the right of the equality sign denote the inviscid limit described by expansion (5.1), while dots within parentheses denote any asymptotically smaller terms arising from a match with (5.21). In this notation we have $\tau_1 \rightarrow 1$ as $\bar{y} \rightarrow 0$.

For a sketch of the four-layered boundary layer structure discussed so far see figure 5 (a).

5.3. Similarity solutions

In order to obtain first non-trivial solutions we seek for the simplest form of nonlinear turbulent boundary layer flow, which is apparently provided by means of a similarity transform applied to (5.2). Furthermore, self-preserving flow will prove to be very instructive for outlining how the reduction of our nonlinear theory presented so far reduces to the classical one in the case of a small velocity defect.

5.3.1. Inviscid limit: $Re^{-1} = 0$

It is readily verified that all commonly used models in principal allow for self-similar solutions of the inviscid shear layer approximation (5.2) of the basic equations of motion (2.1). This is the case if the transformed stream function f and Reynolds shear stress t , respectively, given by

$$\psi = \delta U_e f(x, \eta; \alpha), \quad \tau = \alpha U_e^2 t(x, \eta; \alpha), \quad \eta = y/\delta(x; \alpha), \quad (5.24)$$

do not depend on x in zeroth order with respect to the expansions (5.1) and (5.7). (We mention that the boundary conditions (5.2b) together with the existence of the finite wall slip $U_s(x; \alpha)$ suggests also a defect transformation of the form $\psi = \delta U_e [1 - (1 - U_s/U_e)f]$. However, inserting it into (5.2a) then shows that it does not allow for self-similar boundary layer flow apart from the exception $U_s/U_e = \text{const}$ in leading order, which clearly coincides with ansatz (5.24).) Then the necessary conditions allowing for self-preserving solutions of the nonlinear leading-order problem (5.2) equal the requirements given in (3.19), (3.20) for equilibrium flow in the case of a small defect. They follow from inserting the appropriate expansions of the transformed variables given by

$$\delta = \alpha \delta_0(x) + O(\alpha^2); \quad f = f_0(x, \eta) + O(\alpha), \quad t = t_0(x, \eta) + O(\alpha) \quad (5.25)$$

into (2.1a). If the boundary layer thickness varies approximately linearly with x , i.e. $\delta_{0x} = a = \text{const}$, and, setting the in principle arbitrary virtual origin x_o to zero, the imposed outer-flow velocity obeys a power law, i.e. $U_e \propto x^m$, (5.2) may reduce to an ordinary boundary value problem determining $f_0(\eta)$, $t_0(\eta)$,

$$m \left(f_0'^2 - 1 \right) - (m+1) f_0 f_0'' = t_0'/a; \quad f_0(0) = t_0(0) = 0, \quad f_0'(1) = 1, \quad t_0(1) = 0. \quad (5.26)$$

Supplementing (5.26) with a suitable closure for t_0 , the rate of increase a of δ_0 has to be regarded as an eigenvalue. It should be noted that the resulting equation for f_0 closely resembles the Falkner–Skan equation for laminar self-preserving flows.

For a general turbulent boundary layer flow the displacement and momentum thicknesses δ^* and δ^{**} , respectively, are defined by

$$\delta^* \equiv \int_0^\delta \left(1 - \frac{u}{U_e} \right) dy = \delta(1 - f_e), \quad \delta^{**} \equiv \int_0^\delta \frac{u}{U_e} \left(1 - \frac{u}{U_e} \right) dy = \delta \left(f_e - \int_0^1 f'^2 d\eta \right). \quad (5.27)$$

Herein the transformed stream function at the outer edge, $f(x, 1; \alpha)$, is denoted by f_e . Integrating (5.26) from $\eta = 0$ to $\eta = 1$ gives rise to the leading-order integral momentum balance in the case of strict equilibrium exhibiting a velocity defect of $O(1)$ in the limit $Re^{-1} = 0$, expressed through the well-known equilibrium shape parameters G and H_{21} :

$$G \equiv 1 - H_{21} \sim \frac{1 + 3m}{1 + 2m}, \quad H_{21} \equiv \frac{\delta^{**}}{\delta^*}. \quad (5.28)$$

From (5.28) together with the boundary conditions in (5.26) it immediately follows that self-similar wakes (that means $f_0' \leq 1$) exposed to an adverse pressure gradient exist only within the limits $-1/3 < m < 0$. Furthermore, δ_0 increases apparently with a positive rate a . The case of the flat plate, $m = 0$, for nonlinear flow then describes an isolated solution exhibiting a reverse-flow region (that means $f_0' < 0$) within some distance from the wall such that δ^{**} vanishes. Considering the other extreme, $m = -1/3$, problem (5.26) becomes singular as the only solution is given by the trivial one, $f_0' \equiv 1$ and $t_0 \equiv 0$. Thus by varying the normalized slip velocity $f_0'(0)$ from its negative limit it takes for $m = 0$ up to 1, $G(m)$ is increased from 0 to 1, where the dependency of the exponent m on $f_0'(0)$ will be found numerically.

The problem (5.26) and the relationship (5.28) have already been considered in the investigation of the so-called Stratford flow, i.e. a boundary layer having zero skin friction throughout even for finite Re , which is presented in Gersten & Herwig (1992) and Schlichting & Gersten (2000): There this profile is regarded as the inviscid limit of a class of boundary layers slowly approaching separation for high but finite Re , and a nonlinear self-preserving wake layer of finite thickness and zero wall slip is proposed. However, the analysis carried out lacks an asymptotic background and, furthermore, gives no hint on the existence of nonlinear wake solutions exhibiting finite $f_0'(0)$ and thus, according to (5.20), finite wall shear. Within the framework of the asymptotic theory presented, the Stratford flow is apparently covered as a special case of a separating profile, characterized by vanishing slip velocity in the inviscid limit $Re^{-1} = 0$. For a recent extensive experimental study of such flows the reader is referred to Elsberry *et al.* (2000).

For the purpose to obtain a whole set of non-trivial numerical solutions of (5.26), parametrized by a varying wall slip $f_0'(0)$ of $O(1)$, the exponent m has to be regarded as a further eigenvalue besides a . To this end, an arbitrary value of $f_0'(0) < 1$ is prescribed, giving rise to an additional boundary condition. It is interesting to note that in consideration of Prandtl's mixing length (5.13) the condition of zero wall shear is indeed implied by the requirement of bounding the velocity at the wall. Otherwise the square root law would be superseded by a log-behaviour which is clearly inconsistent with a finite wall slip. Therefore, $t_0(0) = 0$ has to be interpreted as a kind of solvability condition which allows to add one boundary condition in (5.26) such that the solution gives rise to a second eigenvalue. Of course, computing m as a function of $f_0'(0)$ will induce a perturbation of the outer flow due to an expansion of m according to (5.1) if higher orders are regarded.

In line with the corresponding remarks in the last paragraph of § 5.1.2, we consider the two-tiered wake as a single layer, giving rise to the square root velocity law for $\eta \rightarrow 0$. Thereby we account for the effect of finite α and thus expect a qualitatively correct behaviour of the solutions within a distance $\eta = O(\alpha^{1/2})$ from the wall, even for flows on the verge of separation where $f_0'(0)$ tends to zero. Some aspects of the numerical integration of problem (5.26) which has been carried out using the model (3.21) with $\alpha = c_\ell^2$, are outlined in Appendix B. Results for the leading order $m = m_0$ of the exponent and a as a function of the wall slip $f_0'(0)$ are plotted in figure 6.

For the sake of simplicity and with respect to (5.13) instead of κ_0 the value $\kappa_\infty = \kappa(\infty) = 0.59$ which approximately holds on the verge of separation was adopted in (3.21) throughout our calculations.

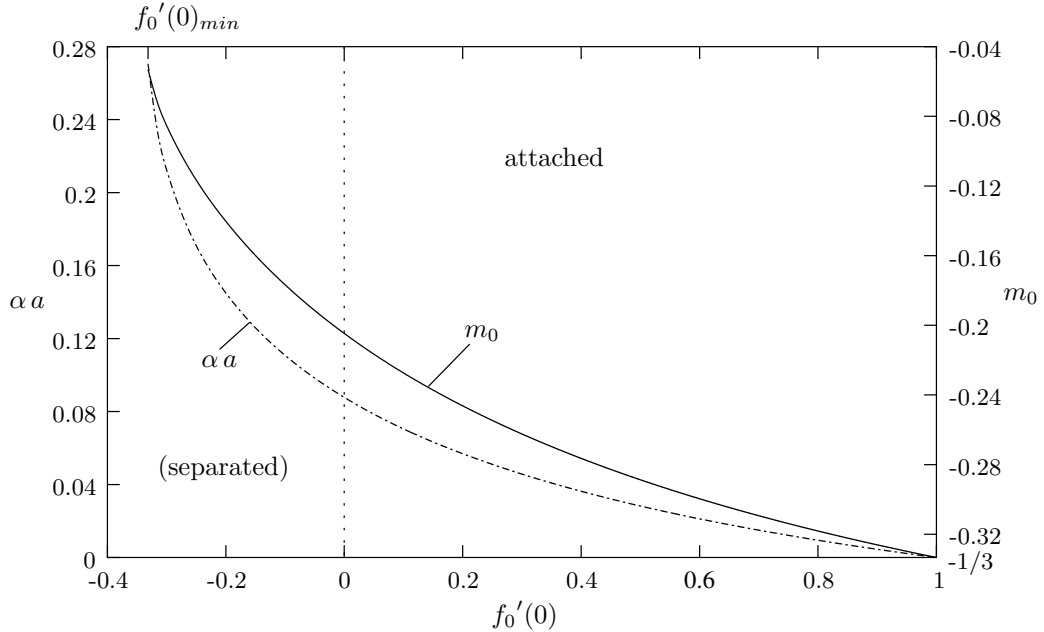


FIGURE 6. Eigenvalues: outer-flow exponent m_0 and $a = \delta_{0x}$. Varying $f_0'(0)$, numerical difficulties occur for $f_0'(0)_{min} \doteq -0.3314$ where $a \doteq 37.461$ and $m \doteq -0.0531$. As commented in the text, applying our theory to distinctly separated solutions seems questionable.

With regard to the skin friction law (5.20), that arises from the perturbed structure due to finite Re as expounded in the foregoing sections, this is only correct if $f_0'(0) = O(Re^{-1/3})$. In the inviscid case considered here a separating profile exists for the flow parameters $\alpha a \doteq 0.0878$, $-m_{sep} \doteq 0.2047$, $G_{sep} \doteq 0.6534$ and the corresponding value of $H_{21} \doteq 0.3466$. That inviscid limit of the Stratford profile has been calculated in Schlichting & Gersten (2000) by means of the common Michel's model with $\kappa_\infty \approx 0.6$. It is interesting to note that in this study only slightly larger values for the quantities cited here are quoted, apart from the clearly more pronounced boundary layer growth given by $\alpha a \doteq 0.145$ there. This maybe reflects an overprediction of turbulence intensity caused by the omission of the intermittency factor in (3.21).

Due to numerical difficulties inhering the solutions with negative wall slip the values of $f_0'(0)$ are limited by some $f_0'(0)_{min}$, see figure 6, almost meeting the flat-plate flow where $m = 0$. From an inspection of (5.26) it is readily verified that $t_0 \geq 0$ for the interval $-1 < f_0'(0) \leq 1$. Therefore, the solutions investigated with negative m exhibit a positive shear gradient at the wall; and the quantity

$$\Lambda / (x U_e^2) = m \left(f_0'(0)^2 - 1 \right)$$

is positive, even in the case of backflow. The corresponding family of profiles f_0' and t_0 is depicted in figure 7. According to (5.11), the wake-like profiles for f_0' show a square root behaviour as $\eta \rightarrow 0$. Due to the finite mixing length the solutions vary quadratically with η as $\eta \rightarrow 1$.

If flows with a negative velocity of $O(1)$ near the wall are considered, i.e. if $f_0'(0) < 0$, one expects a negative wall shear stress τ_w in the case of finite Re . This is supported by the skin friction law (5.20), and the log-profile now points in opposite direction as for attached flow. Concerning the transition layer, see § 5.2, Prandtl's mixing length hypothesis predicts a coincidence in leading order of the location where

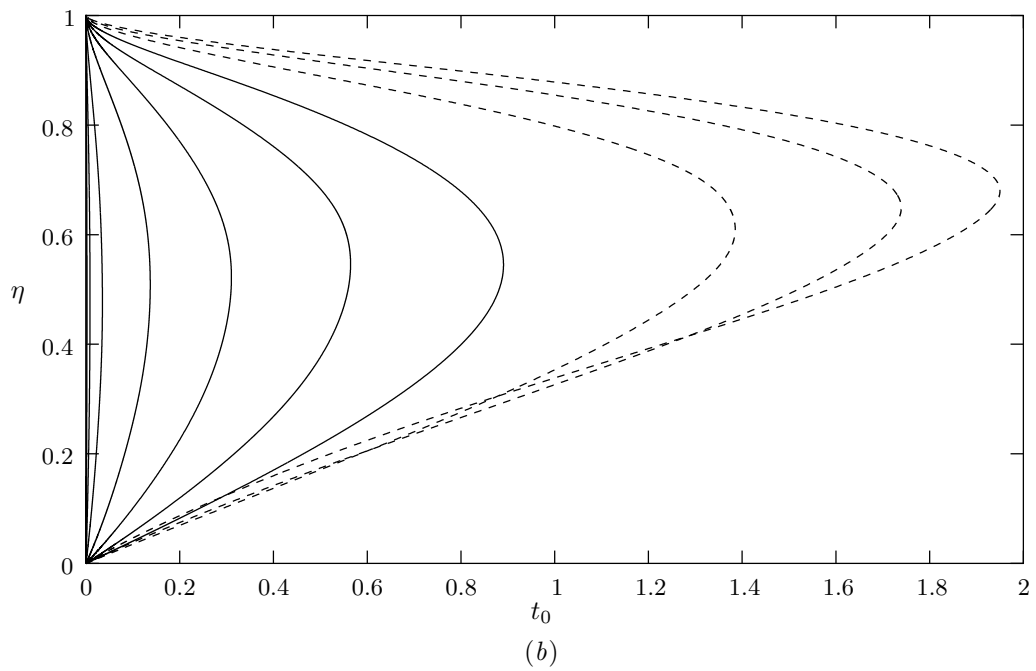
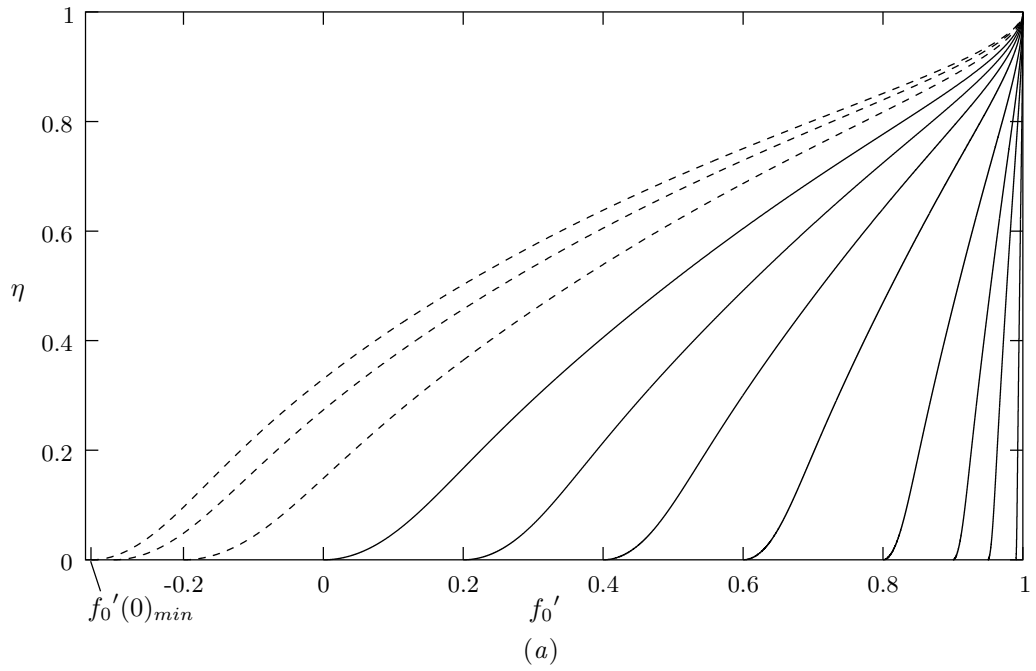


FIGURE 7. Similarity profiles for the related (a) streamwise velocity, f_0' , and (b) Reynolds shear stress, t_0 , parametrized by $f_0'(0)$. The maxima in the distributions for t_0 are shifted to the right as $f_0'(0)$ decreases. Starting with the trivial case, the wall slip $f_0'(0)$ varies from 1 over 0.99, 0.95, 0.9, 0.8, 0.6, 0.4, 0.2, 0.0, -0.2 , -0.3 to $f_0'(0)_{min}$.

the nearly linearly varying Reynolds shear, cf. (5.16), changes sign with the turning point of the velocity profile where $u_y = 0$. However, to the author's knowledge the universal profile (5.17) contradicts empirical data available for strongly separated reverse-flow regimes, where the local dependency of τ on the velocity gradient as expressed by (3.8) seems not adequate. Thus the theory developed so far is probably not capable of allowing for a perturbation of solutions describing separated flows due to high but finite Re . Therefore, these are printed only dashed and results regarding substantially separated profiles have to be accepted with some reservation (cf. the corresponding figures in this and the subsequent section).

The postulate of a nonlinear self-preserving description of the outer part of turbulent boundary layers that gives rise to a finite wall slip must be attributed to Clauser (1956), who established the well-known eddy viscosity concept on basis of a laminar-like flat-plate profile. Equilibrium flows at incipient separation exhibiting a large defect and the square root law have been considered by several authors, see, for example, Perry, Bell & Joubert (1966), Chawla & Tennekes (1973), Schofield (1981), Durbin & Belcher (1992) or Afzal (1996). However, none of those approaches are within a correct asymptotic framework as they lack the need of the Re -independent perturbation parameter α first recognized by Melnik (1989). Inspired by the work of Clauser (1956), he demonstrated good agreement of attached nonlinear wake-like equilibrium solutions with the ones obtained by Mellor & Gibson (1966) which arise from the classical small-defect theory. In fact, this seems less surprising as Melnik's theory is not derived by means of a genuine two-parameter asymptotics and thus does not account for the self-consistent wake structure presented here, giving rise to vanishing skin friction in the limit $Re^{-1} = 0$. Therefore, in Melnik's shear stress profiles exhibit a finite wall shear in leading order which is only correct if Re is high but finite.

5.3.2. Finite values of Re

In order to account for the real physics, the eigensolutions of (5.26) discussed so far have to be perturbed due to finite values of Re by means of the appropriate expansions (5.23), (5.21) holding in the outer and inner wake, respectively. In that case integration across the boundary layer yields

$$G = \frac{1 + 3m}{1 + 2m} + \dots - \operatorname{sgn}(\tau_w) \frac{\gamma^2}{\alpha} \frac{1}{a(2m + 1)(1 - f_0(1))} + \dots \quad (5.29)$$

With respect to the asymptotic relationship (5.28) here the dots on the left abbreviate the inviscid higher-order disturbances of $O(\alpha)$, in accordance with the expansions (5.1), (5.7). Thus as long as the wall shear stress $\tau_w = \operatorname{sgn}(\tau_w)u_\tau^2$ is finite (and negative for separated flows) the inviscid limit is primarily perturbed by the latter. The right-hand dots in (5.29) denote terms of $O(\gamma^2)$ that are induced by the full set of Reynolds equations, see (2.1). Compared to the inviscid case, for a given $f_0'(0)$ the curves are shifted to smaller values of G as m slightly varies in parametric dependency on γ .

Let $\epsilon = \kappa_0/\ln Re$ denote the leading-order contribution to $\gamma_s \sim \gamma f_0'(0)$, given by the generalized skin friction law (5.20). Then in figure 8 the outermost curve designated by $\epsilon = 0$ represents the inviscid limit (5.28), and the abscissa $G \equiv 0$ the trivial irrotational solution. Regarding the perturbed case of finite Re , and m not too close to $-1/3$ and m_{sep} , respectively, the upper branches of the inner curves may be calculated for various values of ϵ by means of (5.29), using the model (3.21). A qualitative diagram similar to the one presented here has already been suggested by Winter & East (1982).

The case of separation, i.e. $\tau_w \equiv 0$ (Stratford flow), was attacked also by Gersten & Herwig (1992), who adopted the concept proposed by Melnik (1989) and solved (5.26) in order to gain solutions for the outer part of the wake. Again, as the wall slip $f_0'(0)$ then is seen to be of $O(Re^{-1/3})$ matching of the Re -independent intermediate layer to the wall layer with a thickness of $Re^{-2/3}$ is problematical and reveals the inconsistencies in Melnik's theory mentioned before. The correct treatment of the boundary

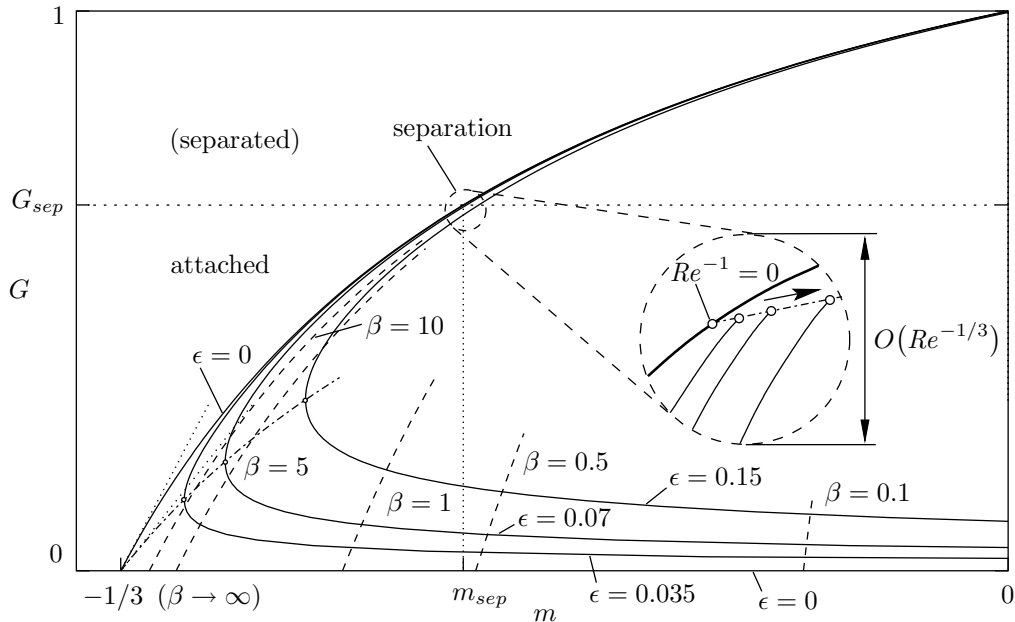


FIGURE 8. Multiple structure of turbulent equilibrium boundary layers. The values of $\beta \sim \beta_0 = \text{const}$ along the dashed curves have been approximated within the moderate-defect approach yielding (4.5).

layer structure in the case $\gamma = O(Re^{-1/3})$ and $\gamma/\gamma_s = O(1)$ or smaller, as sketched in figure 5 (b), will be performed in § 6.2.1. As a consequence of the failure of (5.20) in that case in figure 8 the curves in the immediate vicinity of $m \sim m_{sep}$, $G \sim G_{sep}$ have to be considered as only qualitatively correct ones. If γ vanishes the relationship (5.29) reduces formally to the inviscid limit (5.28). Nevertheless, for negligible wall shear the duple $m \sim m_{sep}$, $G \sim G_{sep}$ characterizing separation if $Re^{-1} = 0$ then is slightly disturbed due to terms of $O(Re^{-1/3})$. Thus the deviation from the inviscid limit (5.28) in the zoomed picture symbolizes viscous higher-order perturbations of $O(Re^{-1})$, mainly resulting from switch-back effects caused by the wall layer.

5.4. Small defect — connecting flow

For a given $\mu = m + 1/3 > 0$ the velocity defect and $a = \delta_{0,x}$ are considered as quantities of $O(1)$. Near $\mu \sim 0_+$ the defect becomes of $O(\mu)$ and thus allows for linearizing the flow about $u = U_e$, i.e. $f = \eta$. This strikingly contrasts the approach suggested by Melnik (1989) where the undesired coupling given by $\alpha^{1/2} = O(1/\ln Re)$, resulting from the requirement that in leading order $\tau \rightarrow \tau_w$ as $\bar{y} \rightarrow 0$, prohibits a linearization of the convective terms in (5.2a).

The expansions (5.25) holding in the outer layer then are superseded by corresponding two-parameter expansions with respect to α and, independently, to μ as a measure of the velocity defect. If μ is defined in this way the following investigation is clearly not restricted to equilibrium flows. Accounting also for the perturbed case due to finite Re , which has been outlined in general in § 5.2.1, one obtains the appropriate expansions

$$Q = Q_{00} + \mu Q_{01} + \dots + \alpha(Q_{10} + \mu Q_{11} + \dots) + \dots + \frac{\gamma^2}{\alpha\mu^2} \bar{Q}_1 + \dots, \\ \text{with } Q = \Delta, F, T; \quad \delta = \alpha\mu\Delta, \quad f = \eta - \mu F, \quad t = \mu^2 T. \quad (5.30)$$

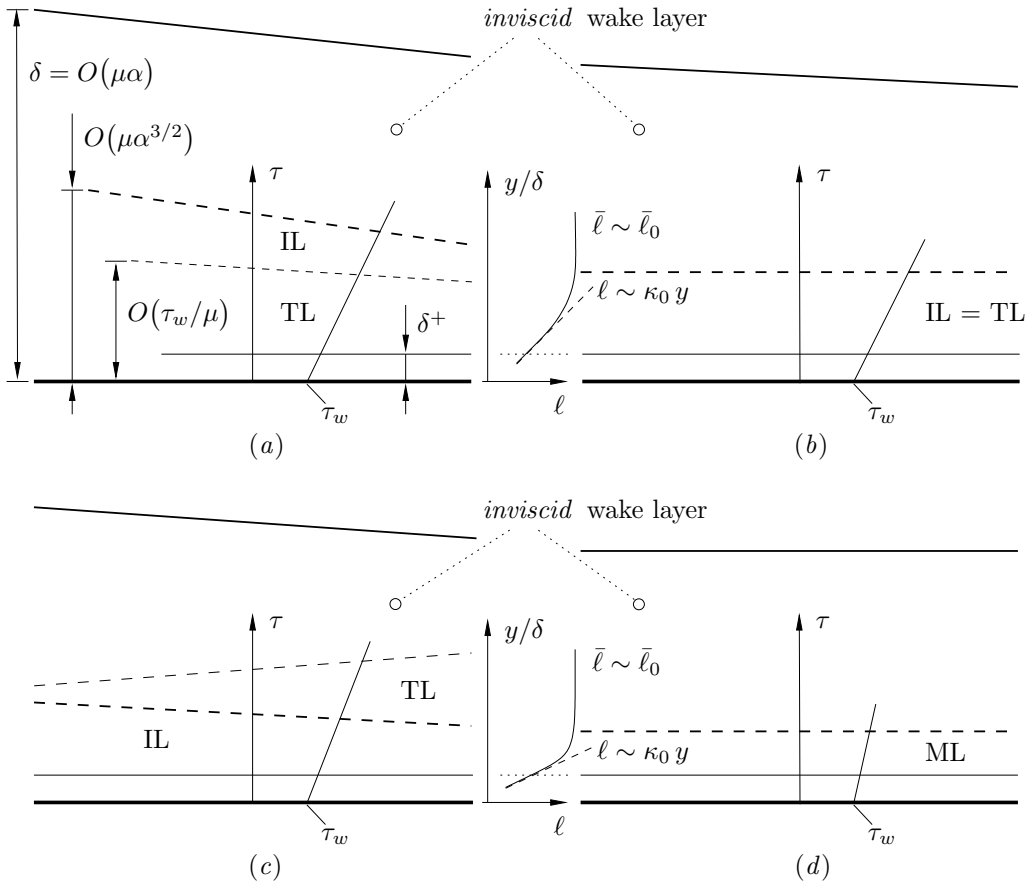


FIGURE 9. Asymptotic boundary layer structure in an adverse pressure gradient if the velocity defect is measured by some small parameter μ , giving rise to the universal scalings of the different layers; IL = *intermediate* layer, TL = *transition* layer, ML = *middle* layer. In the cases (a) $\mu \gg \gamma/\alpha^{3/4}$ and (b) $\mu = O(\gamma/\alpha^{3/4})$ of a ‘moderately’ large defect the transition layer accounts for the linearly varying leading-order distribution of the shear stress given by $\tau = \tau_w + \Lambda_0 y + \dots$, $\Lambda_0 = O(\mu)$; if (c) $\gamma/\alpha^{3/4} \gg \mu \gg \gamma/\alpha^{1/2}$ the inner wake and transition layer have interchanged their position. Finally, if (d) $\mu = O(\gamma/\alpha^{1/2})$ the classical small-defect theory is recovered.

As elucidated previously, contributions of $O(\alpha\mu)$ arise from effects due to Reynolds normal stresses, the pressure gradient perpendicular to the wall as well as the boundary layer displacement. The viscosity-affected term of $O(\gamma^2/(\alpha\mu))$ is attributed to the finite wall shear, cf. (5.23). Thus the quantities Q_{0i} , $i = 0, 1, \dots$ are solely determined by the inviscid shear layer approximation. In turn, the corresponding inner wake expansions, see (5.7) and (5.21), have to be linearized accordingly with respect to μ .

In general $\ell = O(\alpha^{1/2}\delta)$, cf. also (3.21), but the boundary layer thickness is a quantity of $O(\alpha\mu)$. Therefore, in the small-defect case the magnitude of the mixing length ℓ reduces to $O(\alpha\mu^{3/2}\mu)$. The resulting scalings of the particular layers of the linearized four-tiered structure are seen from figure 9 (a).

With regard to the wake flow for finite values of Re , it appears convenient to introduce the asymptotically large Rotta–Clauser parameter β defined through (3.18) and (5.27), in order to provide a coupling

between the independent perturbation parameters α , μ and γ which simplifies the analysis drastically:

$$\beta \equiv -\frac{\delta(1-f_e)U_e U_{e,x}}{\tau_w} = -\frac{\alpha\mu^2}{\gamma^2} \frac{\Delta F_e U_{e,x}}{U_e}.$$

The latter representation is based on the scalings in (5.30) and becomes relevant if $\mu \ll 1$ and the basic requirement (4.4) known from our moderate-defect approach is met. Then β may be expanded as demonstrated in (4.5) if $\bar{\gamma}$ is formally replaced by μ such that $\mu = \gamma(\beta_0/\alpha)^{1/2}$. In the same way the expansions (5.30) supersede (4.3) and the relationships (5.14) are revealed. In particular, from the analysis of the linearized intermediate layer, see §5.1.1, the relationships (5.14) for U_s and Λ immediately follow in the case of a weak wake. For the scalings of the universal transition layer see §4.1.1. Introducing an additional parameter $\Gamma = \mu\beta_0$ by analogy to (4.10c) in order to account for the finite wall shear yields $T_1 \rightarrow 1/\Gamma$ as $\eta \rightarrow 0$.

Therefore, all the results presented in §4 are maintained as far as the magnitude μ of the velocity defect is chosen independently of α and γ . As μ formally takes the place of $\bar{\gamma}$, serving as the principal perturbation parameter if we deal with (quasi-)equilibrium flow, the leading-order contribution μ_1 to μ , see (4.25), is apparently rescaled to 1.

However, the flow in the inviscid outer wake is governed by the moderate-defect problems (4.7) and 4.10, respectively, supplemented with a closure accounting for $\bar{\ell} \rightarrow \bar{\ell}_0$ as $\eta \rightarrow 0$.

We now return to the case of quasi-equilibrium flows, that is $m = -1/3 + \mu$ and $a = \mu\Delta_0 = 3/F_{e0}$, the latter relation follows from (3.18). If $\mu = O(\gamma^{2/3}/\alpha^{1/3})$ or, equivalently, Γ is assumed to be of $O(1)$ the integral momentum balance (5.29) reads in leading order

$$G \sim 9\mu - \gamma^2/(\alpha\mu^2) = \mu(9 - 1/\Gamma).$$

Setting $G = \mu G_0$ and noticing that $\mu_1 = 1$, the condition (4.28) is recovered if the effects gathered in the term II_0^2 are disregarded. In fact, from an inspection of (5.30) they turn out to be by $O(\alpha)$ smaller than it has been the case in §4.3 where α was seen as a parameter of $O(1)$. Finally, applying (4.29) we reveal the fundamental relationship (4.30). Thus the linearized theory allows for a continuation of the nonlinear regime in figure 8 where β , $\Gamma = O(\alpha/\tau_w)$ to the vicinity of the turning point of the curves where $\Gamma = O(1)$. Indeed, we have made up the completion of the bifurcation diagram presented in figure 4 towards large-defect flow.

Considering equilibrium flows, the lower branches of the curves in figure 8 correspond to small values of Γ as pointed out at the end of §4.3. If for a given Re the defect parameter μ falls below a critical magnitude the transition and intermediate layer may coincide, see figure 9 (b). In this case $\beta = O(\alpha^{-1/2})$, and

$$\bar{T}_0 = 1 + \lambda\bar{\eta} = -(\bar{\ell}/\delta_0)^2 |\partial_{\bar{\eta}}\bar{U}_1| \partial_{\bar{\eta}}\bar{U}_1 \quad (5.31)$$

replaces (4.15) and (5.7b). Therefore, the square root law disappears, and the large- $\bar{\eta}$ behaviour in (4.17) is superseded by the small-defect form of (5.9), given by $\bar{U}_1 \sim -(2\delta_0/3\bar{\ell}_0)\lambda^{1/2}\bar{\eta}^{3/2}$. Note that $\bar{\ell}/\delta_0 = O(1)$, independently of μ .

For smaller values of μ the transition layer is governed by (5.31) in the limit $\bar{\ell} \rightarrow \bar{\ell}_0$ in leading order and suppresses the original intermediate layer to a region more close to the wall, see figure 9 (c). The momentum balance holding in the latter region in leading order is obtained formally from (5.31) for $\lambda \rightarrow 0$ and redefining $\bar{\eta} = \eta/\alpha^{1/2}$. This limiting form of the inner wake layer is characterized by approximately

constant shear stress, $\tau \sim \tau_w$, and vanishing convection. Accordingly, one obtains for the velocity profile:

$$F' \sim -C_0(x) - (2\delta_0/3\bar{\ell}_0) + (\gamma/\mu)\bar{U}_1(x, \bar{\eta}), \quad \bar{U}_1 \sim \begin{cases} (\delta_0/\bar{\ell}_0)\bar{\eta} & \dots \bar{\eta} \rightarrow \infty, \\ -\kappa_0^{-1} \ln \bar{\eta} - \bar{C}(x) & \dots \bar{\eta} \rightarrow 0. \end{cases} \quad (5.32)$$

The function $C_0(x)$ is imposed by the outermost layer and shifted by the transition layer as known from the analysis presented in §4.1.1. On the other hand, the contribution $\bar{C}(x)$ to the total slip velocity $U_s \sim U_e - \mu\beta_0^{1/2}(C_0 + 2\delta_0/3\bar{\ell}_0) + \gamma\bar{C}$ induced by the outer wake layer depends on an appropriate model for the mixing length distribution $\bar{\ell}$ as provided by (3.21), for instance.

This structure clearly breaks down if the transition layer merges with the linearized outer wake. This happens if μ approaches its lower limit where $\beta = O(1)$, revealing the classical small-defect structure as depicted in figure 9(d). Now embedded within the nonlinear theory primarily based on the smallness of α it has to be re-interpreted as a three-layered one. Thus $\delta = O(\gamma\alpha^{1/2})$, and the passive inner wake described by (5.32) has a thickness of $O(\gamma\alpha)$. Recalling the results from §3.1.2, this velocity profile, which matches with the linearized outer defect flow in a regular manner and the log-profile in the overlap to the wall layer, may also be obtained from an inspection of (3.12) in the regime where $\eta = O(\alpha^{1/2})$.

6. Separation process

The nonlinear theory developed so far now enables us to study the situation if the wall shear τ_w vanishes for any given high but finite Re : First of all, it immediately follows from (5.20) that the asymptotic structure presented in §5 ceases to be valid as u_τ becomes of $O(Re^{-1/3})$ or $\gamma_s = O(1)$, respectively. That means that then also the slip velocity $U_s(x; \alpha)$ caused by the inviscid wake limit is a quantity of $O(Re^{-1/3})$. Thus in the inviscid limit, $Re^{-1} = 0$, separation is associated with flows that have U_s tending to zero or even its sign changed. Afterwards this inviscid solutions will be perturbed due to finite Re such that τ_w is finite but may change sign, too.

6.1. Inviscid limit: $Re^{-1} = 0$

In contrast to the investigation of self-similar flows in §5.3 we now focus on numerical solutions of the zeroth-order shear layer problem (5.2) by prescribing an appropriate adverse pressure gradient $p_{0,x} = -U_e U_{e,x}$ that drives the boundary layer towards the verge of separation, i.e. $U_s \rightarrow 0$. Since the asymptotic hierarchy of the two-tired wake structure due to the expansions (5.1) and (5.7) ceases to be valid if $U_s = O(\alpha^{3/4})$, a correct treatment of the flow near the wall in that interesting case requires the inviscid wake to comprise both the outer and the inner layer as proposed by the more detailed discussion in §5.1.2. Again, this will be provided by employing the simple closure (3.21) which implicates (5.13) (see also the corresponding considerations for self-preserving flow in §5.3).

We remark that Melnik (1989) considered $u_s \rightarrow 0$ in the outer wake limit $\alpha = 0$ only.

Since the behaviour of the wall slip is qualitatively determined by its zeroth-order approximation $U_s \sim \psi_{0,y}(x, 0)$ even in the case $U_s = O(\alpha^{3/4})$, higher-order perturbations of the inviscid limit according to (5.12a) due to the effects of finite α will be neglected in the following.

6.1.1. Numerical results — marginally separated flow

For adjusting the intensity of the pressure gradient in problem (5.2) the imposed outer-edge velocity U_e is taken to depend on a control parameter termed χ . The specific choice

$$U_e(x; \chi) = (1.0 + x)^m \left[1.0 + \chi (\exp(-5.0 x^2) - 1.0) \right] \quad (6.1)$$

allows for a similarity solution that satisfies (5.26) and thus fixes the exponent m to serve as an initial profile at the location $x = 0$, in order to initiate the marching procedure downstream. The factor in the exponential in (6.1), which controls the bias of U_e with respect to x , as well as the initial values for the wall slip, $U_s = f_0'(0) = 0.76$, and $U_e = 1.0$ at $x = 0$ have been chosen properly, such that the region of separation will be located about $x \approx 1$.

Solving the problem (5.26) gives rise to the eigenvalues $m = p_{0,x}(x = 0) \doteq -0.3147$ and $a = \delta_{0,x}(x = 0) \doteq 1.6019$. In order to obtain suitably scaled solutions the – in principle arbitrary – virtual origin x_o (see §3.1.3) which fixes the initial value for the boundary layer thickness itself, $\delta_0 = \delta_{0,x}(-x_o)$ at $x = 0$, has been set to $1 - f_0'(0)$.

Some peculiarities regarding the marching method adopted for solving (5.2) under the action of a pressure gradient $p_{0,x}(x; \chi)$ determined by (6.1) that arise from the finite boundary thickness $\delta_0(x)$ are pointed out in Appendix B. Distributions for the wall slip U_s associated with solutions of (5.2) for increasing values of χ are plotted in figure 10. Prandtl's mixing length yields the clearly identifiable half-power law (5.11) which holds for small distances from the wall.

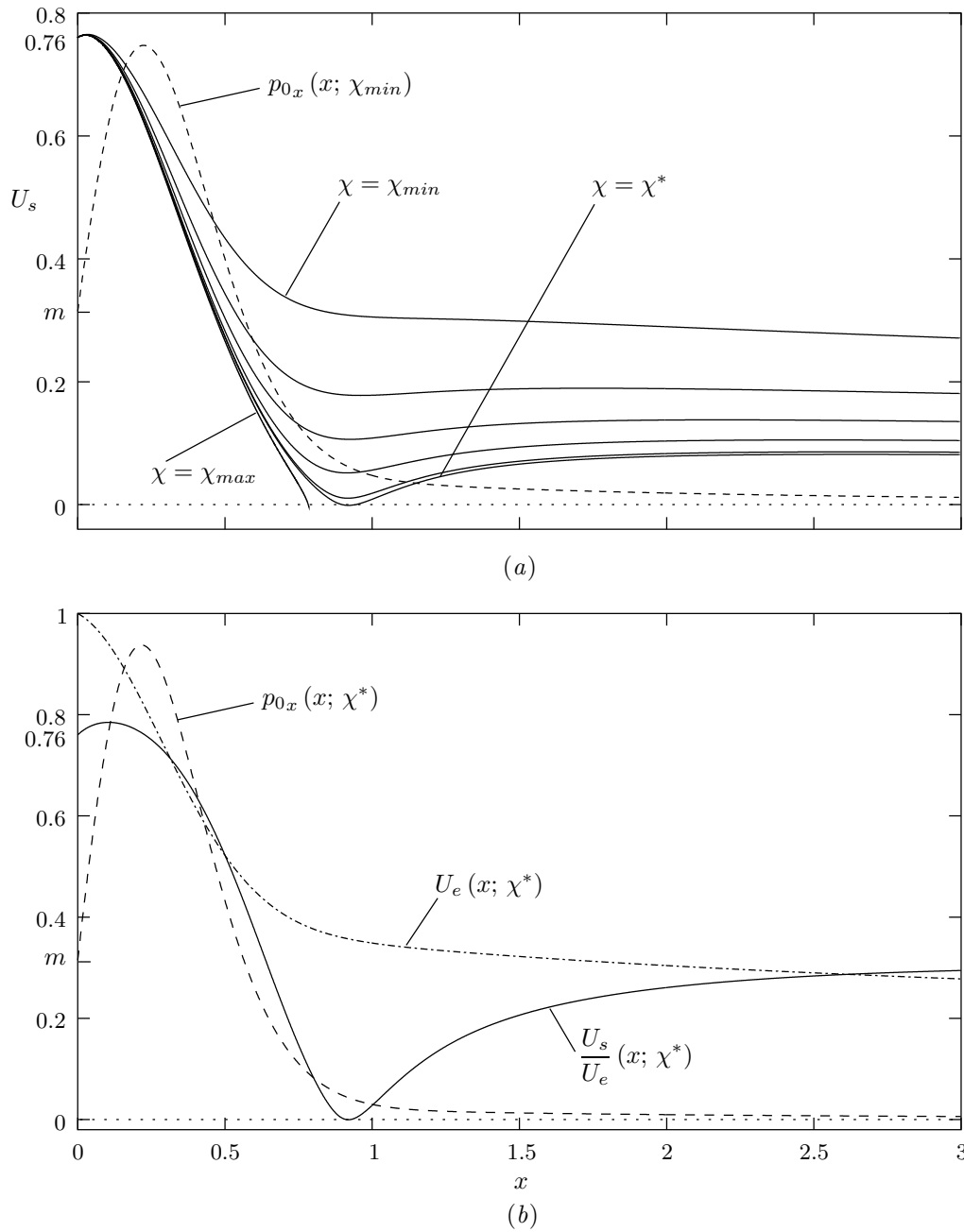


FIGURE 10. (a) Distributions of U_s if the adverse pressure gradient $p_{0x}(x; \chi)$ is intensified according to χ varying from $\chi_{min} = 0.4$, via $\chi = 0.5, 0.54, 0.56, 0.568$, and the critical value $\chi^* \doteq 0.569091$ limiting the existence of continuous solutions up to $\chi_{max} = 0.575$. The latter gives rise to the cutoff-branch which demonstrates breakdown of the calculation. Lower curves correspond to larger values of χ . (b) Related slip velocity U_s/U_e for the case $\chi = \chi^*$.

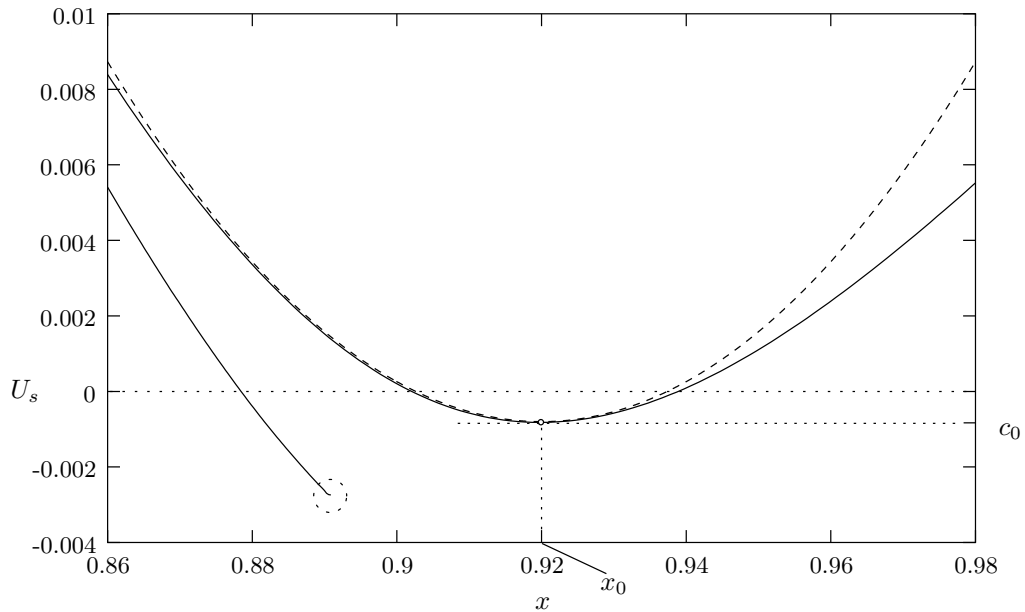


FIGURE 11. Local behaviour of U_s exhibiting backflow. In order to obtain a pronounced separation bubble for $\chi = \chi^*$ the originally fixed step size of 10^{-5} has been increased carefully where U_s changes sign to take on about 10^{-4} at $x = x_0$ and reaches the old value again at the point of reattachment.

If the prescribed pressure gradient is strong enough but χ chosen properly a small reverse-flow eddy arises. The results depicted in figure 10 indicate that converged solutions with negative wall slip can be obtained for a rather narrow range of $\chi \leq \chi^*$ only. However, this difficulty is most probably caused by numerical instabilities associated with the presence of a reversed flow region, as demonstrated by the solution obtained for $\chi = \chi_{max}$ which breaks down suddenly due to the occurrence of strong oscillations where $U_s < 0$. In figure 11 the local numerical distribution of U_s for the critical case $\chi = \chi^*$ is compared with the analytical result (dashed) given by (6.16) for the overall wall slip which results from the local asymptotic analysis of incipient inviscid separation presented in the next section. The minimum value of U_s occurs at $x = x_0 \approx 0.920$.

In the solution for $\chi = \chi_{max}$ exhibiting numerical breakdown in figure 11 the strong oscillating behaviour which starts at the endpoint of the curve within the dashed circle has been displayed here for reasons of lucidity. The failure of the calculations may be shifted to larger values of χ or, for χ held constant, to more negative values of U_s downstream if the step size in x -direction is increased. This undesirable behaviour of the results agrees with the well-known numerical deficiencies of pure downstream-integration schemes to handle the phenomena of non-uniqueness of the exact solution of a boundary layer problem, triggered instantaneously at the origin of a backflow region. We will focus on this matter from an analytical point of view in the next section.

Figure 12 shows the profiles of the corresponding quantities $f_0' = \psi_{0y}/U_e$ and $t_0 = \tau_0/U_e^2$, respectively. The much weaker intensities of the related shear stress t_0 as compared to the self-similar case (see figure 7, *b*) for a given relative wall slip $f_0'(0)$ are clearly visible.

The regular behaviour of solutions obtained within the framework of pure boundary layer theory that exhibit small reversed flow zones strikingly contrasts the case of laminar marginal separation, resulting from a qualitatively similar pressure distribution. This problem was studied by Ruban (1981) and inde-

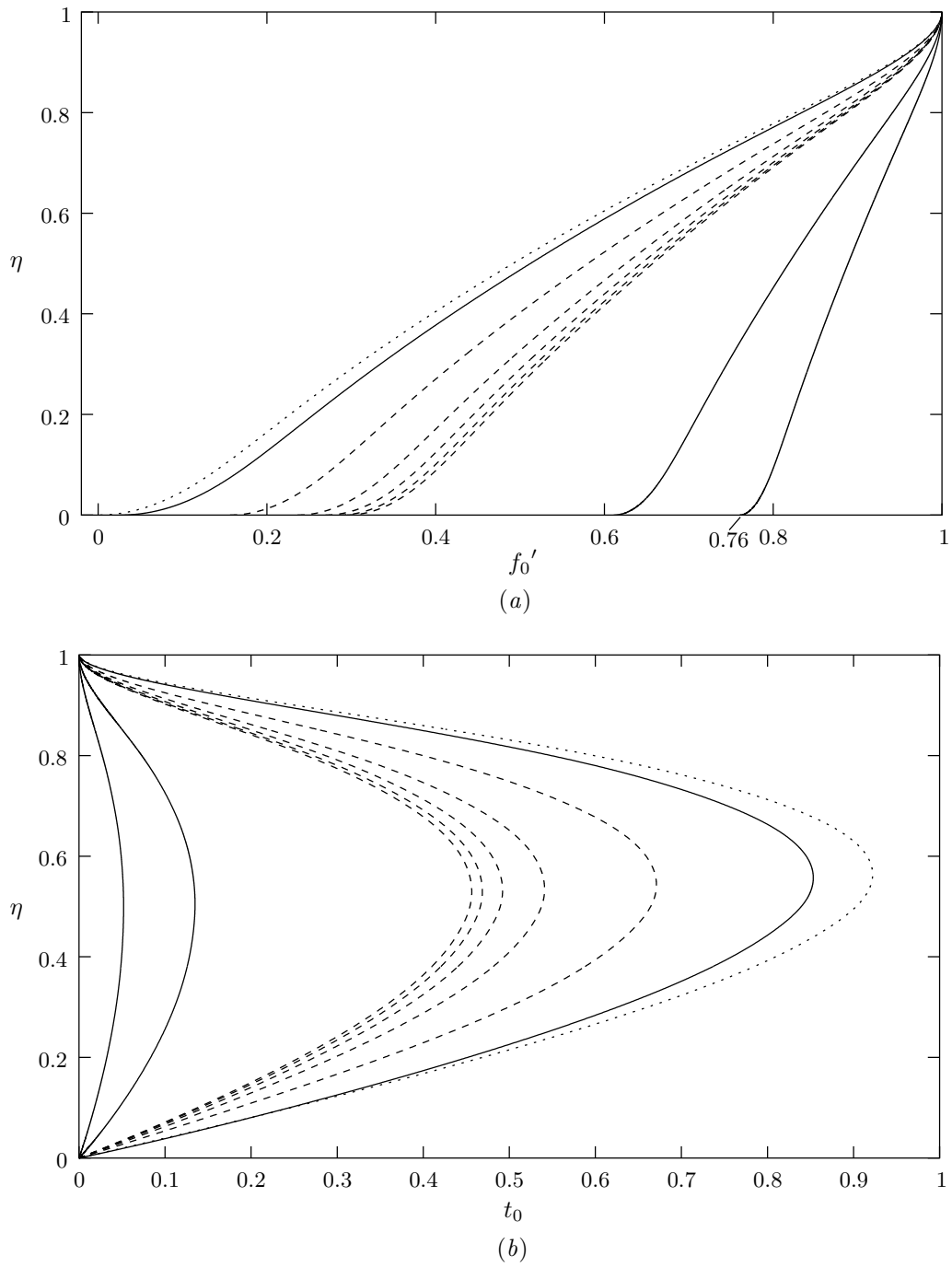


FIGURE 12. Related (a) velocity and (b) shear stress profiles against η at the (equidistantly spaced) locations: $x = 0, x \doteq 3/7, 6/7$ (solid, from the right to the left); $x \doteq x_0$ (dotted, within the reverse-flow region); $x \doteq 9/7, 12/7, 15/7, 18/7, 3.0$ (dashed, from the left to the right).

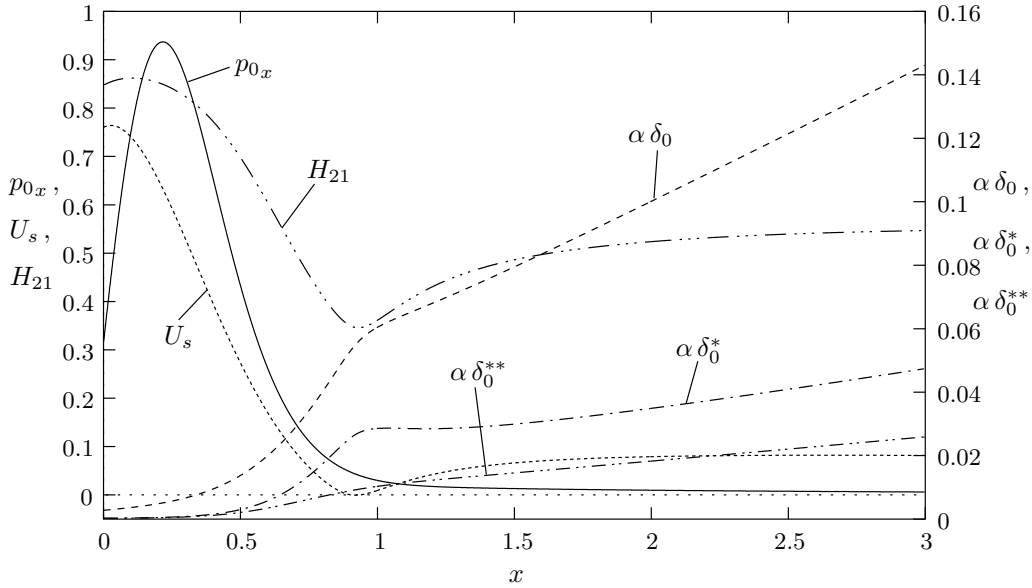


FIGURE 13. Global quantities in the case $\chi = \chi^*$.

pendently by Stewartson, Smith & Kaups (1982) who showed that the boundary layer approximation is rendered invalid due to the occurrence of a weak singularity at the point of vanishing skin-friction if χ exceeds a critical value. Consequently, laminar flow calculations come to an end and cannot be continued into the separated flow regime. In the turbulent case, the perturbation of the regular inviscid solution at incipient separation discussed so far due to high but finite Re is carried out in §6.2. It finally allows for the asymptotic description of marginally separated flow regions within the viscous sublayer as the wall shear stress may change sign.

For the limiting case $\chi = \chi^*$ several global quantities including the leading-order distributions of the displacement and the momentum thicknesses δ_0^* and δ_0^{**} , respectively, and the shape factor $H_{21} = \delta_0^*/\delta_0^{**}$, as defined in (5.27) with respect to the expansion (5.1), are plotted in figure 13. As a consequence of the specific choice of (6.1) the solution exhibits a pronounced relaxing behaviour before it attains its initial similarity form, determining the exponent m in (6.1); cf. also figure 10 (b). (Interestingly, choosing the flat-plate distribution such that $U_e \rightarrow const$ for $x \rightarrow \infty$ would implicate $\psi_{0\bar{y}} \rightarrow U_e$, $\tau_0 \rightarrow 0$ far downstream, i.e. the trivial irrotational solution of problem (5.2a).)

6.1.2. Local analytical solutions for $U_s \rightarrow 0$

In the case we refer to as *marginal* separation the occurrence of a reverse-flow regime is restricted to the viscous wall layer whose thickness is of $O(Re^{-2/3})$. In the inviscid limit, $Re^{-1} = 0$, that small bubble therefore collapses into a single point at the wall, denoted by $x = x_0$: Then U_s vanishes in this point only and is positive up- and downstream, respectively. In the following we shall term this flow situation the ‘critical’ case and the velocity profile at $x = x_0$ a ‘critical’ one. With regard to the numerical results of the last section, this ‘critical’ solution is associated with a pressure gradient fixed by a certain $\chi = \chi_{crit}$ where $\chi_{crit} < \chi^*$.

In order to investigate the numerical results near $\chi = \chi_{crit}$ analytically we seek for local solutions about $x = x_0$ of the boundary layer approximation (5.2) such that both the outer and the inner wake

layer are taken into account as they are again treated as a single layer for a given finite α . Therefore, we let $U_s \rightarrow 0$ for α held fixed. Furthermore, restricting the behaviour of the mixing length for $\bar{y} \rightarrow 0$, α fixed to its leading-order term provided by Prandtl's hypothesis, $\bar{\ell} \sim \kappa \bar{y} / \alpha^{1/2}$, will render the analysis independent of any specific shear stress closure.

Introducing a local streamwise coordinate $s = x - x_0$ the critical limit to be examined may be written as $s \rightarrow 0_{\mp}$, α finite. This solution then has to be perturbed due to small values of $\epsilon = \chi - \chi^*$, measuring the deviation of the imposed pressure gradient from the critical distribution. Therefore, we assume the possibility of only short reverse-flow regions or, equivalently, marginally separated flow which is supported by the numerical results presented in § 6.1.1.

For arbitrarily chosen ϵ we decompose the imposed outer-edge velocity $U_e(x; \chi)$ according to the distribution (6.1) proposed for our numerical example and represent it locally by means of its Taylor expansion:

$$U_e(x; \chi) = U_0(x; \chi^*) + \epsilon U_1(x), \quad U_e = U_{00} + U_{01}s + U_{02}\frac{s^2}{2} + \dots + \epsilon(U_{10} + \dots). \quad (6.2)$$

Bernoulli's law, cf. (5.2a), yields in turn

$$p_{0x} = P_{00}(1 + P_{01}s + \dots) + \epsilon P_{10}(1 + \dots); \\ P_{00} = -U_{00}U_{01}, \quad P_{01} = U_{02}/U_{01} + U_{01}/U_{00}, \quad P_{10} = -U_{00}U_{10}. \quad (6.3)$$

We first assume $\chi = \chi_{crit}$, $\epsilon = 0$. Inspection of the leading-order equation (5.2a) in combination with (5.3) and taking into account Prandtl's law (3.8) then reveals the existence of the flow regimes IIa as depicted in figure 14(a), where all terms in the boundary layer approximation are retained in leading order. The appropriately defined local stream function f and boundary layer coordinate η are regarded as quantities of $O(1)$ there,

$$\psi_0 = \frac{\kappa_0^2 P_{00}^{1/2}}{\alpha} (\mp s)^{3/2} f(\mp s, \eta), \quad \tau_0 = \frac{\kappa_0^2 P_{00}}{\alpha} (\mp s) \eta^2 f''^2; \quad \eta = \frac{\alpha \bar{y}}{\kappa_0^2 (\mp s)}. \quad (6.4)$$

Here and in the following primes denote derivatives with respect to η and the upper and lower signs the up- and downstream case, respectively. However, for the sake of clearness we do not distinguish between these as we use the same notation for the dependent quantities. The substitution (6.4) transforms (5.2a) into

$$\mp \left[\frac{1}{2} f'^2 - \frac{3}{2} f f'' + (\mp s) (f' \partial_{(\mp s)} f' - f'' \partial_{(\mp s)} f) \right] = -(1 + P_{01}s + \dots) + (\eta^2 f''^2)'. \quad (6.5)$$

Equation (6.5) has to be supplemented with the inviscid boundary conditions following from (5.2b),

$$\eta \rightarrow 0: \quad f \rightarrow 0, \quad \eta f'' \rightarrow 0. \quad (6.6)$$

In turn, they imply the square root law in the behaviour for the related velocity profile f' near the wall.

In the limit $s = 0$ the boundary layer problem given by (6.6) and (6.6) reduces to

$$\mp \left(\frac{1}{2} f_0'^2 - \frac{3}{2} f_0 f_0'' \right) = -1 + (\eta^2 f_0''^2)', \quad f_0 \sim C \eta^{3/2} \quad \text{as } \eta \rightarrow \infty. \quad (6.7)$$

The condition at infinity with any $C = O(1)$ results from the match to the solution at $s = 0$ in the outer flow regime Ia, where \bar{y} is regarded to be of $O(1)$ due to the scaling of ψ_0 given in (6.4). Numerical integration of this nonlinear equation, initialized by the lower boundary conditions (6.6) but arbitrary slip $f_0'(0)$, suggested that the simple solution

$$f_0 = \frac{4}{3} \eta^{3/2} \quad (6.8)$$

is the only one with non-exponential growth. Thus it is unique with regard to the upstream side, i.e. for

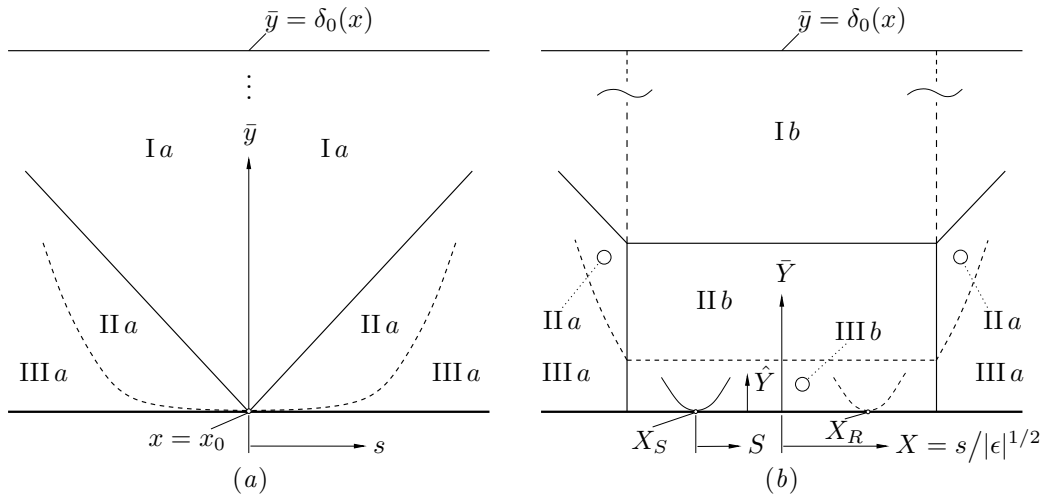


FIGURE 14. Local asymptotic structure at separation in the limit $Re^{-1} = 0$: (a) for $\epsilon = 0$, (b) for finite ϵ .

the upper sign holding on the left-hand side in (6.7). Studying the downstream case, any non-negative $f_0'(0)$ implies algebraic behaviour for $\eta \rightarrow \infty$ in (6.7) but (6.8) only then matches to the critical profile of the streamfunction at $s = 0$. So it constitutes the basic solution we shall linearize about on both the up- and downstream side. (Note the square root singularity $U_s \sim f_0'(0)(\mp P_{00}s)^{1/2}$ which would occur in the case of positive $f_0'(0)$.)

Therefore, both sides of (6.7) vanish identically and the critical near-wall profile at $x = x_0$ is characterized by a shear stress gradient balancing the local pressure gradient or, equivalently, vanishing inertia terms. As a consequence from (6.8), any region emerging for small values of η turns out to be passive as the flow there is governed by the simple balance of the gradient of τ_0 and P_0 in leading order at vanishing convection.

As $s \rightarrow 0_{\mp}$, we expect an asymptotic expansion of the solution in regions II a of the form

$$f = f_0(\eta) + (\mp s)^\lambda f_\lambda(\eta) + (\mp s)^{2\lambda} f_{2\lambda}(\eta) + \dots + P_{01}s f_{01}(\eta) + \dots + \varphi(\mp s)f_0'(\eta) + \dots \\ + \epsilon \left[(\mp s)^\mu g_\mu(\eta) + (\mp s)^{\mu+\lambda} g_{\mu+\lambda}(\eta) + \dots + P_{10}/P_{00} f_{10}(\eta) + \dots \right] + \epsilon^2 (\mp s)^{2\mu} g_{2\mu}(\eta) + \dots \quad (6.9)$$

with the real exponents λ, μ to be determined. The latter arises due to some, for the present unknown, disturbance of the strength ϵ evoking locally an eigensolution g_μ which satisfies the linearized boundary layer operator. As will turn out below, see § 6.2, such a perturbation leads to a breakdown of the similarity structure. Thus we first treat the undisturbed solution, i.e. the case $\epsilon = 0$, and discuss the perturbed one afterwards. The regular series in (6.9) with the coefficient functions f_{ij} , $i, j = 0, 1, \dots$ is caused by the expanded Bernoulli's law given by (6.3).

Of course, the operator in (6.5) linearized about $f = f_0$ allows for the occurrence of eigensolutions of the form $\varphi(\mp s)f_0'$ as stated in (6.9) where the in principle arbitrary function $\varphi(\mp s)$ is considered to be asymptotically small in the regions II a, which dominate the oncoming-flow structure, see figure 14. Note that such perturbations do not satisfy the second boundary condition given in (6.6) as they give rise to a constant shear stress in the regimes II a. However, in the following the expansion (6.9) will turn out to be rendered invalid in the regions III a where $(\mp s)^\lambda f_\lambda$ becomes of the same magnitude as f_0 . Therefore, an eigensolution governed by $f_0' = 2\eta^{1/2}$ must apparently be caused by the solution to a problem resulting from a linearization about the leading-order term of the corresponding expansion holding in the latter

region. In fact, the analysis below will show the existence of disturbances with φ varying exponentially with s .

Inserting the expansion (6.9) into (6.5) yields the set of equations

$$\eta^2 h''' + \left(\frac{3}{2}\eta \mp \eta^2\right) h'' \pm (1 + \nu) \eta h' \mp \left(\frac{3}{4} + \frac{\nu}{2}\right) h = 0, \quad h = f_\lambda, g_\mu, \quad \nu = \lambda, \mu; \quad (6.10a)$$

$$\begin{aligned} \eta^2 f_{2\lambda}''' + \left(\frac{3}{2}\eta \mp \eta^2\right) f_{2\lambda}'' \pm (1 + 2\lambda) \eta f_{2\lambda}' \mp \left(\frac{3}{4} + \lambda\right) f_{2\lambda} = \\ \frac{\eta^{1/2}}{2} \left[\mp \left(\frac{1}{2} + \lambda\right) f_\lambda'^2 \pm \left(\frac{3}{2} + \lambda\right) f_\lambda'' f_\lambda - \left(\eta^2 f_\lambda''^2\right) \right]; \end{aligned} \quad (6.10b)$$

$$\eta^2 f_{ij}''' + \left(\frac{3}{2}\eta \mp \eta^2\right) f_{ij}'' \pm (1 + j) \eta f_{ij}' \mp \left(\frac{3}{4} + \frac{j}{2}\right) f_{ij} = \frac{\eta^{1/2}}{2}, \quad i, j = 0, 1. \quad (6.10c)$$

The linear equations (6.10) have to be subjected to the accordingly expanded homogeneous boundary conditions (6.6) and to the requirement of non-exponential growth as $\eta \rightarrow \infty$ in order to allow for a match with the solution in region Ia (figure 14), comprising the main part of the boundary layer. Considering the problem (6.10a), it is shown in Appendix C that the eigenvalues ν then have to satisfy the solvability condition (C2), causing the homogeneous solution h to be a polynomial of degree $\nu + 3/2 = n + 1$ where $n = 0, 1, 2, \dots$. Therefore, the exponents take on their minimum values for $\lambda = 3/2$ and $\mu = -1/2$, giving rise to the first eigensolutions

$$f_{\frac{3}{2}} = c_0 (\eta \mp \eta^2/3 + \eta^3/30), \quad g_{-\frac{1}{2}} = c_1 \eta. \quad (6.11)$$

Eigensolutions belonging to larger values of λ and μ and, as a consequence, weaker perturbations in (6.9) of the critical solution f_0 influence the flow only quantitatively and thus will be disregarded. Clearly, the coefficients c_0 and c_1 are reckoned as quantities of $O(1)$ as they have to be considered as functions of α and, reflecting the dependency of the local solutions on the upstream history, on χ_{crit} .

Taking into account the general form of the polynomial f_λ , the bracketed term on the right-hand side of (6.10b) turns out to be a polynomial in η of degree $2\lambda = 2n - 1$, i.e. of third degree in the interesting case $\lambda = 3/2$. Accordingly, the nonlinearities in (6.5) are responsible for the further inhomogeneous equations

$$\eta^2 g_1''' + \left(\frac{3}{2}\eta \mp \eta^2\right) g_1'' \pm 2\eta g_1' \mp \frac{5}{4} g_1 = \eta^{1/2} \left(\mp 2 + \frac{2}{3}\eta\right), \quad \eta^2 g_{-1}''' + \left(\frac{3}{2}\eta \mp \eta^2\right) g_{-1}'' \mp \frac{1}{4} g_{-1} = 0.$$

As the homogeneous parts of these problems and problem (6.10b) given by (6.10a) for $\nu = 1, -1$ and $\nu = 2\lambda$ contradict the solvability condition (C2) their homogeneous solutions as pointed in Appendix C have to be discarded. However, particular solutions satisfying the expanded boundary conditions (6.6) are found to be

$$f_3 = c_0^2 \eta^{3/2} \left(\mp \frac{4}{3} + \frac{14}{27}\eta \mp \frac{26}{405}\eta^2 + \frac{76}{42525}\eta^3\right), \quad g_1 = c_0 c_1 \eta^{3/2} \left(\mp \frac{4}{3} + \frac{2}{9}\eta\right), \quad g_{-1} = 0.$$

The solutions of the corresponding higher-order equations are pure polynomials, too. By analogy, the solutions to (6.10c) read

$$f_{01} = \frac{2}{3} \eta^{3/2} \left(1 \mp \frac{2}{15}\eta\right), \quad f_{10} = \frac{2}{3} \eta^{3/2}. \quad (6.12)$$

It should be noted that from an inspection of (6.5) one might propose a generalized ansatz for the perturbation functions in (6.9) of the form

$$(\mp s)^\nu \ln^\sigma (\mp s) h(\eta)$$

with some real σ : This leaves the homogeneous equation (6.10a) unchanged but causes a term of $O((\mp s)^\nu \ln^{\sigma-1} (\mp s))$, governed by equation (6.10a) which now exhibits the inhomogeneity $\pm \sigma (\eta h' - h/2)$

on the right-hand side. With respect to the analysis presented in Appendix C, we denote the contribution of highest degree to the homogeneous solution h with $d\eta^{n+1}$, $n = 0, 1, 2, \dots$, such that the monomial of highest degree in the inhomogeneous term reads $\pm\sigma d(n+1/2)\eta^{n+1}$. It may be shown that it gives rise to a particular solution growing exponentially as $\eta \rightarrow \infty$. Thus σ must be zero and logarithmically varying disturbances have to be excluded.

The results quoted so far give rise to the (primarily) regular expansion of the solution in the outer main part *Ia* of the boundary layer,

$$q_0 = q_{00}(\bar{y}) + s q_{01}(\bar{y}) + \frac{s^2}{2} q_{02}(\bar{y}) + \dots + \epsilon(q_{10}(\bar{y}) + \dots) + \epsilon^2(q_{20}(\bar{y}) + \dots) + \dots, \quad \text{with } q_0 = \psi_0, \tau_0. \quad (6.13)$$

We note that the class of general eigensolutions mentioned before will induce also terms of the form $\mp s\varphi(\mp s)(\kappa_0^2/\alpha)\psi_{00}'$ in the expansion of the stream function. Using the original variable $y = \alpha\bar{y}$, matching with the sublayer solutions (6.8), (6.11) yields the small- \bar{y} behaviour of the separating profiles given by $q_{00} + \epsilon q_{10} + O(\epsilon^2)$ at the critical point $s = 0$:

$$\begin{aligned} \psi_{00} &= \frac{P_{00}^{1/2}}{\alpha} \left(\frac{4}{3} \frac{y^{3/2}}{\kappa_0} + \frac{4}{45} \frac{P_{01}}{\kappa_0^3} \frac{y^{5/2}}{\kappa_0^3} + \frac{c_0}{30} \frac{y^3}{\kappa_0^4} + O(y^4) \right), \\ \tau_{00} &= \frac{P_{00}}{\alpha} \left(y + \frac{2}{3} \frac{P_{01}}{\kappa_0^2} \frac{y^2}{\kappa_0^2} + \frac{2}{5} \frac{c_0}{\kappa_0^3} \frac{y^{5/2}}{\kappa_0^3} + \frac{P_{01}^2}{9} \frac{y^3}{\kappa_0^4} + O(y^{7/2}) \right); \end{aligned} \quad (6.14a)$$

$$\begin{aligned} \psi_{10} &= \frac{P_{00}^{1/2}}{\alpha} \left(c_1 y + \frac{2}{3} \frac{P_{10}}{P_{00}} \frac{y^{3/2}}{\kappa_0} + \frac{2}{9} \frac{c_0 c_1}{\kappa_0^3} \frac{y^{5/2}}{\kappa_0^3} + O(y^{7/2}) \right), \\ \tau_{10} &= \frac{P_{10}}{\alpha} y + \frac{c_0 c_1 P_{00} + P_{01} P_{10}}{3\alpha} \frac{y^2}{\kappa_0^2} + \frac{c_0 P_{10}}{5\alpha} \frac{y^{5/2}}{\kappa_0^3} + O(y^3). \end{aligned} \quad (6.14b)$$

Higher-order terms not quoted explicitly result from weaker eigensolutions, see Appendix C. Inserting (6.13) into (5.2a) shows that in regime *Ia* the flow is locally dominated by inertia. The solutions for the next terms in the expansion of ψ_0 then read

$$\left. \begin{aligned} \frac{\psi_{01}}{\psi_{00}'} &= \int_0^{\bar{y}} \frac{-P_{00} + \tau_{00}'(z)}{\psi_{00}'(z)^2} dz, & \frac{\psi_{11}}{\psi_{00}'} &= \int_0^{\bar{y}} \frac{-P_{10} + \tau_{10}'(z)}{\psi_{00}'(z)^2} dz, \\ \frac{\psi_{02}}{\psi_{00}'} &= \int_0^{\bar{y}} \frac{-P_{01} + \tau_{01}'(z) - \psi_{01}'(z)^2 + \psi_{01}(z)\psi_{01}''(z)}{\psi_{00}'(z)^2} dz, & \frac{\psi_{21}}{\psi_{00}'} &= \int_0^{\bar{y}} \frac{\tau_{20}'(z)}{\psi_{00}'(z)^2} dz; \end{aligned} \right\} \quad (6.15)$$

corresponding formulas are found for the higher-order contributions. Note that terms q_{20} are caused solely by the nonlinear expression for the shear stress arising from Prandtl's mixing length.

Indeed, expanding the boundary layer thickness $\delta_0(x)$ according to (6.13), using the boundary conditions given in (5.2b) and applying Bernoulli's law (6.3) to (6.15) yields $\psi_{00\bar{y}} = U_{00}$, $\psi_{01\bar{y}} = U_{01}$, $\tau_{00} = \tau_{01} = 0$, and so on at $y = \delta_{00}$. In turn, the conditions $\psi_{00\bar{y}\bar{y}} = \psi_{00\bar{y}\bar{y}} = \tau_{00\bar{y}} = \tau_{01\bar{y}} = U_{01}$, etc. providing the aforementioned continuous patching to the irrotational outer flow are revealed.

From combining (6.4), (6.9) and (6.11) we obtain for the slip velocity given by $U_s = \psi_{0\bar{y}}$ at $\bar{y} = 0$ within the pure boundary layer approximation adopted here

$$U_s \sim P_{00}^{1/2}(\mp s)^{1/2} f'(\mp s, 0) = P_{00}^{1/2} \left(c_0 s^2 + \epsilon c_1 + O(s^3) \right), \quad (6.16)$$

higher order contributions result primarily from the weaker eigensolutions for larger values of λ . From a careful analysis of the numerical results obtained by replacing κ_0 with $\kappa_\infty = 0.59$ in the case $\chi = \chi^* = \chi_{crit} + \epsilon$ the values $c_0 \approx 2.647$ and $\epsilon c_1 \approx -8 \times 10^{-4}$ for the constant shift in the wall slip distribution are detected. This in turn allows for sketching the dashed parabola representing (6.16) in figure 11. Due

to the influence of higher order effects as well as the numerical difficulties associated with the problem of non-unique solutions (treated below) occurring in the backflow region the measured values for c_0 and c_1 , respectively, have to be accepted with some reservation. However, the discrepancy between the asymptotic solution and the branch obtained numerically reflecting this uncertainty is seen to be weak, at least as far as the solution upstream of $x = x_0$ is concerned.

The asymptotic picture of the flow pointed out so far is based on the assumption $(\mp s) \gg \epsilon$. Then (passive) sublayers denoted by III *a* in figure 14 are recognized where $\eta = O(c_0^2 s^3)$ and $f_0 = O(U_s)$. That means that there the leading-order disturbance described by f_λ in (6.9) has the same magnitude as the critical solution f_0 or, equivalently, the wall slip becomes of the same order as the square root part of the inviscid velocity profile near the wall. Introducing an appropriate coordinate $\bar{\eta}$,

$$\eta = c_0^2 (\mp s)^3 \bar{\eta},$$

the solution in these regions behaves as

$$f = c_0^3 (\mp s)^{9/2} (\bar{f}_0 + O(\mp s)) + \epsilon c_1 c_0^2 (\mp s)^{5/2} \bar{\eta} + \dots, \quad \bar{f}_0 = \frac{4}{3} \bar{\eta}^{3/2} + \iota \bar{\eta} \quad \iota = +1. \quad (6.17)$$

With regard to (6.5), the convective part becomes of $O((\mp s)^3)$. However, eigensolutions denoted by $\bar{g}(\bar{\eta})$ which emerge in regions III *a* due to a linearization about the leading-order term \bar{f}_0 of the stream function are only possible if their derivatives with respect to $(\mp s)$ dominate over the linearized inertia terms. In fact, adding a perturbation of the form

$$(\mp s)^\nu \exp\left(-\omega / (3(\mp s)^3)\right) (\bar{g}(\bar{\eta}) + (\mp s) \bar{h}(\bar{\eta}) + \dots), \quad (6.18)$$

where ν, ω are real and higher-order contributions account for the nonlinearities in (6.5), to (6.17) and inserting (6.18) into (6.5) gives rise to the leading-order problem

$$\omega \left[\bar{\eta}^{-1/2} \bar{g} - (2\bar{\eta}^{1/2} + \iota) \bar{g}' \right] = 2(\bar{\eta}^{3/2} \bar{g}'')'; \quad \bar{\eta} \rightarrow 0 : \bar{g} \rightarrow 0, \quad \bar{\eta} \bar{g}'' \rightarrow 0, \quad \bar{\eta} \rightarrow \infty : \bar{g} = 0(\bar{\eta}^{1/2}). \quad (6.19)$$

with $\iota = +1$. The requirement of dominating inertia terms at infinity now corresponds with the aforementioned appearance of eigensolutions of the form $\varphi(\mp s) f_0'$ in the flow regimes II *a*, see (6.9), in turn yielding the aforementioned exponential dependency of φ on $\mp s$. As outlined in Appendix C, non-trivial solutions to (6.19) with non-exponential growth as $\bar{\eta} \rightarrow \infty$ exist only for all $\omega \geq 0$. These solutions show a finite, in principle arbitrary slip $\bar{g}'(0) = \bar{g}'_0 + \epsilon \bar{g}'_1 + O(\epsilon^2)$ which is assumed to exhibit further dependencies on ω as well as on the upstream history. The continuous spectrum of the eigenvalue problem (6.19) allows for an exponentially small overall disturbance $\int_0^\infty (\mp s)^{\nu(\omega)} \exp(-\omega / (3(\mp s)^3)) \bar{g}(\bar{\eta}) d\omega$, $\mp s$ small, of the stream function. Without going into detail, we note that the dependency of ν on ω is fixed by the inhomogeneous next-order problem determining $\bar{h}(\bar{\eta})$. However, as a result, the local wall slip distribution is indeed primarily governed by the regular expansion (6.16).

6.1.3. Reverse-flow regime — multiple solutions

An apparent breakdown of the structure presented so far is encountered if $\epsilon = O(U_s)$, i.e. $s^2 = O(\epsilon)$. Then $(\mp s)^{3/2} f_{\frac{3}{2}}$ and $\epsilon(\mp s)^{-1/2} g_{-\frac{1}{2}}$ become of the same magnitude in (6.9), and the sublayer expansion (6.17) ceases to be valid. Introducing stretched quantities

$$X = \frac{s}{|\epsilon|^{1/2}}, \quad \bar{Y} = \frac{\alpha}{\kappa^2} \frac{\bar{y}}{|\epsilon|^{1/2}}; \quad \bar{\Psi} = \frac{\alpha}{\kappa^2 P_{00}^{1/2}} \frac{\psi_0}{|\epsilon|^{3/4}} \quad (6.20)$$

accounts for the emerging flow regime II *b* as depicted in figure 14 (*b*). Note that here and in the following κ_0 has been replaced by its generalized form $\kappa(K)$ in consideration of the coupling between ϵ and

Re performed in § 6.2 below: This distinct limit will be associated with finite values of the Bradshaw parameter K defined by (3.5) which then becomes of $O(1)$.

From (6.5) and (6.6) one obtains the boundary layer problem

$$\left. \begin{aligned} \Psi_{\bar{Y}} \Psi_{\bar{Y}X} - \Psi_X \Psi_{\bar{Y}\bar{Y}} &= -(1 + |\epsilon|^{1/2} P_{01} X + \dots) + (\bar{Y}^2 \Psi_{\bar{Y}\bar{Y}^2})_{\bar{Y}}; \\ \bar{Y} \rightarrow 0 : \Psi &\rightarrow 0, \quad \bar{Y} \Psi_{\bar{Y}\bar{Y}} \rightarrow 0. \end{aligned} \right\} \quad (6.21)$$

Again, it has to be supplemented with the condition of non-exponential growth as $\bar{Y} \rightarrow \infty$, in order to allow for a match with the solution in the main region I *b*, see figure 14 (*b*). Inserting the appropriate expansion

$$\Psi = \Psi_0 + |\epsilon|^{1/2} \Psi_1 + |\epsilon|^{3/4} \Psi_2 + |\epsilon|^{5/4} \Psi_3 + \dots + \Phi(X) \Psi_{0\bar{Y}} + \dots, \quad (6.22)$$

cf. (6.9), into (6.21) and matching with the solution in the upstream region II *a* characterized by $X \ll -1$ gives rise to the simple polynomial solutions

$$\Psi_0 = \frac{4}{3} \bar{Y}^{3/2}, \quad \Psi_1 = P_{01} \left(\frac{2X}{3} \bar{Y}^{3/2} + \frac{4}{45} \bar{Y}^{5/2} \right), \quad \Psi_2 = \text{sgn}(\epsilon) c_1 \bar{Y} + c_0 \left(X^2 \bar{Y} + \frac{X}{3} \bar{Y}^2 + \frac{1}{30} \bar{Y}^3 \right), \quad (6.23)$$

cf. (6.8), (6.12) and (6.11). The expansion for the region I *b* is then found if s is replaced by $|\epsilon|^{1/2} X$ in (6.13), whereas the corresponding solutions (6.14) and (6.15) remain unchanged. The same holds for the (passive) region III *b* and the according expansion (6.17). Accordingly, the asymptotically correct form of (6.16) is also obtained by means of this simple transformation, i.e.

$$U_s \sim |\epsilon|^{1/4} P_{00}^{1/2} \Psi_{\bar{Y}}|_{\bar{Y}=0} = |\epsilon| P_{00}^{1/2} \left(c_0 X^2 + \text{sgn}(\epsilon) c_1 + O(\epsilon^{3/2}) \right). \quad (6.24)$$

Therefore, the regimes denoted by *b* which reflect the breakdown of the similarity structure due to the deviation from the critical state of flow given by $\epsilon = 0$ turn out to be passive ones as the solutions therein match term by term with their oncoming counterparts. Thus matching with the solutions holding in the emerging downstream regions also denoted by *a* appears to be a self-consistent process, too.

For $\epsilon < 0$ the slip velocity U_s is shifted towards positive values at $X = 0$, see (6.24). Note that c_1 which depends solely on χ_{crit} is apparently negative. In the opposite case $\epsilon > 0$ the flow separates at $X = X_S \sim -(-c_1/c_0)^{1/2}$ with respect to the solution $\Psi_1(X, Y)$ in (6.23) and reattaches at $X = X_R \sim (-c_1/c_0)^{1/2}$, cf. figure 14 (*b*). Let

$$\hat{Y} = \bar{Y}/|\epsilon|^{3/2}$$

denote a wall coordinate suitable for the sublayer III *b*, the separating streamline bounding the recirculation regime occurring in that region reads $\hat{Y} \sim (9/16)(c_1 + c_0 X^2)^2$.

Recalling the analysis of the subregions III *a* carried out in the previous section, the perturbations $\Phi(X) \Psi_{0\bar{Y}}$ in (6.22) are at first induced by the family of exponentially varying eigensolutions which are obtained by applying the transformation (6.20) to (6.18). However, in order to investigate the excitement of further eigensolutions, in particular if they are issuing from the separation point $X = X_S$ into the reverse-flow region, an additional analysis is seen to be necessary accounting for the limit $X \rightarrow X_S$, ϵ kept fixed. To this end, we define a rescaled wall slip \bar{U}_S and appropriate local variables

$$S = X - X_S; \quad \bar{\eta} = \bar{Y}/|\bar{U}_S|^2, \quad \bar{U}_S = \Psi_Y|_{\bar{Y}=0} \sim -2\epsilon^{3/4}(-c_1 c_0)^{1/2} S,$$

see the corresponding flow regimes sketched in figure 14 (*b*). There the unperturbed regular solution behaves as

$$\Psi = |\bar{U}_S|^3 \left[\bar{f}_0 + \left(\frac{2}{3} \bar{\eta}^{3/2} - \frac{1}{6} \bar{\eta}^2 \right) \bar{S} + O(\bar{S}^2, \epsilon^{1/2}) \right]; \quad \bar{f}_0 = \frac{4}{3} \bar{\eta}^{3/2} - \bar{\eta}, \quad \bar{S} = -4\epsilon^{3/2} c_1 c_0 S. \quad (6.25)$$

An inspection of the boundary layer equation (6.21) then suggests a further class of possible eigensolutions

given by

$$\bar{S}^\nu \exp(\omega/\bar{S}) (\bar{g}(\bar{\eta}) + \bar{S} \bar{h}(\bar{\eta}) + \dots), \quad (6.26)$$

by analogy to (6.18). In order to maintain a linearization and to prevent an unacceptable breakdown of the undisturbed asymptotic structure as S approaches zero, we require $\omega/S < 0$. Inserting (6.26) into (6.21) gives rise to (6.19) with the difference that $\iota = -1$ now. Clearly, the discussion of the problem presented in Appendix C recovers the continuous spectrum given by $\omega \geq 0$ describing oncoming perturbations at the upstream side. Interestingly, it also reveals the existence of a one-parametric family of solutions parametrized by $\bar{g}'(0)$ for the distinct value $\omega = -9$, excited instantaneously at $S = 0_+$.

Note that these exponentially weak downstream disturbances exhibit vanishing derivatives with respect to S in any order at $S = 0$, allowing for a patching with the upstream solution at the separating point, independently of the specific choice of $\bar{g}'(0)$. This indetermination or non-uniqueness explains the occurrence of the numerical difficulties we faced in § 6.1.1.

The solution of (6.19) in the case $\omega = -9$, $\iota = -1$ is found in closed form (cf. Appendix C),

$$\bar{g}(\bar{\eta}) = \bar{g}'(0) \left[1 - 2\bar{\eta}^{1/2} - (1 + 4\bar{\eta}^{1/2}) \exp(-6\bar{\eta}^{1/2}) \right] / 6. \quad (6.27)$$

Making use of the regular expansion (6.25) and inserting (6.26) into (6.21) yields the inhomogeneous problem for the next order governed by $\bar{h}(\bar{\eta})$, which determines the exponent ν of the algebraically varying portion of the leading-order perturbation:

$$\begin{aligned} \omega \left[\bar{\eta}^{-1/2} \bar{h} - (2\bar{\eta}^{1/2} - 1) \bar{h}' \right] &= 2(\bar{\eta}^{3/2} \bar{h}'')' \\ -\bar{g}'(0) \bar{\eta}^{-1/2} \left[1/9 - \exp(-6\bar{\eta}^{1/2}) (1/9 + (\nu - 11/6) \bar{\eta}^{1/2} - (4\nu - 31) \bar{\eta} - 36\bar{\eta}^{3/2}) \right] &; \\ \bar{\eta} \rightarrow 0 : \bar{h} \rightarrow 0, \quad \bar{\eta} \bar{h}'' \rightarrow 0, \quad \bar{\eta} \rightarrow \infty : \bar{h} &= 0(\bar{\eta}^{1/2}). \end{aligned} \quad (6.28)$$

A particular solution is apparently possible only if the eigenvalue ν takes on the value $1/3$, see also Appendix C. For the sake of completeness, it is written as

$$\bar{h}(\bar{\eta}) = \bar{g}'(0) \left[-105 + 194\bar{\eta}^{1/2} + \exp(-6\bar{\eta}^{1/2}) (105 + 436\bar{\eta}^{1/2} + 582\bar{\eta} - 648\bar{\eta}^{3/2}) \right] / (3 \times 648). \quad (6.29)$$

For reasons becoming clear in the subsequent section examining the downstream propagation of the two types of eigensolutions represented by (6.18) and (6.26) towards the backflow region where $X - X_s = O(1)$ does not seem relevant for the further analysis. We only mention that no more eigensolutions are triggered at the point of reattachment. The respective investigation for $X \rightarrow X_R$ is almost identical to the one at separation inasmuch as it leads to (6.19) again, but for the case $\iota = +1$.

6.2. Accounting for finite Re

The asymptotic picture pointed out above describing solutions on the verge of separation of the boundary layer approximation (5.2), where $U_s = O(\epsilon)$ depends on the strength of the local pressure gradient, has to be perturbed in order to account for the effect of finite values of Re . Since α is held fixed, the limit process to be examined is given by $U_s \rightarrow 0$ as $Re \rightarrow \infty$, which in turn implies a meaningful coupling between U_s , thus ϵ , and Re , allowing for a definition of marginal separation in an asymptotic sense.

The descriptions of the viscous wall layer, see § 3.1.1, as well as the transition layer elucidated in § 5.2 remain upright as long as $\gamma_s = u_\tau/U_s \ll 1$. These two layers emerging in the case of finite Re perturb the local asymptotic structure for $x \rightarrow x_0$ of the inviscid wake, which is recalled by means of figure 15 (a) for ϵ assumed to be finite. Therefore, expanding the induced disturbances evoked by transition layer solution, see the large- ζ behaviour in (5.18), as has been discussed in § 5.2.1 in terms of small U_s and adopting the similarity transformation (6.4) gives rise to corresponding perturbations due to small but finite values of γ_s .

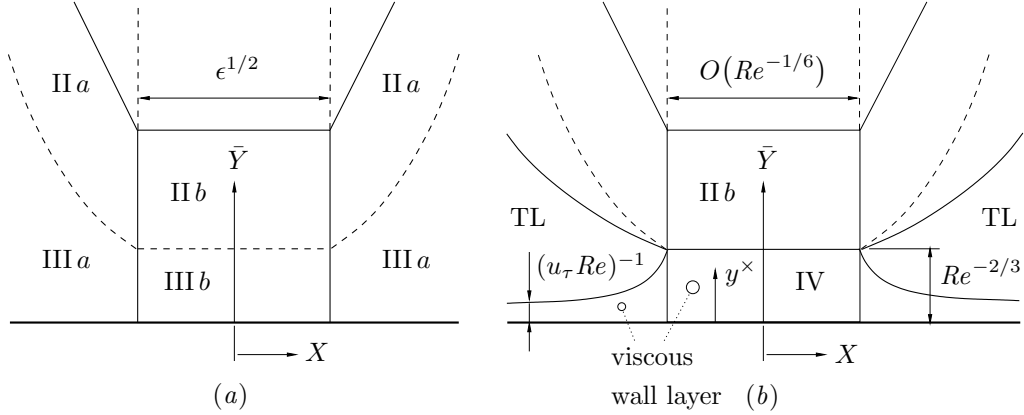


FIGURE 15. Local asymptotic structure at separation: (a) in the limit $Re^{-1} = 0$, (b) for Re finite: TL = transition layer; separation as well as reattachment may take place in region IV. In (b) the regions belonging to the inviscid wake (α finite, $Re^{-1} = 0$) are separated by thin lines.

in the regions II *a* which dominates the boundary layer flow locally. Neglecting logarithmic contributions inducing a pressure gradient of the same magnitude (cf. (5.19*a*) and (5.21)) for the sake of clearness, we only consider the leading-order term reflecting the finite wall shear which is determined by the skin friction law (5.20) in combination with the wall slip distribution (6.16),

$$f = \dots - \frac{c_0^2 (\mp s)^3 \gamma_s^2}{\kappa_0^2 P_{00}} \left(f_0' + O((\mp s)^{3/2}) \right) + \dots, \quad \gamma_s = \frac{\kappa_0}{\ln Re} \left(\frac{\ln(Re/U_s^3)}{\ln Re} + 3 \frac{\ln(\ln Re)}{\ln Re} + O\left(\frac{1}{\ln Re}\right) \right).$$

The leftmost dots abbreviate the inviscid expansion (6.9).

The attached-flow structure collapses if U_s and thus u_τ become of $O(Re^{-1/3})$ as already outlined at the beginning of §6. Independently of the specific behavior of U_s , this situation is associated with a merge of the wall layer with the transition layer as both their thicknesses equal $\delta^\times = O(Re^{-2/3})$ (cf. the respective scalings in §5.2) and summarized by

$$U_s, u_\tau = O(Re^{-1/3}) \quad \text{or} \quad \gamma_s = O(1). \quad (6.30)$$

Thus it also covers the case of self-similar flow where U_s is presupposed to be sufficiently small at all. The corresponding structure is sketched in figure 5 (b). As an important consequence, the log-law characteristic of their overlap (cf. (5.18)) apparently then disappears. We remark that none of the investigations carried out by Melnik (1989) and Gersten & Herwig (1992) are capable of capturing the inevitable breakdown of the skin friction formula as the need of the inviscid wake limit exhibiting a slip velocity and accounting for Prandtl's mixing length at the wall has not been recognized so far.

Contrarily, our approach even allows for the occurrence of negative skin friction, which then becomes a second-order term in the large- y^+ behaviour $\tau^+ \sim Ky^+$ of the wall layer expansions (3.6*a*). As the inviscid slip velocity U_s admits a regular behaviour when it changes sign the assumption

$$\epsilon Re^{1/3} = O(1), \quad (6.31)$$

which couples the regions of breakdown of both the inviscid and viscosity-affected flow cases represents an appropriate basis for describing the flow in the merging wall layer, without loss of generality. Note that (6.31) formally even comprises the case $\epsilon \rightarrow 0$ if c_1 in (6.24) is regarded as small. The arising structure is displayed in detail in figure 15 (b). As pointed out in the last section, the flow may separate in the limit

$Re^{-1} = 0$ within region III *b* which is replaced by the resulting wall layer IV if Re is finite. *Marginal* separation then occurs for high but finite Re if the reverse-flow regime is totally covered by the latter region.

6.2.1. Near-wall structure allowing for separation and reattachment

Regardless of the specific properties of the inviscid wake flow on the verge of separation, the behaviour in the overlap of the merging wall region IV and the mainly inviscid part of the boundary layer, see figure 15 (*b*), is readily found from (5.17) by examining the limits

$$U_s \rightarrow 0 \quad \text{and} \quad U_{sx} \rightarrow 0: \quad \Lambda \sim -U_e U_{ex}, \quad \Lambda \zeta \sim K y^+ \rightarrow \infty. \quad (6.32)$$

In order to account also for the case of separation where u_τ is no longer an adequate reference velocity, the velocities in region IV are referred to

$$u_p = (-U_e U_{ex}/Re)^{1/3} = O(Re^{-1/3}).$$

Therefore, the scalings (3.4) of the oncoming strictly attached wall layer in regime IV are suitably expressed by means of the familiar notations

$$y = \delta^\times y^\times, \quad \delta^\times = 1/(Re u_p); \quad u = u_p u^\times, \quad \tau = u_p^2 \tau^\times, \quad (6.33)$$

see e.g. Durbin & Belcher (1992), Gersten & Herwig (1992). Then the effect of the local mainstream pressure gradient which may provoke separation on the wall shear stress τ_w is measured by means of the Bradshaw parameter K introduced by (3.5) and expressing the ratio of the two velocity scalings appropriate for the wall layer:

$$K = (u_p/u_\tau)^3 = O(1); \quad u^+ = K^{1/3} u^\times, \quad \tau^+ = K^{2/3} \tau^\times, \quad y^+ = |K|^{-1/3} y^\times. \quad (6.34)$$

Furthermore, $\tau_w = \text{sgn}(\tau_w) u_p^2 K^{-2/3}$ is the wall shear stress, and the Bradshaw parameter clearly tends to $+\infty$ and $-\infty$ at the locations of separation and reattachment, respectively. In turn, one obtains by analogy to (3.6)

$$\tau^\times + u_{y^\times}^\times \sim \frac{\text{sgn}(K)}{K^{2/3}} + y^\times + \frac{1}{Re u_p \epsilon^{1/2}} \int_0^{y^\times} \left(\frac{u_{px}}{u_p} u_0^{\times 2} + u_0^\times u_{0x}^\times - u_0^\times z \int_0^z u_{0x}^\times d\zeta \right) dz; \quad (6.35a)$$

$$u^\times = u_0^\times + \frac{1}{Re u_p \epsilon^{1/2}} u_1^\times + \dots \quad (6.35b)$$

Considering (6.31), the convective contribution to the momentum balance (6.35a) is of $O(Re^{-1/2})$ and accounts for the at first unknown dependency of u_0^\times on x , which does not play a role in the limit $K \rightarrow 0$ as is seen from (3.6a). Note that the case of self-similar flow as discussed at the end of § 5.3.2 is formally implied if one assumes $\epsilon = O(1)$. Finally, restricting the considerations to the overlap closure to Prandtl's law (5.13) again and applying it to u_0^\times as $y^\times \rightarrow \infty$, yields the continuation of the large- ζ behaviour quoted in (5.18) in accordance with (6.32) and (6.34),

$$u_0^\times(y^\times, K) = \frac{2}{\kappa(K)} y^{\times 1/2} + C(K) - \frac{K^{-2/3}}{\kappa(K)} y^{\times -1/2} + \frac{1}{2\kappa(K)^2} y^\times + \frac{K^{-4/3}}{12\kappa(K)} y^{\times -3/2} + \dots \quad (6.36)$$

Here the term of $O(1/y^\times)$ is caused by the viscous stress, $\partial u^\times / \partial y^\times$, which is of the same order as τ^\times in (6.35a). Thus the overlap behaviour is governed by the square root law but any logarithmic portion has disappeared.

The parametric dependency of the velocity profile u_0^\times solely on K is justified as follows: As convective terms in the momentum balance (6.35a) vanish as $Re \rightarrow \infty$, the gradient u_y is not influenced by the state

of flow in the outer fully turbulent regime and the upstream conditions are given by the universal velocity profiles $u_0^+(y^+)$ and $U_1(\zeta)$ (see (5.17)), respectively. Dimensional reasoning then suggests a generalization of the universal character of the flow in the wall region as outlined in §3.1.1 for finite values of K ,

$$u_{y^\times}^\times \sim f(y^\times, K), \quad \tau^\times \sim g(y^\times, K) \quad \text{as } Re \rightarrow \infty.$$

This relation also indicates the dependency of the near-wall behaviour on K as already indicated in connection with (3.10), which is rewritten as

$$\tau^\times \sim A^\times(K) y^{\times 3}, \quad u^\times \sim K^{-2/3} y^\times + 1/2 y^{\times 2} - A^\times(K)/4 y^{\times 4}; \quad A^\times(K) = K^{-5/3} A^+(K) \quad \text{as } y^\times \rightarrow 0.$$

The universal functions $A^+(K)$, $A^\times(K)$ are not known at all at present but may be obtained by means of experiments. However, $A^\times(K)$ is assumed to attend a finite limit for $|K| \rightarrow \infty$. We emphasize that no further predictions regarding the properties of the wall layer flow in leading order are possible without adopting an appropriate wall closure scheme (the validity of the ones available at present must be considered at least questionable as separation is approached). Nevertheless, the most interesting feature is obtained from matching (6.36) to the solution in the flow region $\text{II}b$, see figure 15 (*b*). There the expansion

$$\Psi = \Psi_0 + \dots + \frac{\alpha}{\kappa^2 P_{00}^{2/3}} \frac{(K Re)^{-2/3}}{|\epsilon|^{1/2}} (\Psi_{0\bar{Y}} + |\epsilon|^{1/2} \Psi_{1\bar{Y}} + \dots) + O(Re^{-1})$$

holds, using the scaling (6.20). The dots denote its inviscid limit (6.22), which is apparently perturbed by terms of $O(Re^{-1/2})$. As $-U_e U_{e,x} \sim P_{00}$ locally, the half-power law given by Ψ_0 matches identically, but from inspection of the next order we draw the important conclusion

$$C(K) \sim U_s / u_p. \quad (6.37)$$

Note that U_s is given by (6.24), in agreement with (6.30). Interestingly, we infer from (6.37) that C varies approximately with $x^{(m+1)/3}$ in the case of self-preserving flow.

The coupling condition (6.37) provides the desired asymptotically correct extension of the skin friction law (5.20). Once $C(K)$ is known e.g. by means of experiments, inversion of (6.37) yields the associated wall shear stress. Measurements of the two empirical universal functions $\kappa(K)$ and $C(K)$ determining the wall layer flow on the verge of separation are presented by Vieth (1996) and Schlichting & Gersten (2000). Their data fitting reflects the requirements

$$\kappa(\infty) = \kappa(-\infty), \quad C(\infty) = C(-\infty), \quad A^\times(\infty) = A^\times(-\infty), \quad (6.38)$$

expressing the continuity of κ and C at separation and reattachment, respectively. Moreover, it proposes a symmetric dependency $\kappa(K) = \kappa(-K)$ with κ weakly increasing monotonically for increasing $|K|$. More interestingly, matching with the attached flow by using (5.20) and a careful interpretation of the measured intercept in the velocity distribution holding in the overlap within the framework of the present approach yields the relationships

$$C(K) \begin{cases} \sim \kappa_0^{-1} K^{-1/3} (\ln(4/|K|) + \kappa_0 C^+ - 2) & \dots |K| \rightarrow 0, \\ \approx C(\infty) + 5 K^{-1/3} & \dots |K| \rightarrow \infty. \end{cases}$$

Therefore, a linear relationship between u_τ and U_s is suggested at separation and reattachment, respectively. Unfortunately, for $|K| \rightarrow \infty$ only few data are available which exhibit relatively large inaccuracies, obviously due to difficulties arising from measurement. Thus they have to be accepted with great reservation and much further experimental effort is apparently needed for validation. However, at separation

the values given by

$$\kappa(\infty) = \kappa_\infty \approx 0.59 \dots 0.88, \quad C(\infty) = C^\times \approx -3.2 \quad (6.39)$$

are strongly supported by the studies cited.

In the current literature the half-power law as provided by (6.36) has been associated with the point of vanishing skin friction alone, and the coefficients usually denoted by κ_∞ and C^\times , respectively, stress the contrast to the log-law for attached flow, see (3.9). However, the theory presented allows for a smooth transition within the region IV (figure 15, *b*), from $\kappa(0) = \kappa_0$ and $C(0) = C^+$ to their counterparts κ_∞ , C_∞ indicating separation. If C^\times is negative as proposed by (6.39) separation (as well as reattachment) will occur for negative values of the inviscid slip velocity U_s , imposed on the wall layer. This fact has already been accounted for in the zoomed sketch in figure 8, characterizing strict equilibrium flows in the immediate vicinity of separation.

7. Conclusions — further outlooks

As the core of this work a self-consistent theoretical explanation for the occurrence of local separation zones within a turbulent boundary layer has been presented. The smooth transition from attachment towards separation inevitably results from a perturbation of an inviscid wake limit, characterized by a small slenderness parameter α , due to high but finite Re , based on matched asymptotic expansions. Furthermore, this theory immediately implies an extension of the classical small-defect approach which covers the empirically well-known phenomenon of non-uniqueness of self-preserving flows.

Apart from more experimental work in order to verify the essential results of the new theory proposed so far further progress on basis of matched asymptotic expansions is seen to be required due to several aspects which remain still open in the present work.

Firstly, the question arises whether the theoretical explanation of non-uniqueness of quasi-equilibrium flow for large β given in § 4, may be extended to small-defect flows where $\beta = O(1)$. In that case a rapid transition towards a nonlinear flow exhibiting a large defect, joined to the classical upstream solution by means of appropriate jump conditions following from first principles, is suggested. Such a drastic change in the structure of a boundary layer would explain how to connect two states of self-similarity which are represented by points lying on the lower and upper branch, respectively, of one of the curves parametrized by finite $\epsilon = O(1/\ln Re)$ in figure 8. Such a transition may be regarded as a nonlinear extension of the so-called connecting flow addressed in § 4.3, represented by the dashed curve in figure 4.

Secondly, the treatment of the nonlinear outer wake layer alone governed by (5.2) in the limit $\alpha = 0$ which is primarily perturbed due to finite α by the inner wake has not been addressed in the present work. This would allow for the treatment of the regular behaviour of the composite wall slip U_s according to (5.12) as $U_s \rightarrow 0$ within an asymptotically correct context. In the sense of a separate treatment of both wake layers it is not clear for the present whether the occurrence of small separation bubbles is accompanied by interaction of the boundary layer with the outer irrotational flow due to the induced pressure gradient.

Furthermore, to the author's mind the theoretical considerations leading to the asymptotic picture presented in § 6.2.1 which describes the case of marginal separation without employing any assumptions concerning a specific wall closure may be revised most likely by means of Direct Numerical Simulation. Therefore, it seems relevant for resolving the emergence of a small separation bubble located totally within the viscous sublayer that for high Re the thickness of this flow regime is asymptotically comparable to Kolmogoroff's micro-length scale $\tilde{\ell}_K$, cf. also § 2: From the turbulent mean kinetic energy budget readily follows that turbulent dissipation denoted by $\tilde{\epsilon}$ must be of the same magnitude as the production term $\tilde{\tau} \tilde{u}_{\tilde{y}}$, in order to maintain turbulent mean energy balance, cf. (5.6). This estimate in connection with the equilibrium between viscous and turbulent shear stresses up to leading order, i.e. actually the definition of a viscous sublayer, gives rise to the asymptotic relationship

$$\tilde{\ell}_K \equiv (\tilde{\nu}^3/\tilde{\epsilon})^{\frac{1}{4}} \sim (\tilde{\nu}/\tilde{u}^*) = \tilde{\delta}^*.$$

The superscript * signifies + or \times , respectively, and tildes denote dimensional quantities such that δ^* and u^* used elsewhere then are made non-dimensional with respect to their global reference scales, \tilde{L} and \tilde{U}_0 , see § 2).

Thus it seems evident that the marginal excitement of time-mean reverse flow in the sense of usual Reynolds (or time) averaging essentially originates from instantaneous separation, evoked by the smallest eddies whose diameter is comparable to $\tilde{\ell}_K$. For a validation of this mechanism by means of extensive

semi-theoretical studies of near-wall turbulence the reader is referred to the survey paper of Walker (1998). More theoretical effort may highlight the properties of near-wall turbulence if separation is approached.

Appendix A. Homogeneous problem for large β_0

We rewrite the leading-order problem (4.20) using (3.7), that is $R = (lH'')^2$, where $l = l(\eta)$ in order to uphold the assumption of complete similarity,

$$2\eta H' = H(1) (l H'')^2; \quad H(0) = H''(0) = 0, \quad H'(1) = 0 \iff H''(1) = 0. \quad (\text{A } 1)$$

Then $H(1)$ might be regarded as an eigenvalue. Any simple but asymptotically correct closure for $l(\eta)$, i.e. supplemented with Prandtl's universal wall condition (3.8), may serve exemplarily for constructing an unique non-trivial solution besides the evident trivial one, $H \equiv 0$ and thus $R \equiv 0$:

From integrating (A 1) one gets

$$H'(\eta) = \frac{1}{2H(1)} \left(\int_{\eta}^1 \frac{\zeta^{1/2}}{l(\zeta)} d\zeta \right)^2. \quad (\text{A } 2)$$

Repeated quadrature yields the solution for $H(\eta)$ and in particular

$$H(1) = \left[\frac{1}{2} \int_0^1 \left(\int_{\eta}^1 \frac{\zeta^{1/2}}{l(\zeta)} d\zeta \right)^2 d\eta \right]^{1/2}.$$

Thus the near-wall behaviour (4.21) may be verified by examining (A 2) for $\eta \rightarrow 0$.

In order to gain numerical results we adopt the closure for $l = \ell/\delta$ proposed throughout this work, (3.21). Integration gives $H(1) \doteq 5.6913$ and $H'(0) \doteq 14.004$. Hence, in accordance with (4.21), $\lambda \doteq 4.9211 g(x_0)^2$. In the case of self-preserving flow, i.e. $F \equiv H$, the increase of δ in the high- β_0 limit then is approximately given by $\delta_x \sim \bar{\gamma} \Delta_x$ with

$$\Delta_{0x} = 3/H(1) \doteq 0.5271;$$

see (3.18), (4.4) and (4.23). Furthermore, for the equilibrium shape parameter defined in (4.22) as well as the first contribution to Π_0^2 in (4.28) due to the effect of boundary layer displacement follows

$$G_0 \doteq 8.0815, \quad 8/H(1)^3 \doteq 4.340 \times 10^{-2}. \quad (\text{A } 3)$$

In (4.28) the latter (rather small) value is added to a term containing the integral over the x - and y -contribution to the spur of the Reynolds stress tensor. In order to model these Reynolds normal stress components we follow Schneider (1991) and focus on the shear layer approximation (5.6) of the well-known k -equation describing the transport of the (dimensionless) turbulent mean kinetic energy k : Considering our nonlinear approach elucidated in § 5, which of course covers also the high- β defect limit, see § 5.4, it has been mentioned in § 5.1.1 that the outer main part of the boundary layer is governed by the balance between turbulent dissipation and production in leading order if the parameter α is regarded to be small. As pointed out in Rotta (1972), Schneider (1991), Prandtl's method (Prandtl, 1945) of combining this equilibrium with the mixing length concept (3.7) gives rise to the common leading-order closure for the eddy viscosity ν_t in the well-known Boussinesq's general ansatz for the Reynolds stress tensor. Based on dimensional reasoning, it exhibits a single empirical parameter $c \approx 0.565$ and reads in the two-dimensional case

$$\tau = \nu_t (u_y + v_x), \quad \sigma_{(x)} = 2\nu_t u_x - 2/3 k, \quad \sigma_{(y)} = 2\nu_t v_y - 2/3 k; \quad \nu_t \sim \ell^2 u_y = c \bar{\ell} k^{1/2}.$$

Therefore, $\tau \sim c^2 k$ such that the sum of both normal stresses are related to τ . (Following Townsend, 1961, flows exhibiting a proportionality between τ and k are termed to be in *structural* equilibrium.)

This model is asymptotically correct as $S_{(x)0}$ and $S_{(y)0}$ exhibit a finite limit in the overlap between the outer region and the viscous wall regime; moreover, they vanish at the boundary layer edge, according to

Kolmogoroff's hypothesis. In fact, it is readily verified that it allows for self-similarity if the distribution of $U_e(x)$ obeys a power law, cf. (3.20). Taking into account the continuity equation, the sum $S_0 = S_{(x)_0} + S_{(y)_0}$ is then expressed according to

$$\int_0^1 S_0 d\eta = -\frac{4}{3c^2} \int_0^1 T_0 d\eta \doteq -2.617, \quad -\frac{1}{H(1)} \int_0^1 S_0 d\eta \doteq 0.460.$$

With $T_0 = (lH'')$ and adopting the shear stress closure (3.21) again, the values result from numerical integration of (A 1). Finally, inserting (A 3) into (4.28) one obtains

$$\Pi_0^2 \doteq 0.503, \quad 6/(1 + \Pi_0^2/G_0) \doteq 5.648.$$

Thus our model gives for the factor in (4.31) an about 12.97% larger value than the empirical one cited in Schlichting & Gersten (2000) as given by (4.32). Apart from the asymptotic error encountered, this difference is probably caused by deficiencies regarding the simple normal stress closure.

Appendix B. Numerical method for the nonlinear problem

In order to solve problem (5.26) a finite-difference scheme with relaxation has been employed. To this end, we introduced a new independent variable z with $\eta = z^2$, such that the square root singularity in f_0' arising from Prandtl's mixing length in the closure for t_0 given by

$$t_0 = (l/c_\ell)^2 f_0''^2, \quad \text{with } l \sim \kappa\eta \text{ as } \eta \rightarrow 0,$$

see (3.7), and (3.21), is discarded and all terms in (5.26) behave regularly for $\eta \rightarrow 0$. Thus the mesh $z_0 = 0, z_1, z_2, \dots$ constructed by the solver itself in order to satisfy a given error tolerance has been spaced approximately uniformly on the interval $0 \leq z \leq 1$.

Starting with an initial profile, in our case given by a similarity solution f_0, t_0 according to (5.24), the leading-order turbulent boundary layer problem (5.2) has been solved by means of a very efficient modification of the second-order accurate Keller-Box scheme which may also be interpreted as a simple finite-volume scheme: The grid points $\eta_0 = 0, \eta_1, \eta_2, \dots$ and thus the numerical accuracy were prescribed by the finite-difference routine solving the initial ordinary boundary value problem and kept fixed during downstream integration. However, studying the performance of different codes revealed that reducing the number of mesh points will give rise to the same accuracy as if a conventional Keller-Box scheme (known from laminar flow) would have been used, especially in the case of backflow, if downstream integration of (5.2a) is based on its conservative representation

$$(U F_\eta)_x - (U F_x)_\eta = \delta_0 U_e U_{ex} + T_\eta, \quad \text{with } \eta = y/\delta_0(x).$$

To this end, we introduced a stream function, streamwise velocity and Reynolds shear stress, respectively, defined by

$$F(x, \eta) = \psi_0(x, \bar{y}), \quad U(x, \eta) \equiv \psi_{0\bar{y}} = F_\eta/\delta_0, \quad T(x, \eta) = \tau_0(x, \bar{y}) = l^2 (U_\eta)^2.$$

Employing our model (3.21), the latter equality reflects the mixing length formulation (3.7). The closure enters the first-order system approach the Keller-Box method provides in expressing the gradient U_η through T .

Appendix C. Local eigensolutions for $U_s \rightarrow 0$

The linearized boundary layer equation (6.10a) is clearly solved by $h = f_0' = 2\eta^{1/2}$. Since this solution does not meet the second boundary condition given in (6.6) requiring vanishing wall shear, a solution of

(6.10a) satisfying all boundary conditions is constructed by means of reduction of order:

$$h(\eta) = \frac{c}{2}\eta^{1/2} \int_0^\eta H_\nu(\zeta) d\zeta; \quad H_\nu(\eta) = \eta^{-1/2} w_\nu(z), \quad z = \pm\eta. \quad (\text{C } 1)$$

The coefficient c remains undetermined, and the upper and lower signs refer to the upstream ($s < 0$) and downstream ($s > 0$) case, respectively. The latter transformation in (C 1) reduces the homogeneous second-order problem for H_ν to the standard form,

$$z w_\nu'' - (z - b) w_\nu' - a w_\nu = 0; \quad a = -\nu - 1/2, \quad b = 2,$$

which is the well-known Kummer's (or confluent hypergeometric) equation. For a detailed discussion see e.g. Abramowitz & Stegun (1972): Two independent solutions for $w_\nu(z)$ are provided by Kummer's functions, denoted by $M(a, b, z)$ and $U(a, b, z)$. Since the latter behaves as $U \sim z^{1-b}$ for $z \rightarrow 0$ it must be discarded with respect to the integration in (C 1). The first one exhibits a regular behaviour starting with $M(a, b, 0) = 1$ and thus gives rise to finite values of the wall slip $h'(0)$. Regarding the upstream side, it exhibits non-exponential growth as $z \rightarrow \infty$ or $\eta \rightarrow \infty$ only if the condition $a = -n$ equivalent to

$$\nu = n - 1/2, \quad n = 0, 1, 2, \dots, \quad (\text{C } 2)$$

is met. Considering the downstream side, an algebraic behaviour $M = O((-z)^{-a})$ as $-z \rightarrow \infty$, i.e. $\eta \rightarrow \infty$, is obtained for any real ν . With respect to (6.9) the solution h must match with the critical profile $\psi_{00}(\bar{y})$, cf. (6.14a). As the near-wall behaviour of the latter is determined by a match with the solution in region IIa for $s < 0$, in the corresponding region for $s > 0$ admissible values of ν are also restricted to the discrete series of the eigenvalues given in (C 2). Thus we obtain a set of eigenfunctions $M(-n, b, z)$ which are polynomials of degree n for both the up- and downstream flow.

Regarding the limit $\epsilon = 0$ in (6.9) we eliminate the case $n = 0$ for $\nu = \lambda$ must be positive; the case $n = 1$ describes a regular separating solution of (6.5) which exhibits a linearly varying slip velocity, i.e. $f'(\mp s, 0) \sim cs$, giving rise to an unbounded backflow region for $s > 0$. As in the marginal case investigated here U_s immediately recovers, we omit also the first eigenvalue. Therefore, the strongest eigensolution perturbing f_0 is then given for $\lambda = 3/2$ by $w_2 = M(-2, 2, z) = 1 + z + z^2/6$. However, in the regions IIa the perturbations of $O(\epsilon(\mp s)^\mu)$ are considered to be asymptotically small for any μ . Thus in the case $\nu = \mu$ the minimum exponent $\mu = -1/2$ is fixed by $n = 0$, so that the strongest disturbance possible is governed by the solution $w_0 = M(0, 2, z) = 1$. Applying (C 1) and setting $c = c_0$ and $c = c_1$ yields the corresponding solutions for f_λ and g_μ , respectively, quoted in (6.11).

We now consider the case of eigensolutions varying exponentially with s , which are governed by (6.19). Again, the solution $\bar{g} = \bar{f}'_0$ (cf. (6.25)) must be discarded by means of

$$\bar{g}(\bar{\eta}) = c \left(2\bar{\eta}^{1/2} + \iota \right) \int_0^z G_\omega(\zeta) d\zeta; \quad z = 2\iota(|\omega|\bar{\eta})^{1/2}, \quad \iota = \pm 1, \quad (\text{C } 3)$$

with arbitrary c known from upstream history. This yields the thereby reduced homogeneous problem

$$z \left(z + |\omega|^{1/2} \right) G_\omega'' + 3z G_\omega' \pm \left(z + |\omega|^{1/2} \right)^2 G_\omega = 0; \quad G_\omega(0) = 0, \quad G_\omega'(0) = 1. \quad (\text{C } 4)$$

Here the upper and lower signs denote the cases $\omega > 0$ and $\omega < 0$, respectively. It is readily verified that due to the first boundary condition the solution for G_ω admits a regular behaviour as $z \rightarrow 0$ such that $\bar{g} = \bar{g}'(0) + O(\bar{\eta}^{3/2})$ as $\bar{\eta} \rightarrow 0$, in order to satisfy the condition of zero wall shear, cf. (6.6). The second boundary condition in (C 4) fixes the constant c by $\bar{g}'(0) = 2\iota c|\omega|$.

A general analytical solution of (C 4) has not been found. However, considering the existence of two

independent fundamental solutions of equation (C4), one obtains for $\omega > 0$ and $|z|$ large

$$G_\omega(z) = z^{-3/2} \left[A(\omega) \cos(z + \omega^{1/2} \ln z/2) (1 + O(|z|^{-1})) + B(\omega) \sin(z + \omega^{1/2} \ln z/2) (1 + O(|z|^{-1})) \right].$$

where the coefficients $A(\omega)$ and $B(\omega)$ depend on the overall solution. As the integral in (C3) then converges, the solution \bar{g} oscillates but varies with $\bar{\eta}^{3/2}$ for $\bar{\eta} \rightarrow \infty$, as requested in (6.19) and allowing for a match with the solution in the region where $\eta = O(1)$. Conversely, in the more interesting opposite case $\omega < 0$ the analysis gives

$$G_\omega(z) = C_+(\omega) \exp(z) z^{(|\omega|^{1/2}-3)/2} (1 + O(|z|^{-1})) + C_-(\omega) \exp(-z) z^{(-|\omega|^{1/2}-3)/2} (1 + O(|z|^{-1})).$$

The solution now exhibits an undesired exponential growth, apart from the possibility of discrete eigenvalues $\omega = \omega^*$ with $C_+(\omega^*) = 0$ (case $\iota > 0$) or $C_-(\omega^*) = 0$ (case $\iota < 0$). Then G_ω decays exponentially and \bar{g} again admits its desired asymptotic behaviour for $\bar{\eta} \rightarrow \infty$.

Note that (C4) allows for a representation of the original function $\bar{g}(\bar{\eta})$ for the cases $\omega \rightarrow 0_+$ and $\omega \rightarrow 0_-$, respectively, in the region $z = O(1)$: There the solution may be written in terms of (modified) Bessel functions, see e.g. Abramowitz & Stegun (1972),

$$G_\omega = |\omega|^{1/2} F_\mp(z)/(2z) + O(\omega), \quad F_-(z) = J_1(z) \quad (\omega < 0), \quad F_+ = I_1(z) \quad (\omega > 0);$$

$$\text{and } G_\omega = |\omega|^{1/2} \left\{ 1/4 - 1 / \left[2(1 + 2\iota \bar{\eta}^{1/2})^2 \right] \right\} + O(\omega^{3/2})$$

where $\bar{\eta} = O(1)$, fixing the coefficient of the former expressions by matching. This reveals the unique solution $\bar{g} \equiv 0$ of (6.19) for $\omega = 0$. However, starting with the analytical limiting solution for $\omega = 0_-$ the initial value problem (C4) has been solved numerically by decreasing ω , in order to find the roots of $C_+(\omega) = 0$ and $C_-(\omega) = 0$. In the case $\iota = +1$ (positive wall slip, see (C3), i.e. $z \rightarrow \infty$, all solutions exhibit exponential growth and thus must be discarded. In contrast, for $\iota = -1$ (negative wall slip) we examine (C4) for $z \rightarrow -\infty$ where a single zero of $C_-(\omega)$ was found, apparently for $\omega = -9$. In fact, only in the case $|\omega| = 9$ a special ansatz allows for a simple analytical solution of problem (C4). For $\omega = -9$ it reads

$$G_{-9} = \frac{z(1 + 2z/3)}{(1 + z/3)^2} \exp(z).$$

Application of (C3) in the interesting case $\iota = -1$ leads to (6.27) and in turn to the inhomogeneity in the problem (6.28), determining the exponent ν . Denoting the accordingly reduced counterpart of the function $\bar{h}(\bar{\eta})$ by $H_\nu(z)$ and abbreviating the homogeneous equation (C4) by $L(G_\omega) = 0$ then yields

$$L(H_\nu) = [2/9 + (11/18 - \nu/3)z + (31/18 - 2\nu/9)z^2 + z^3/3] \exp(z) - 2/9; \quad H_\nu(0) = 0, \quad H'_\nu(0) \neq 0.$$

Like $\bar{g}'(0)$ also the ratio $\bar{h}'(0)/\bar{g}'(0) = H'_\nu(0)$ depends on upstream history and thus remains unknown. Noting that $\omega = -9$, any homogeneous solution of this problem vanishes identically due to the purely homogeneous boundary conditions, i.e. $C_+(-9) = C_-(-9) = 0$. Furthermore, from an analytical study it is deduced that the particular solution $H_\nu(z)$ decays with z^{-2} as $z \rightarrow -\infty$. However, a solution lacking of logarithmic terms which prevent the existence of a real solution for negative z is suggested only if $\nu = 1/3$. Again, the solution $H_{\frac{1}{3}}(z)$ may be expressed in closed form and is transformed into (6.29) by means of (C3).

REFERENCES

- ABRAMOWITZ, M. & STEGUN, I. A., EDS. 1972 *Handbook of mathematical functions*, 9th edn. Dover.
- AFZAL, N. 1996 Wake layer in a turbulent boundary layer with pressure gradient: a new approach. In *Proc. IUTAM Symp. Asymptotic Methods for Turbulent Shear Flows at High Reynolds Numbers* (ed. K. Gersten), pp. 95–118. Kluwer Academic.
- ALVING, A. E. & FERNHOLZ, H. H. 1996 Turbulence measurements around a mild separation bubble and downstream of reattachment. *J. Fluid Mech.* **322**, 297–328.
- BUSH, W. B. & FENDELL, F. E. 1972 Asymptotic analysis of turbulent channel and boundary-layer flow. *J. Fluid Mech.* **56**, 657–681.
- CHAWLA, T. C. & TENNEKES, H. 1973 Turbulent boundary layers with negligible wall stress: A singular perturbation theory. *Int. J. Engng Sci.* **11**, 45–64.
- CLAUSER, F. H. 1954 Turbulent Boundary Layers in Adverse Pressure Gradients. *J. Aeronaut. Sci.* **21**, 91–108.
- CLAUSER, F. H. 1956 The Turbulent Boundary Layer. *Adv. Appl. Mech.* **4**, 1–51.
- DURBIN, P. A. & BELCHER, S. E. 1992 Scaling of adverse-pressure-gradient turbulent boundary layers. *J. Fluid Mech.* **238**, 699–722.
- ELSBERRY, K., LOEFFLER, J., ZHOU, M. D. & WYGNANSKI, I. 2000 An experimental study of a boundary layer that is maintained on the verge of separation. *J. Fluid Mech.* **423**, 227–261.
- FENDELL, F. E. 1972 Singular perturbation and turbulent shear flow near walls. *J. Astro. Sci.* **20**, 129–165.
- GERSTEN, K. & HERWIG, H. 1992 *Strömungsmechanik*. Vieweg.
- KÁRMÁN, TH. VON 1930 Mechanische Ähnlichkeit und Turbulenz. *Nachr. Ges. Wiss. Göttingen, Math.-Phys. Klasse*, 58–76.
- MELLOR, G. L. 1966 The effects of pressure gradient on turbulent flow near a smooth wall. *J. Fluid Mech.* **24**, 255–274.
- MELLOR, G. L. 1972 The large Reynolds number, asymptotic theory of turbulent boundary layers. *Int. J. Engng Sci.* **10**, 851–873.
- MELLOR, G. L. & GIBSON, D. M. 1966 Equilibrium turbulent boundary layers. *J. Fluid Mech.* **24**, 225–253.
- MELNIK, R. E. 1989 An asymptotic theory of turbulent separation. *Computers & Fluids* **17** (1), 165–184.
- MICHEL, R., QUÉMARD, C. & DURANT, R. 1969 Hypothesis on the mixing length and application to the calculation of the turbulent boundary layers. In *Proc. Computation of turbulent boundary layers – 1968 AFOSR-IFP-Stanford Conference* (ed. S. J. Kline *et al.*), Vol. I, pp. 195–207. Stanford University.
- MILLIKAN, C. B. A. 1938 A critical discussion of turbulent flows in channels and circular tubes. In *Proc. 5th Int. Congress of Theoretical and Applied Mechanics*, pp. 386–392. MIT Press.
- NARASHIMA, R. 1996 Different approaches to asymptotic expansions in turbulent boundary layers. In *Proc. IUTAM Symp. Asymptotic Methods for Turbulent Shear Flows at High Reynolds Numbers* (ed. K. Gersten), pp. 5–16. Kluwer Academic.
- NEISH, A. & SMITH, F. T. 1992 On turbulent separation in the flow past a bluff body. *J. Fluid Mech.* **241**, 443–467.
- PERRY, A. E., BELL, J. B. & JOUBERT, P. N. 1966 Velocity and temperature profiles in adverse pressure gradient turbulent boundary layers. *J. Fluid Mech.* **25**, 299–320.
- PRANDTL, L. 1904 Über Flüssigkeitsbewegung bei sehr kleiner Reibung. In *Verhandlg. d. III. Intern. Mathem.-Kongr., Heidelberg 1904*, pp. 484–491. Teubner.
- PRANDTL, L. 1925 Bericht über Untersuchungen zur ausgeprägten Turbulenz. *Z. Angew. Math. Mech.* **5**, 136–139.
- PRANDTL, L. 1933 Neuere Ergebnisse der Turbulenzforschung. *Z. VDI* **77**, 105–114.
- PRANDTL, L. 1945 Über ein neues Formelsystem für die ausgebildete Turbulenz. *Nachr. Akad. Wiss. Göttingen, Math.-Phys. Klasse*, 6–19.
- ROTTA, J. C. 1972 *Turbulente Strömungen*. B. G. Teubner.
- RUBAN, A. I. 1981 Singular solution of boundary layer equations which can be extended continuously through the point of zero surface friction. *Fluid Dyn.* **16** (6), 835–843.
- SCHLICHTING, H. & GERSTEN, K. 2000 *Boundary-layer theory*. Springer.

- SCHNEIDER, W. 1991 Boundary-layer theory of free turbulent shear flows. *Z. Flugwiss. Weltraumforsch.* **15**, 143–158.
- SCHOFIELD, W. H. 1981 Equilibrium boundary layers in moderate to strong adverse pressure gradients. *J. Fluid Mech.* **113**, 91–122.
- STEWARTSON, K., SMITH, F. T. & KAUPS, K. 1982 Marginal Separation. *Stud. in Appl. Math.* **67**, 45–61.
- SYCHEV, VIK. V. 1983 Asymptotic theory of turbulent separation. *Fluid Dyn.* **18** (4), 532–538.
- SYCHEV, V. V. 1987 On Turbulent Boundary-Layer Separation. In *Proc. IUTAM Symp. Boundary-Layer Separation* (ed. F. T. Smith & S. N. Brown), pp. 91–107. Springer.
- SYCHEV, V. V. & SYCHEV, VIK. V. 1987 On turbulent boundary layer structure. *PMM U.S.S.R.* **51**, 462–467.
- SYKES, R. I. 1980 An asymptotic theory of incompressible turbulent boundary-layer flow over a small hump. *J. Fluid Mech.* **101**, 647–670.
- TOWNSEND, A. A. 1961 Equilibrium layers and wall turbulence. *J. Fluid Mech.* **11**, 97–120.
- TOWNSEND, A. A. 1976 *The structure of turbulent shear flow*. Second edition. Cambridge University Press.
- VIETH, D. 1997 Heat and momentum transfer in turbulent boundary layers in the presence of strong adverse pressure gradients. In *Proc. IUTAM Symp. Asymptotic Methods for Turbulent Shear Flows at High Reynolds Numbers* (ed. K. Gersten), pp. 155–168. Kluwer Academic.
- WALKER, J. D. A. 1998 Turbulent Boundary Layers II: Further Developments. In *Recent advances in boundary layer theory* (ed. A. Kluwick), CISM Courses and Lectures - No. 390, pp. 145–229. Springer.
- WINTER, K. G. & EAST, L. F. 1982 The Design of Optimum Diffusers for Incompressible Flow. In *Recent Contributions to Fluid Mechanics* (ed. W. Haase), pp. 312–320. Springer.
- YAJNIK, K. S. 1970 Asymptotic theory of turbulent shear flows. *J. Fluid Mech.* **42**, 411–427.

CURRICULUM VITAE

Name: Bernhard (Frank) Scheichl
Geburtsdatum: 15. April 1969
Geburtsort: Mödling, Niederösterreich
Nationalität: Österreicher
Zivilstand: dzt. ledig
Bekenntnis: ev. AB
Wohnadresse: dzt. Neusiedlerstraße 41/2/3, A-2340 Mödling

Bildungsweg:

1975 – 1979 Volksschule in Mödling.

1979 – 1987 Realistisches Gymnasium, BGuBRG Mödling. Reifeprüfung im Juni 1987.

Oktober 1987 – **Maschinenbau-Studium / Studienzweig Verfahrenswesen**
November 1995 an der Technischen Universität Wien.

Diplomarbeit unter Betreuung von Prof. A. Kluwick:

Nichtlineare Stabilitätsanalyse von Wellenausbreitungsphänomenen in Suspensionen.

Zweite Diplomprüfung im November 1995.

April 1997 – **Doktoratsstudium** im Rahmen der Beschäftigung als **Univer-**
April 2001 **sitätsassistent** an der Technischen Universität Wien am Institut für Strömungslehre und Wärmeübertragung in der Abteilung für Aerodynamik und Wellenausbreitung unter der Leitung von Prof. A. Kluwick.

Proceedings zu GAMM-Vorträgen (1999, 2000):

KLUWICK, A., SCHEICHL, B. (2000) On marginal turbulent separation due to an imposed adverse pressure gradient. In *Z. Angew. Math. Mech. (ZAMM)* **80**, S3, pp. 647–648.

KLUWICK, A., SCHEICHL, B. (2001) Singular Solutions of the Turbulent Boundary Layer Equations in the Case of Marginal Separation as $Re \rightarrow \infty$. To appear in *Z. Angew. Math. Mech. (ZAMM)* **81**, S4 (in press).

Februar 1995 – Zivildienst (Stadtgemeinde Mödling).
Dezember 1995

postgraduale Industrietätigkeiten:

Jänner 1996 – Projekt-Ingenieur bei *Hoerbiger Ventilwerke AG*, Wien.

Dezember 1996

Februar 1997 – *R.T.S. – Real Time Computer Software Ges.m.b.H.*, Wien.

März 1997